Full title

Pattern-informed energetics: Energy allocation modeling for predicting trait variation and population persistence

Short title

Pattern-informed energetics in population models

Authors

Cara A. Gallagher[1,2*], Viktoriia Radchuk[3], Melanie Dammhahn[4,5], & Florian Jeltsch[1]

Affiliations

[1]Plant Ecology and Nature Conservation, Institute of Biochemistry and Biology, University of Potsdam, 14469 Potsdam, Germany

[2]Department of Ecoscience, Aarhus University, 4000 Roskilde, Denmark

[3]Leibniz Institute for Zoo and Wildlife Research, Alfred-Kowalke-Straße 17, Berlin, Germany

[4]Behavioural Biology, Institute for Neuro- and Behavioural Biology, University of Münster, Badestrasse 9, 48149 Münster, Germany

[5]Joint Institute for Individualisation in a Changing Environment (JICE), University of Münster and Bielefeld University, Germany

*Corresponding author: cara.gallagher@ecos.au.dk

Abstract

Ecosystem processes emerge from complex interactions between environmental conditions, individual behavior, fitness, and population dynamics. Energetics is a central mechanism driving these relationships, and individual-based energy budget models have emerged as powerful tools for linking resource dynamics to fitness. However, these models often lack an empirical foundation for how organisms allocate energy to fitness-related processes when resources are limited. Here, we introduce the Pattern-Informed Energetics (PIE) framework, a novel approach that leverages diverse empirical data sources to infer key parameters governing energy allocation. Using a rodent case study, we rigorously calibrated and evaluated PIE against multiple observed patterns, including in population dynamics, morphometrics, energetics, and life-history traits, assessing its ability to replicate experimental results and predict responses to future climate scenarios. Our findings demonstrate that PIE can mechanistically predict how environmental change shapes traits and population trajectories, offering a robust framework for improving biodiversity forecasting. By linking energy allocation to emergent ecological patterns, PIE strengthens the integration of physiological insights into predictive models, advancing our understanding of species' responses to environmental change while accounting for their evolved life histories.

Introduction

Amidst unprecedented environmental change, we face an urgent need to deepen our understanding of ecological dynamics and enhance our ability to predict responses to change. Despite considerable conservation efforts, progress remains limited in halting population declines, species extirpations, and the loss of entire branches of the tree of life, with cascading repercussions for ecosystem functions (1–4). Accurate predictive models are needed to forecast biodiversity change, identify its drivers, guide data collection, prioritize conservation efforts, and develop effective strategies to maximize the use of limited time and resources (4, 5). Predictive models increasingly guide ecosystem management and conservation (6–8), yet our ability to anticipate environmental impacts on species and communities remains hindered by gaps in understanding the processes driving biodiversity dynamics (3). Given the diverse, multiscale, and nonlinear disruptions humans elicit in nature (9), process-explicit models are vital to understand complex interactions and feedbacks between threats and biodiversity responses (4, 10, 11). These models can serve as platforms for weaving ecological knowledge and theory into tools that advance understanding of species and ecosystem dynamics under change and provide much needed projections for conservation management and policy (3).

A key mechanism through which changes in environmental conditions affect animal fitness is by disrupting individual energy balance. Resource availability and behavioral shifts in altered environments can limit foraging success or increase metabolic costs. These disruptions influence energy allocation to maintenance, growth and reproduction, which in turn shape population vital rates (12) and community dynamics (13). As such, energy represents the fundamental currency of biological fitness, mediating survival and reproduction according to the laws of energy and mass balance (14). The ability to meet energetic demands, driven by basal metabolism, activity, reproduction, and tissue production, determines an individual's fitness (15, 16). In life-history theory, animal metabolisms are viewed as products of evolutionary adaptations tailored to specific environmental contexts, wherein the allocation of limited resources between survival, activity, growth, and reproduction is constrained by trade-offs among traits that are suited for their habitats (17, 18). Environmental changes can disrupt these evolved strategies, potentially leading to

mismatches that upset energy balance and impact reproduction and survival (e.g., Clairbaux et al., 2021). To link environmental changes and animal behavior to fitness outcomes and population-level impacts, process-explicit models incorporating individual energy budgets are essential (12).

The history of ecological energy budget models spans over 70 years (e.g., Winberg, 1956). These models have been applied to diverse systems and questions, including the effects of management decisions on mackerel (*Scomber scombrus*) fisheries (21), climate and habitat changes on African elephant (*Loxodonta africana*) populations (22), and thermogenic dynamics in muskoxen (*Ovibos moschatus*) (23). To address this broad range of purposes, diverse energy budget models have been developed, each based on distinct assumptions about the dynamics governing energy expenditure and allocation. These assumptions range from hierarchical prioritization of metabolic processes favoring survival (12) to fixed-fraction allocation in Dynamic Energy Budget (DEB) theory (24) and optimization-based approaches (25, 26). Despite this diversity, the relative performance and predictive power of these approaches remain under-evaluated (27). Moreover, many modern empirical insights remain under considered in energy budget modeling, such as mechanisms regulating body adiposity (28, 29) and energy intake (30), non-linearities in metabolic fuel use and deposition (31, 32), and variations in energy use associated with pace-of-life (17, 33, 34). While models will always be simplifications of nature, and not all processes are relevant to every model's purpose, incorporating advancements in physiological understanding, such as reserve regulation, nonlinear fuel use, and inter-individual variation in energetics, can drive more mechanistic projections of populations under change. These advancements can enhance our ability to understand how populations respond to environmental stressors and inform strategies to mitigate biodiversity loss and ecosystem disruptions

Advances in technology and data collection techniques, which have generated an ever-growing trove of detailed physiological, morphological, and demographic data from both captive and wild settings, present an opportunity for a more strategic integration of this knowledge in informing or testing energy budget models (e.g., Chimienti et al., 2020). Datasets from both classical and emerging approaches offer

opportunities for improving the estimation of energetic parameters that are currently difficult or impossible to measure empirically. Approaches such as pattern-oriented modeling (POM) (*36, 37*) and statistical inference (*38*) hold promise for addressing these gaps.

A significant gap in the literature concerns how suboptimal energy intake affects the allocation of energy between competing demands such as survival, activity, reproduction, and growth (*12, 39, 40*). Current methodologies often rely on arbitrary thresholds or optimization-based approaches to determine when animals should halt resource allocation to processes such as reproduction or growth (*12, 39*), which may not reflect the feedbacks and adaptive behaviors of real-world systems (*41*). Empirical studies linking energy balance or reserves to their effects on processes related to metabolism, such as reproduction probability, remain limited (but see Beltran et al., 2023; Bright Ross et al., 2021; Christiansen et al., 2014; Van Benthem et al., 2017). Collecting such data remains challenging, particularly for cryptic, rare, or elusive species that cannot be studied through captive or repeated experimentation. Nevertheless, recent studies have illuminated patterns in animal morphometrics, physiology, behavior, and life history that offer insights into evolved energy allocation strategies without relying on assumptions rooted in thresholds or optimal behavior. By employing statistical inference and POM, it is possible to elucidate parameters driving the context-dependent relationships governing energy allocation in a species-specific manner, while considering the inherent uncertainty and variation within and between species.

Here, we introduce the Pattern-Informed Energetics (PIE) framework (Figure 1B), an energy budget modeling approach that departs from traditional fixed-allocation models by deriving context-dependent strategies directly from empirical patterns, offering greater ecological realism. The PIE framework provides mechanistic insights into the emergence of individual trait variation, driven by phenotypic plasticity, competitive interactions, and natural selection, and can be used to predict the impacts of environmental change on population dynamics and persistence. This approach allows for allocation strategies to emerge from the patterns they drive, such as morphometrics and growth, reproductive investment and success, and

population dynamics. Additionally, it incorporates underutilized physiological insights, including dual intervention point and Forbes' theories (*28, 32*), which link body fat regulation and metabolic fuel use to body condition. Although PIE is relevant to all animals, the bioenergetic model structure we implement here for illustrative purposes is generic to terrestrial homeotherms, with bank vole (*Myodes glareolus*) populations serving as a case study. Using Approximate Bayesian Computation (ABC) for inverse parameterization (*46*), we derive allocation strategies and then rigorously evaluate the fitted model following POM by replicating an empirical litter manipulation experiment and comparing it to additional independent patterns (Figure 1A). As a demonstration of the framework's capacity for mechanistic understanding of the emergence of individual trait variation and for predicting the impacts of environmental change on population dynamics and persistence, we apply the model to future environmental scenarios, using normalized difference vegetation index (NDVI)(*47*) as a proxy of food availability. We reveal emerging patterns in energetic, morphological, and life history trait variation among populations and forecast changes in population abundance based on projected future climate-driven alterations in food availability. By leveraging diverse empirical knowledge to infer the values of parameters that shape some of the most elusive yet vital energetic processes driving animal fitness (*48, 49*), the PIE approach can shed light on the driving forces behind the evolution of life history strategies and offers potential for improved predictive power.
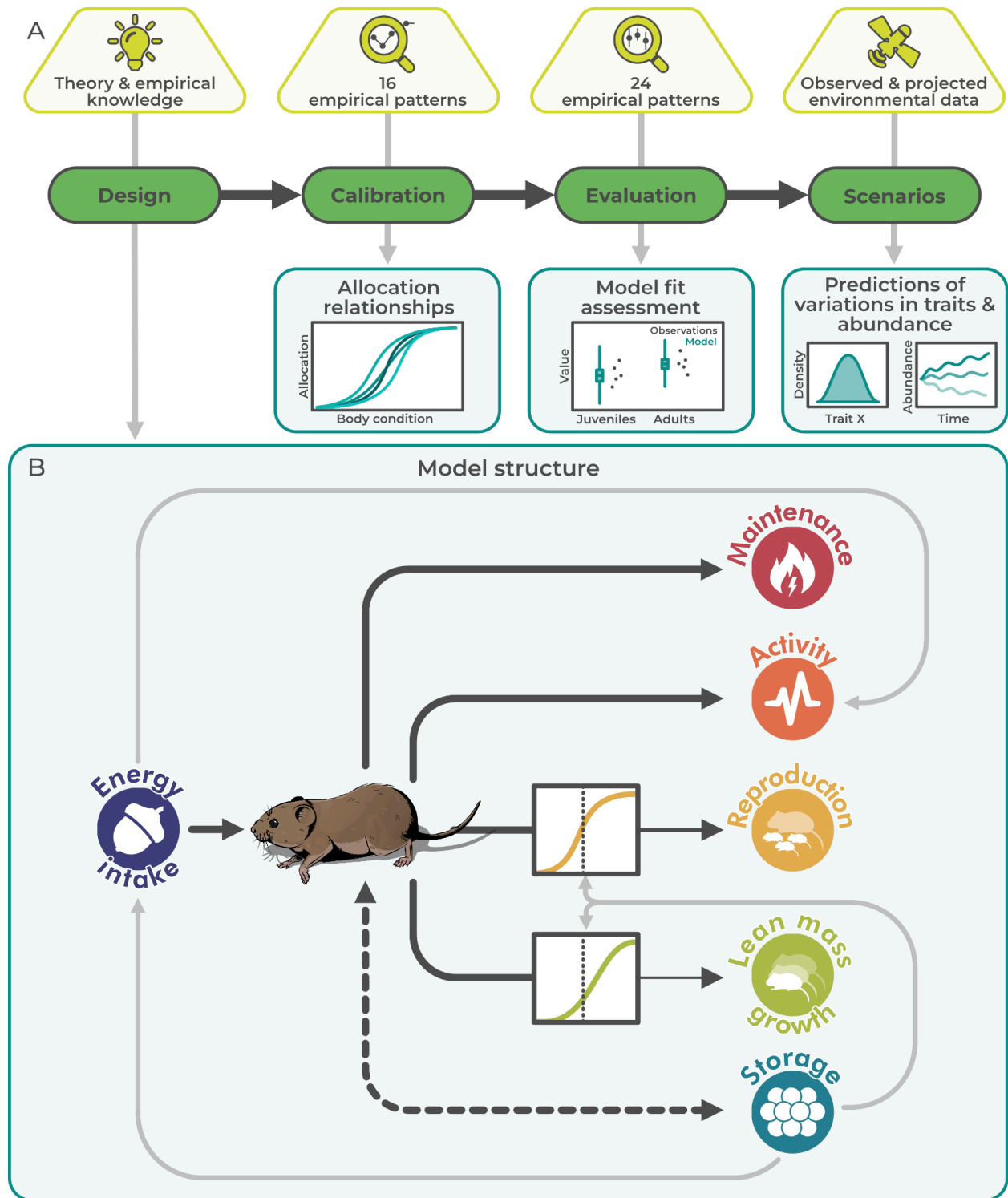
Figure 1. Schematic representing key inputs and outputs of the model development, testing, and application process A). Key processes underlying the energy budget framework B), with light grey lines indicating interactions between

processes. The sigmoidal functions associated with growth and reproduction represent the allocation of energy to these processes. Within the PIE approach, energy allocation is guided by body-condition-dependent relationships, which result from model calibration to empirical patterns.

Results

Model calibration of population densities, energy allocation relationships, and mortality

To ensure that the model represented realistic population densities of bank voles, we initially calibrated the resource parameters of the model to empirical density estimates (*50–53*). Details regarding model development and testing can be found in the supplemental TRACE document (*54, 55*). This calibration yielded maximum resource levels of 140 g per 10 m x 10 m grid cell and resource accumulation rates of 0.011 g per 30-minute timestep, resulting in average population densities of 14.4 ± 13.7 females per hectare, with peaks in mid-summer (empirical mean of 17.5 ± 11.8 females per hectare; TRACE Section 6.1). These initial parameter values were used to ensure realistic population densities in the model for subsequent calibration and evaluation steps, while the maximum resource level was adjusted in the replication of the empirical litter manipulation experiment and in scenarios to simulate seasonal and projected resource dynamics.

To parameterize the underlying relationships linking animal body condition to energy allocation for growth, pregnancy, and lactation, as well as survival, we employed an inverse parameterization approach using ABC and POM (details in TRACE Section 6.2). This allowed us to determine the values of ten parameters by fitting them to 16 empirical patterns derived from bank vole morphometrics, reproduction, and energetics. The parameter sets from the 30 best performing combinations, determined using median absolute scaled error, were found to fit the empirical patterns quite well (Figure 2), with only a few minor discrepancies which were primarily attributed to conflicts between the patterns themselves.

When comparing prior and posterior distributions for the selected parameter sets, the parameter space was considerably reduced, effectively identifying a subset of plausible values consistent with the observed data (TRACE Figure S23). However, three parameters—the slopes of the relationships between storage level and growth, pregnancy, and reproduction—showed less reduction in their parameter space. Further analysis of parameter correlations revealed that these slope parameters were positively correlated with their corresponding midpoint parameters (e.g., the slope and midpoint shaping the growth allocation curve) (TRACE Figure S24). This correlation indicated challenges in estimating these parameters independently, as variations in slopes were less influential on model outputs than the midpoints of the relationships.

We retained the 30 selected parameter combinations (Figure 2N-P) and employed each of them independently in model simulations, with the curves varying among simulation runs to consider uncertainty in model outcomes.
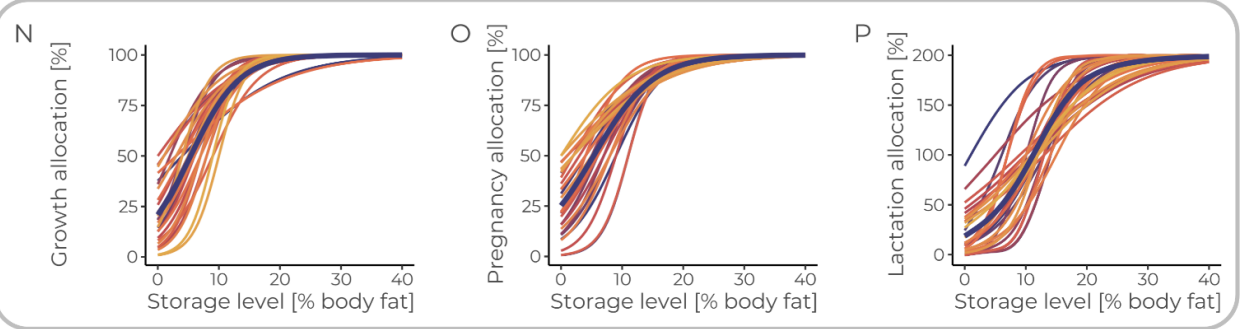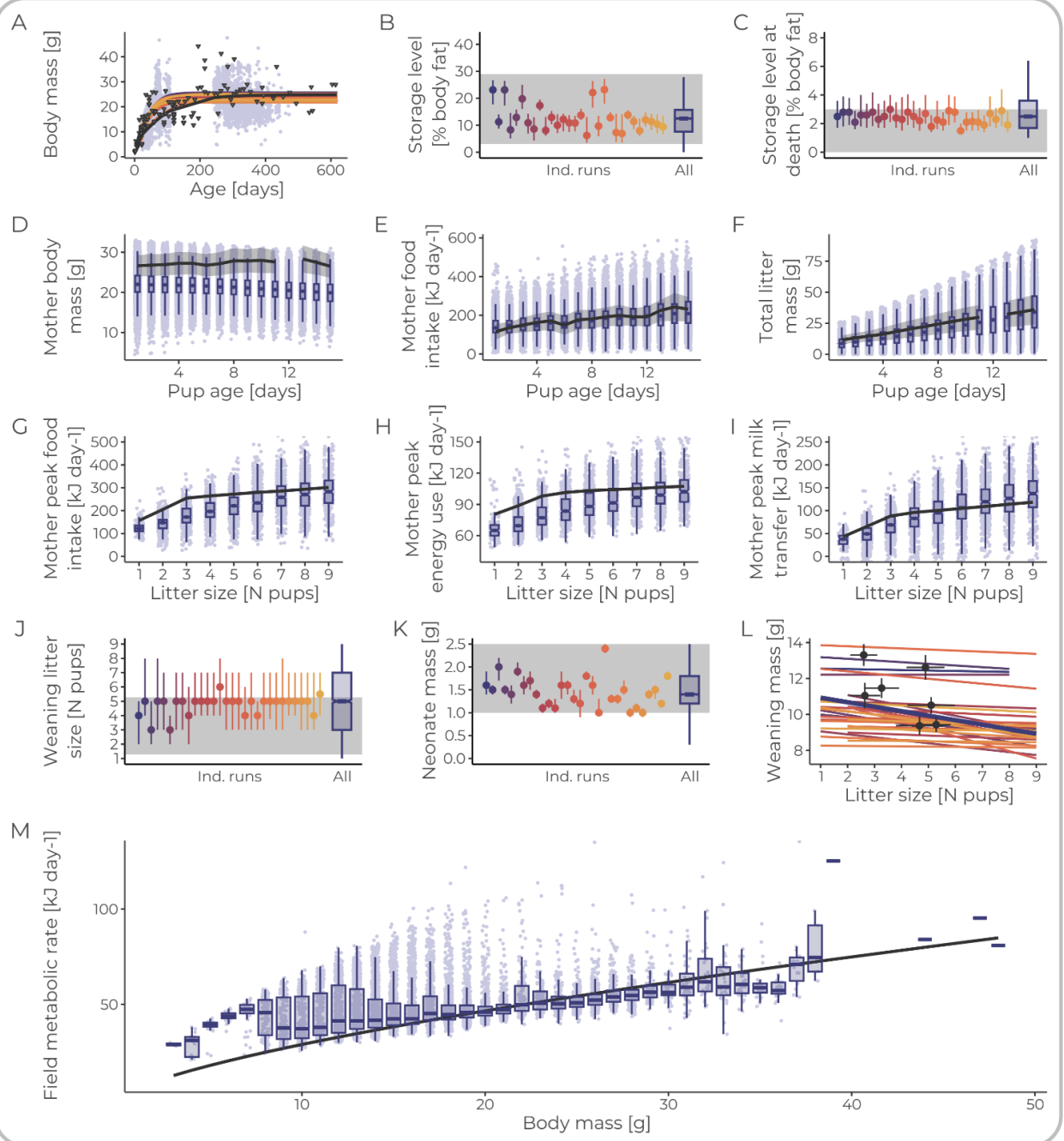
Figure 2. Comparison of model predictions for the 30 best-fitting parameter combinations against the empirical patterns used for calibration (empirical data depicted in black or grey) for A) total body mass, B) percent body fat of living animals, and C) percent body fat at death, D) mother body mass and E) food intake, F) total litter mass with pup age, G) mother peak food intake, H) energy use, and I) milk transfer with litter size, J) litter size at weaning, K) neonate mass, L) weanling mass by litter size, and M) field metabolic rate of non-lactating animals by body mass. Outputs from individual parameter sets are shown in unique colors, with combined results in purple. Colored point ranges represent the median and 95% CIs for each individual parameter set, with light purple points in A, D-I, and M representing individual simulation data points. In panels B-F, J, and K, the grey rectangle indicates the range of empirical values used to assess pattern fit, while the grey shaded region in D-F represents the mean ± SE of the empirical data. For panels A, G, H, I, and M, empirical relations are shown as solid black lines. In panel L, fit was defined qualitatively as a negative relationship, with illustrative points (mean ± SE) from two independent empirical studies (*56*, *57*). In panels A and L, colored lines represent von Bertalanffy and linear relationships fit to outputs for each parameter set. Panels N-P show the selected allocation relationships of the 30 best-fitting parameter sets, illustrating the association between body fat percentage and allocation to N) growth, O) pregnancy, and P) lactation. Approximate Bayesian computation (ABC) was used to evaluate 500,000 parameter combinations, assessing fit with median absolute scaled error for univariate or multivariate patterns and a pass/fail approach for linear relationships. See supplementary TRACE document section 6 "Model output verification" for more details and further patterns used in model development.

Model evaluation and replication of a litter manipulation experiment

To assess the model's ability to replicate real-world observations, we simulated an empirical litter manipulation experiment conducted on wild bank voles in Konnevesi, Finland in 1996-1998 (*50*). Litter manipulation experiments represent a classic

approach in life-history research, where litter sizes of females which have recently given birth are experimentally increased or decreased. Such studies have been used to assess the costs and trade-offs associated with reproduction across various species and settings, from laboratory environments to outdoor enclosures and the wild (*50*, *56*, *57*).

Model outputs were found to be in strong agreement with the 13 observed patterns related to population density and the effects of manipulated litter size on weanling number and body mass, subsequent breeding attempts, and maternal survival (Figure 3). The model captured the seasonal dynamics in population density, with the highest values observed in late summer and the lowest in early summer across all years. It also reflected differences between years, such as the relatively high early summer density and low late summer density in 1997 compared to 1996 and 1998 (Figure 3A).

Observed declines in weanling body mass with both season and manipulation group were also replicated by the model (Figure 3B), highlighting its ability to reflect complex biological processes, such as how varying environmental conditions and maternal investment strategies influence offspring growth.

Simulated litter size at weaning is driven by the female's provisioning during lactation and offspring mortality due to starvation, and outputs varied between manipulation groups and seasons (Figure 3C). The model reproduced observed seasonal patterns, with the largest litter sizes in mid-summer and lowest in late summer. However, the model predicted an overall overestimation of litter size at weaning compared to empirical observations. Additionally, while the model did predict the smallest litter sizes at weaning for reduced litters, as observed, it did not sufficiently capture the pattern that increased litter sizes at birth did not necessarily result in larger litter sizes at weaning, particularly during early and late summer. Instead, the model tended to predict a positive correlation between litter size at birth and weaning across all seasons. However, this effect was less pronounced in late summer, where litter sizes were more consistent across manipulation groups.

In contrast, the model effectively captured the decline in female survival across different seasons and treatment groups, with the lowest survival rates in late summer and among females with enlarged litters (Figure 3D). Although there were some inconsistencies, such as the absence of manipulation group effects in early summer and lower survival rates among control litters in late summer, the model still demonstrated a strong alignment with empirical data, considering the complexity of these patterns.
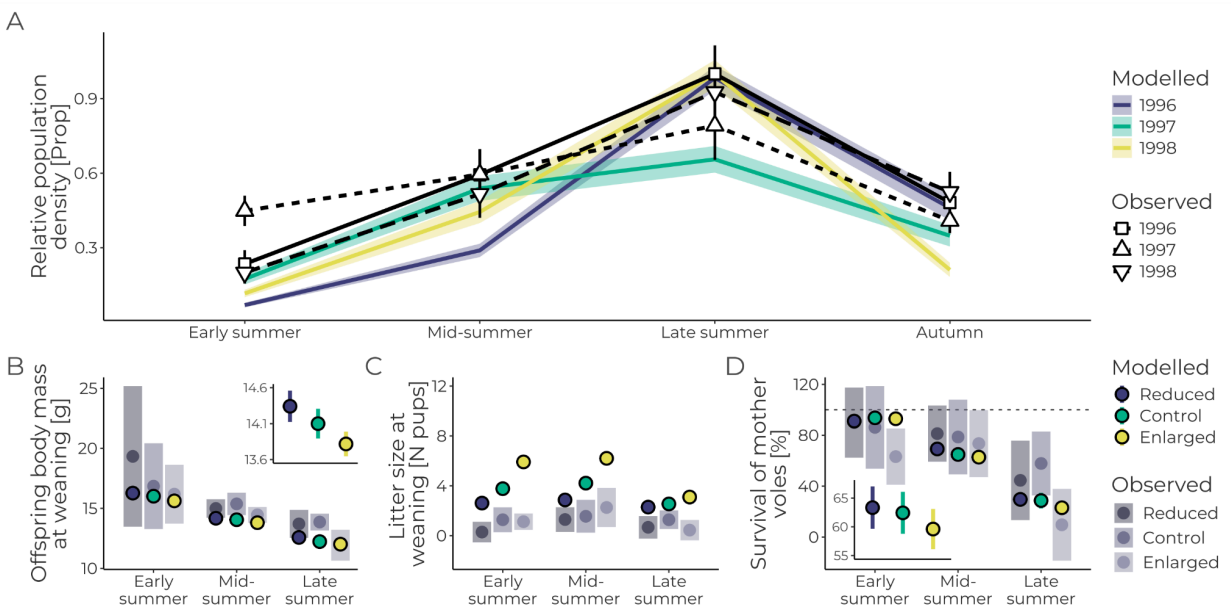
Figure 3. Comparison of model outputs with empirical data from a litter manipulation experiment in Konnevesi, Finland for 1996-1998 (*50*). A) Seasonal population density dynamics per year (proportion of maximum value) (mean ± SE), B) offspring body mass (in grams) at weaning , C) litter size (count pups) at weaning , and D) mother survival (%) to the next breeding period (means ± 95% CIs). Insets panels in B and D display the seasonal averages (means ± 95% CIs), with the dotted line in panel D representing 100% survival. Predictions were generated from 100 simulation replicates. All observed estimates were taken directly from plots presented in Koivula et al. (2003).

Further tests of the model against independent empirical patterns of state-dependent energy consumption and expenditure, survival, life history, and morphometrics, were also observed to be in strong agreement (TRACE Section 8.1). In particular, the total daily field metabolic rates for nonreproducing and lactating animals, as well as the daily food consumption of juvenile, nonreproducing, pregnant, and lactating females, closely matched empirical data from nine independent studies. These patterns, at higher levels of temporal coverage, represent the emergent total metabolism of animals which is driven by their behavior, costs, and allocation strategies and, as such, the agreement found here is particularly encouraging.

More details on model evaluation, including full description of pattern values, observation strategies, and sources, are found in Appendix Section 8.

Scenarios of impacts of temporal variation in resource dynamics on individual traits and population dynamics

With the model successfully replicating key empirical patterns during the evaluation phase, we extended its application to future scenarios. This allowed us to investigate how individual-level trait variation influences population dynamics and to project how population abundance might respond to climate-driven changes, offering a deeper understanding of the mechanisms linking individual energetics to ecological outcomes under shifting environmental conditions.

Resource availability in Konnevesi for recent years was characterized using the normalized difference vegetation index (NDVI) from 2000 to 2022, derived from the Terra MODIS mission (*58*) (Figure 4A), providing a baseline for assessing both historical trends and future projections. Projected NDVI dynamics, based on minimum temperature and precipitation data from three global circulation models (GCMs), were used to determine resource availability through 2099 (Figure 4B). Simulations were run for this 100 year period with 500 repetitions, collecting outputs across six observation days per year (two in spring, summer, and fall). Thirteen traits

were observed in the final five years of both the observed (2018–2022) and projected (2094–2098) periods. Trait values, including body mass, total metabolic rates, and costs of locomotion reproduction, and lean mass deposition, were averaged across all adult individuals (or relevant age groups) for each observation day. Traits like litter size and body mass at weaning were taken as averages for birth and weaning events occurring between observation days, while others, such as lifetime reproductive success and age at death, were updated annually. These traits were selected for their ecological relevance in understanding how resource availability impacts individual fitness and population dynamics. Measures of body mass, metabolic rate, and energy allocation reflect immediate physiological responses, while metrics like lifetime reproductive success and longevity provide insights into key life-history traits.
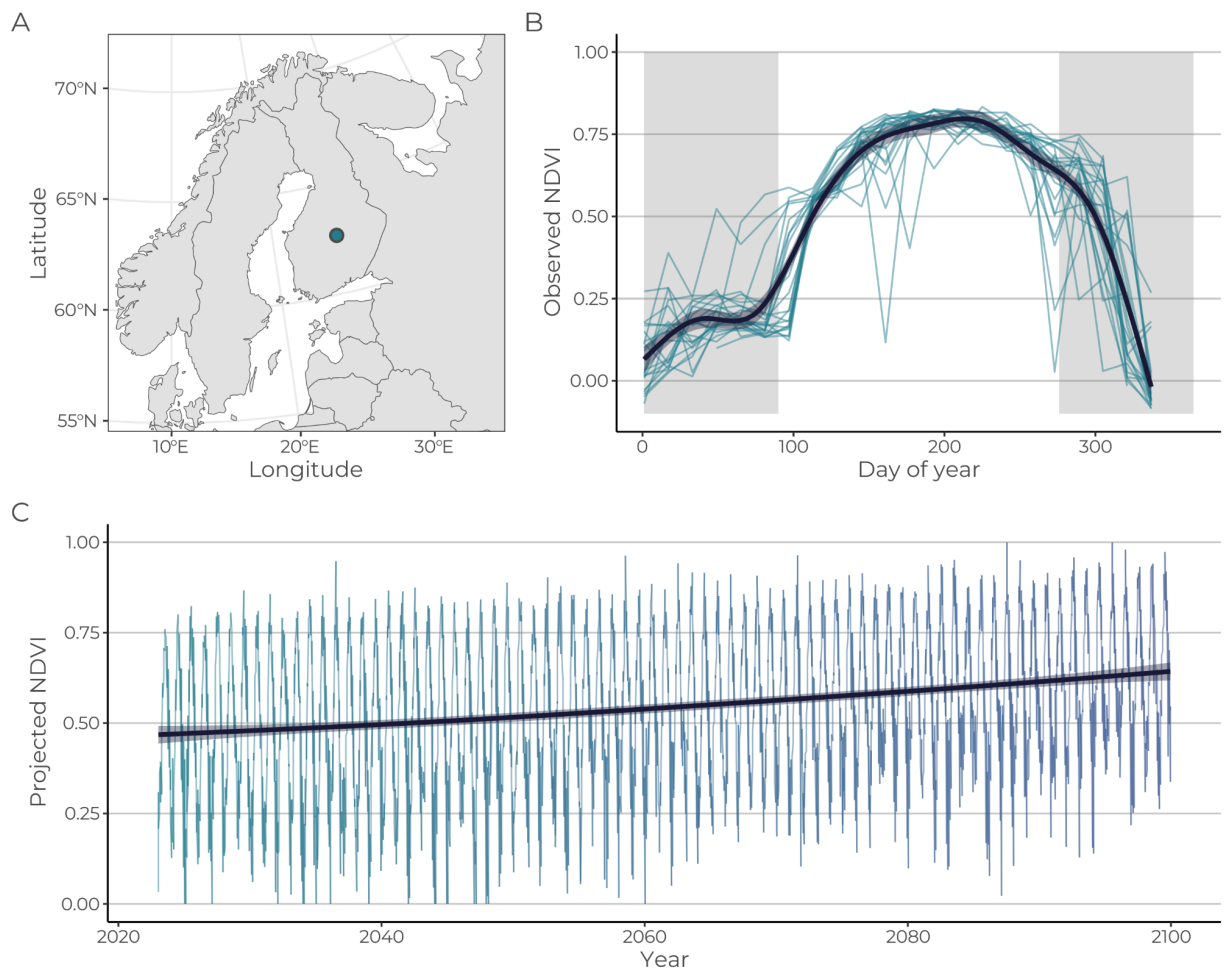
Figure 4. Characteristics of the site used for the replication of a real-world experiment in model evaluation and for scenario simulations in Konnevesi, Finland (A). For the scenarios, B) seasonal variations in observed resource dynamics, represented by NDVI, are shown with colored lines indicating individual years (2000–2022) that drove historical resource dynamics. C) Projected future resource dynamics under the SSP585 emissions scenario, generated based on projected temperature and precipitation changes. Dark lines in B and C represent GAM predictions.

To identify general trends across time periods, we used assessed correlations between all individual-level traits and population metrics for each simulation in each period (df = 498). While we did not explicitly examine how relationships between traits and population metrics change within the year or between years, the output of our model allows for such analyses to be conducted.

Under the observed vegetation dynamics from 2018 to 2022, average population density varied strongly throughout the year, with the lowest values found in late fall and early spring (Figure 5A). Population dynamics were primarily characterized by strong peaks occurring from late August to early September, though in some years, the peak occurred during early summer in late June. Under projected conditions for 2094 to 2098 (Figure 5B), density patterns remained similar, though peak densities were on average higher.

Correlations between averages and variations in 13 individual traits related to energetics, morphometrics, and reproduction, and six population-level outcomes revealed distinct patterns (Figure 5G, see 'Scenarios' in the Methods section for descriptions and units). Under observed conditions, strong negative relationships were found between maximum offspring abundance (A_{peak}) and both storage levels (SL) (r = -0.54, 95%CI: [−0.60,−0.48]; Figure 5D) and mass of offspring at weaning (m_{wean}) (r = -0.65, 95%CI: [−0.70,−0.59]). Additionally, there were strong negative correlations between the timing of peak adult abundance (T_{Apeak}) and timing of peak offspring abundance (T_{Opeak}) (both as day of year) and both locomotion costs (M_L) and

age at first birth ($age_{1st\ birth}$) (T_{Apeak}-M_L: r = -0.64, 95%CI: [−0.69,−0.59]; T_{Apeak}-$age_{1st\ birth}$: r = -0.72, 95%CI: [−0.76,−0.68]; T_{Opeak}-M_L: r = -0.50, 95%CI: [−0.57,−0.43]; T_{Opeak}-$age_{1st\ birth}$: r = -0.84, 95%CI: [−0.87,−0.82]). Positive correlations were observed between the peak number of adults (A_{peak}) and offspring (O_{peak}) and longevity (age_{death}) (A_{peak}-age_{death}: r = 0.61, 95%CI: [0.55,0.66] (Figure 5C); O_{peak}-age_{death}: r = 0.55, 95%CI: [0.48,0.60]). Additionally, a positive relationship was found between the timing of minimum adult abundance (T_{Amin}) and age at first birth ($age_{1st\ birth}$) (r = 0.56, 95%CI: [0.50,0.62]).

Under projected conditions for 2094 to 2098, many of these correlations held, with slightly higher effect sizes across all 171 output combinations (sum absolute *r*: 2018-2022: 52.9; 2094-2098: 56.0) (Figure 5H). Stronger effects were primarily found for timing-related population-level outputs (T_{Apeak}, T_{Opeak}, and T_{Amin}). The strong negative relationship between minimum adult abundance (A_{min}) and total metabolic rate (M_{tot}) held across both time periods (2094-2098: r = -0.55, 95%CI: [-0.61,-0.48]; Figure 5F), related to trends with allocation to reproduction (M_R) and lean mass deposition (M_{LM}) (A_{min}-M_R: r = -0.52, 95%CI: [-0.58,-0.45]; A_{min}-M_{LM}: r = -0.49, 95%CI: [-0.55,-0.42]). Additionally, strong positive relationships between peak adult (A_{peak}) and offspring (O_{peak}) abundance and litter size at weaning (LSW) and lifetime reproductive success (LRS) remained across both periods (2094-2098: A_{peak}-LSW: r = 0.80, 95%CI: [0.77,0.83] (Figure 5E); A_{peak}-LRS: r = 0.79, 95%CI: [0.75,0.82]; O_{peak}-LSW: r = 0.71, 95%CI: [0.67,0.75]; O_{peak}-LRS: r = 0.57, 95%CI: [0.51,0.63]). Full matrices, including analyses of both mean values and variation in outputs, are provided in Appendix Figure S31 and Figure S32. All presented correlations were significant at p < 0.001 (n = 500 per combination).

Overall, the model predicted a general increase in adult female vole density for the remainder of the century (Figure 5C). As a whole, average population density (mean ± SD) increased slightly from 2018-2022 to 2094-2098 (15.7 ± 2.0 vs. 16.8 ± 2.7 female voles per hectare, respectively; mean ± 1SD).
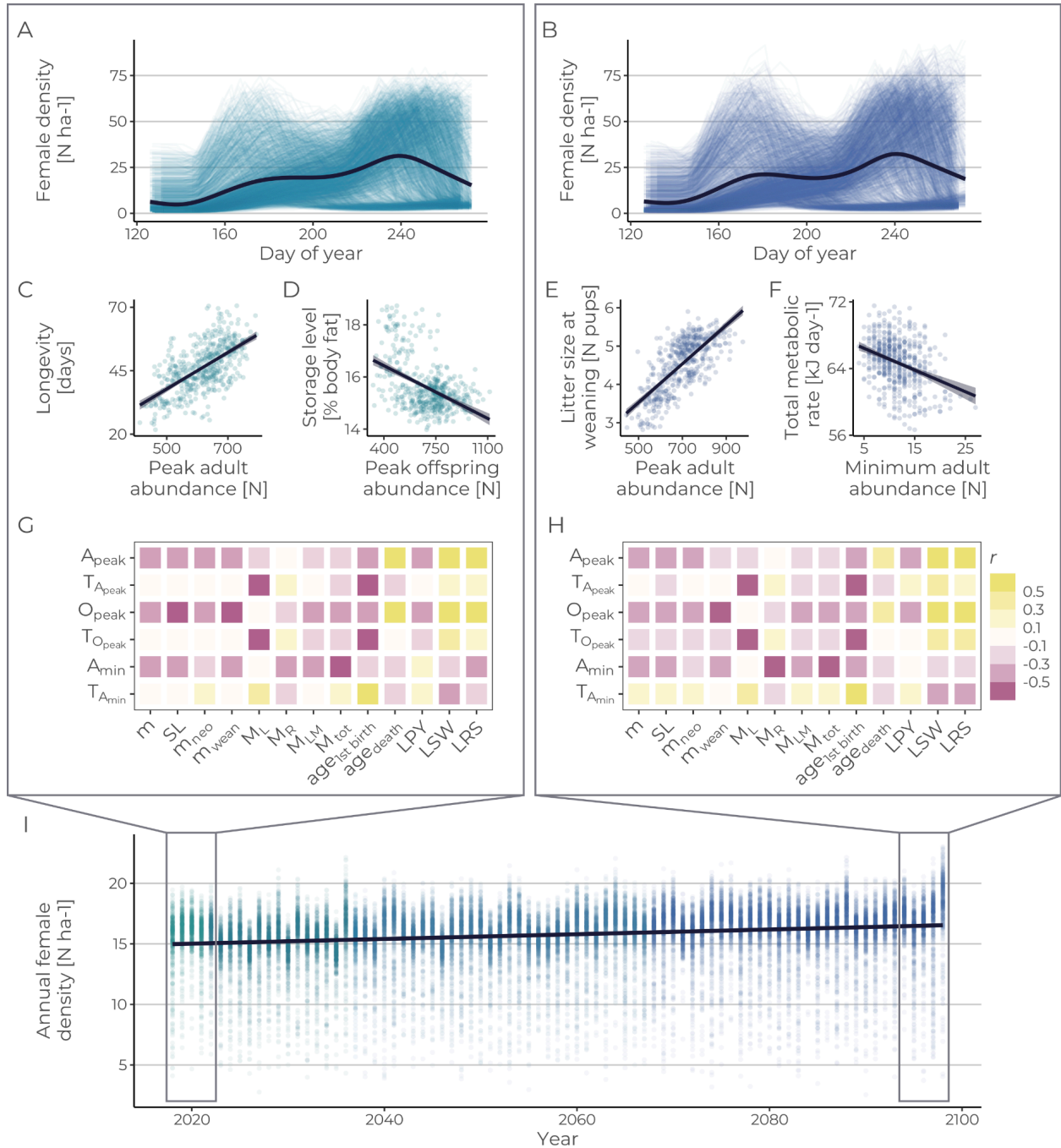
Figure 5. Predicted temporal variations in population dynamics, life history, and morphometric traits under observed and projected resource dynamics, based on the SSP585 emissions scenario. In A, C, D, and G, results are shown for 2018–2022, while B, E, F, and H depict results for 2094–2098. Changes in annual averages of adult female population density over the simulated period are illustrated in I. Panels A and

B show within-year changes in adult female population density, while G and H display correlation matrices between a subset of population-level outputs (x-axis) and individual-level traits (y-axis). Exemplary relationships are shown for the historic period between C) average longevity (in days) and peak adult abundance (count animals) and D) body condition (storage level as percent body fat) and peak offspring abundance (count animals). For the projected period, relationships are shown between E) litter size at weaning (count pups) and peak offspring abundance (count animals) and F) total metabolic rate (in kJ per day) and minimum adult population size (count animals). Densities in A, B, and I were collected at weekly intervals over each five-year period, with annual averages computed per simulation for I. Outputs in C–H were derived from averages of traits and population metrics recorded on six observation days per year (two each in spring, summer, and fall), totaling 30 days per time period per simulation. Correlations thus reflect broad time-period-level relationships, acknowledging that this resolution neglects within- and between-year variations. In A-F and I, colored points and lines represent outputs from each simulation replicate. In G and H, yellow represents negative and pink denotes positive correlations, determined via the Pearson correlation coefficient, with increasing saturation representing stronger effect size. Abbreviations used in G and H include: m = body mass (g), SL = storage level (% body fat), m_{neo} = neonate mass (g), m_{wean} = weaning mass (g), M_L = locomotion costs (J day^{-1}), M_R = reproduction costs (J day^{-1}), M_{LM} = cost of lean mass growth (J day^{-1}), M_{tot} = total metabolic rate (J day^{-1}), $age_{1st\ birth}$ = age at first birth (days), age_{death} = longevity (days), LPY = number of litters per year (N), LSW = litter size at weaning (N pups), LRS = lifetime reproductive success (N pups weaned), A_{peak} = peak adult abundance (N), TA_{peak} = timing of peak adult abundance (day of year), O_{peak} = peak offspring abundance (N), TO_{peak} = timing of peak offspring abundance (day of year), A_{min} = adult minimum abundance (N), and TA_{min} = timing of minimum adult abundance (day of year). Predictions were generated from 500 simulation runs, with thick lines representing generalized additive model (GAM) predictions in A and B and linear model predictions in C-F and I. For alternative scenarios, see Appendix Figures A2-6.

Alternative scenarios were explored to address limitations in the statistical model, which failed to fully capture drivers of some within-year NDVI patterns, such as the flattening of NDVI in summer (Figure 4A). In these scenarios, observed within-year NDVI dynamics were preserved, but their mean values were adjusted to align with the statistical model's projected average annual NDVI. These scenarios resulted in slightly weaker correlations overall (sum absolute r: 52.0) (Figure S33). However, average annual population density was higher by the end of the simulation period (18.5 ± 2.8 female voles per hectare; mean ± 1SD). Similar results were observed under the SSP245 emissions scenario (sum absolute r: 52.5), although average annual population densities remained fairly constant over the projection period (2094-2098: 15.2 ± 2.1 female voles per hectare; mean ± 1SD) (Figure S34).

Discussion

Allocation processes are among the most daunting energetic processes to measure empirically (*12*, *39*). Using a PIE approach, we successfully informed these allocation curves by applying inverse parameter estimation and leveraging measurable patterns driven by underlying allocation dynamics, such as in morphometrics, energy expenditure, and life history. This approach allowed energy allocation patterns to be dynamic and incorporate uncertainty, and the model reliably reproduced the empirical patterns it was compared against. Notably, the model's ability to accurately recreate complex empirical patterns related to animal morphometrics, reproduction, survival, and density when applied to conditions mimicking an empirical litter manipulation experiment underscores the approach's predictive power in simulating real-world biological processes. By better informing some of the most uncertain aspects of animal energetics, this approach can greatly enhance our capacity to predict how organisms will respond to environmental changes, particularly those affecting foraging efficiency and resource dynamics. Individual-based bioenergetic models are increasingly recognized as powerful tools for predicting the effects of change on animal populations (Pirotta, 2022; Rose et al., 2024). The PIE approach has the potential to elevate these models by precisely fitting energy allocation dynamics to the unique needs of individual species. This capability makes the approach highly suitable for applied cases, such as informing policy and management decisions.

Moreover, PIE allows us to address fundamental questions in ecology and evolution, including those related to the emergence and consequences of individual variation (*33*, *61*), by integrating plasticity and dynamic variation in individual energetics, morphometrics, and life history traits and directly linking these traits to the resource environment. Additionally, as these allocation strategies may themselves be subject to selection, leading to observed differences in pace of life both between and potentially within species (*62*, *63*), investigating eco-evolutionary dynamics could offer valuable insights into the role of resource dynamics in selection processes. Furthermore, since the model is grounded in first principles, it could be particularly useful for assessing the combined effects of multiple co-occurring environmental changes (*64*, *65*).

By replicating the conditions of the real-world experiment (*50*), the model effectively reproduced empirical observations and provided a mechanistic explanation for its successes and limitations. Notably, it excelled in predicting seasonal dynamics, showing lower averages for litter size, offspring mass, litter mass at weaning, and female survival in late summer, consistent with reproductive trade-offs under resource limitation and high population densities (*50*, *56*, *66*). The model also captured qualitative trends driven by allocation processes, such as smaller weaning masses for offspring from enlarged litters and reduced survival and subsequent litter masses in females with larger initial litters. However, a key discrepancy emerged: the phenomenon where enlarging litter size at birth does not increase the number of offspring successfully weaned, commonly observed in vole litter manipulation studies (*56*, *57*, *67*), was not adequately captured in model outputs. While females with enlarged litters did lose the most offspring, this effect was not strong enough to equalize litter size at weaning. These gaps may stem from unmodeled maternal behaviors, such as selective feeding or infanticide in enlarged litters, which could influence offspring outcomes. Additionally, litter sizes at weaning were generally larger than observed in the empirical data. Offspring survival in the wild is likely influenced by various non-energetic factors, such as predation, and since the empirical study observed animals at a minimum of 30 days old, dispersal processes may have already been at play (Mazurkiewicz & Rajska, 1975), reducing the observed number of successfully weaned offspring. These factors likely contributed to the

model's overestimation of empirical results. Despite this limitation, the model successfully captured complex seasonal and experimental dynamics, demonstrating that its implemented mechanisms can reproduce high-level ecological patterns.

When applied to scenarios, the model demonstrated how changes in individual traits due to environmental shifts relate to broader ecological patterns, such as adult and offspring abundances, as well as the timing of population peaks and reproductive success. While the causality of these relationships was not assessed here due to matters of design, it could be explored in future studies. The model highlighted key factors shaping the responses of individuals and populations to environmental change, as assessed via correlations between individual-level traits and population metrics. For example, body mass was linked to the peak abundance of both offspring and adults, while reproductive costs influenced the timing of peak and minimum adult abundance. Life-history traits like longevity, lifetime reproductive success, and litter size at weaning typically corresponded with higher abundances but were often negatively associated with morphometric and energetic factors, such as body mass and total metabolic costs, and age at first birth.

While an inverse relationship between body mass and peak abundance is consistent with broader mass-abundance patterns, where resource limitations constrain the number of individuals or total biomass in an environment (*68–70*). However, in cyclical rodents, like bank voles, body size tends to increase during the population increase and peak phases, a phenomenon known as the Chitty effect (*71*). These phases have also been associated with enhanced survival and suppressed reproduction, with the hypothesis that this suppression redirects energy toward body growth, resulting in the Chitty effect (*72, 73*). Evidence suggests that this increased allocation to growth may be heritable (*74*). Although increased longevity was observed with higher peak abundances, true cyclical population dynamics were not seen in the model, likely due to the absence of driving factors such as these shifts in energy allocation patterns, as well as predation, dispersal, and social factors (e.g. Radchuk et al., 2016). Nonetheless, the model's mechanistic flexibility allows for testing alternative hypotheses to explore conditions under which such cycles might emerge, while considering detailed energetic factors.

By bridging the gap between micro-level processes (such as energy expenditure and morphometrics) and macro-level phenomena (such as population density), these findings shed light on how individual-level alterations in response to environmental variability relate to broader shifts in population dynamics. Previous research suggests that physiological constraints drive life history strategies both across (*76*) and within species (*77*), with trait-demography relationships documented in species like small mammals and seabirds (*45, 78, 79*). This approach offers a mechanistic understanding of how these trait correlations arise through competition for resources and energy allocation, providing valuable insights for identifying causal pathways linking environmental change to emergent population outcomes (*80*). Moreover, findings suggest potential conservation implications, such as the association between higher locomotive costs and reduced peak population abundance. In European brown hares (*Lepus europaeus*), increased activity behavior, and consequently higher locomotive costs, have been linked to changes in resource dynamics (*81*). The model's results suggest that such impacts may relate to a decline in adult abundance.

Population density was predicted to increase under projected resource availability, with scenarios forecasting a 7.0% rise in average annual density and a 13.1% increase in peak abundance within a year by the end of the century. However, NDVI increased by 21.5% over this period, suggesting that even when implemented as a direct relationship, resource availability and ecological responses may not be 1:1, even in simplified settings such as here, where only density- and resource-dependent factors were considered.

In generating the presented scenarios, several assumptions were made that may have influenced findings. One key assumption in this study was that NDVI serves as a reliable proxy for resource availability. Although NDVI has been proposed or applied in this context, particularly for herbivores (*22, 82, 83*), it does not necessarily reflect the actual availability of resources consumed by the target species. Despite this limitation, NDVI can still be useful for capturing seasonality, offering a comparative measure of relative differences and enabling the quantification of temporal and spatial patterns in model outcomes. Depending on the modeling effort's goal and

the study system, the best-suited proxy should be determined, which may be NDVI, other vegetation indices such as the Enhanced Vegetation Index (*84*), abiotic measures like precipitation, or ideally more direct estimates of food availability, when available (*82*). Certain processes, such as masting events (e.g., Reil et al., 2015), predation (Korpela et al., 2014; Radchuk et al., 2016), interspecific competition (Eccard & Ylönen, 2002, 2003), and site-specific habitat structure (Ecke et al., 2002), are known to influence vole population dynamics and could influence predictions. However, they were not incorporated here to maintain the model's tractability and specific scope. In cases requiring absolute forecasts, these factors should be informed by empirical data when possible. Moreover, the three GCMs used to drive projections represent a limited selection of available GCMs within CMIP6 (*85*). The selected GCMs provided the high spatial and temporal resolution needed for the temperature and precipitation values used in the projections. Despite these limitations, the model outcomes effectively demonstrated how variations in resource dynamics can influence trait changes and population patterns under potential future conditions, providing valuable insights into ecological responses to environmental shifts.

In addition to the assumptions underlying the demonstrative scenarios, the proposed PIE framework also relies on several key assumptions in its formulation. Firstly, using empirical patterns to inform the allocation dynamics grounds the model dynamics in observed knowledge of the study system. However, this approach inherently assumes that these patterns can be trusted as accurate indicators of a system's functioning. Factors such as measurement or reporting error, study conditions (e.g., field versus lab settings), sample size, and variability in methodology could all affect the accuracy and transferability of empirical patterns (*36*). These challenges can be met by using multiple and diverse patterns spanning various levels of the ecological hierarchy modeled, and we adhered to this practice here (*36*, *37*). Additionally, methods like the virtual ecologist approach (*86*) can be employed to collect pattern outputs under conditions similar to the empirical observations, thereby minimizing the effect of contextual differences between the model and observations. Moreover, the current approach implicitly assumes that many of these patterns remain static over time. However, many patterns are driven by local context (e.g., habitat structure and climate, resource availability, inter- and intraspecific

interactions) and may change through adjustment (e.g., phenotypic plasticity), local adaptation, and evolutionary processes (e.g., Edelaar & Bolnick, 2019). Particularly when making predictions under changing conditions and under longer timescales, it may be crucial to consider evolution and adaptation (*88*). Ideally, an understanding of how specific patterns vary across time and space would best inform model processes. In lieu of such rare knowledge sources, considering a diverse range of patterns has been shown to suffice in driving realistic model behavior (*89*).

While our understanding of ecological systems necessitates incorporating assumptions and imperfect data sources into models, the rapid pace of environmental change compels us to leverage available tools and knowledge to address emerging threats and safeguard biodiversity (*5, 90*). Given that energy serves as a crucial link between environmental conditions and animal fitness, advancements in empirical knowledge of animal physiology, coupled with a more direct approach to informing allocation patterns, can enhance the representation of diverse physiological and life history patterns in predictive models (*18*). Although this approach offers a pathway to better inform energetic processes and represent species more accurately, it inevitably introduces added complexity. This complexity might exceed what is necessary for certain research questions, yet it is indispensable for others that demand a detailed understanding of energetic dynamics. Any realized gains in predictive power of the PIE approach have not yet been assessed in comparison to other methods that represent energy dynamics and allocation patterns (e.g. Kooijman, 2000; Mangel, 2015; Sibly et al., 2013). In reality, there has been minimal work comparing existing approaches in this manner. Animal metabolism and allocation trade-offs are inherently complex phenomena, and the roles of plasticity and drivers of energy intake and expenditure remain unresolved (*28, 92–94*). The complex model presented here offers a tool for assessing these influences, yet rigorous inter-model comparisons, grounded in statistical validation and utilizing independent, spatiotemporally explicit multivariate data, will be needed for assessing any improvements in predictive performance (*3*). Understanding under which conditions the consideration of animal energetics at various levels of detail is necessary or can improve our ability to make robust population predictions is essential for the advancement of predictive ecology.

The fundamental concept of the PIE framework, where energy allocation curves are informed by empirical patterns, is not limited to the specific model structure presented in this study. This approach could be integrated into existing energy budget modeling methodologies (*12*, *24*) to drive allocation processes based on animal nutritional status in a manner consistent with empirical knowledge. By leveraging empirical patterns, researchers can avoid *ad hoc* approaches to inform energy allocation dynamics, making the PIE framework a valuable tool for those implementing bioenergetics models. Moreover, the full model structure can be readily applied to other terrestrial homeotherms, provided relevant data are available. Although movement and foraging processes may need updating if animals are not central place foragers, the core principles of the PIE framework remain applicable. In applying the model to other systems, we suggest using patterns that generally relate to the dynamics between energy demand, energy intake, and body condition, with outcomes measured in terms of morphometrics, reproductive output, and survival. Emerging empirical methods are additionally increasingly capturing more directly applicable patterns in wild settings, further enhancing the potential of the PIE framework. For example, recent studies have linked body condition and mass gain to reproductive performance and success in polar bears (*Ursus maritimus*), badgers (*Meles meles*), and elephant seals (*Mirounga angustirostris*) (*42*, *43*, *95*). These advancements in empirical methods provide patterns that can be readily incorporated into the PIE structure, offering immense potential for improving the accuracy and realism of bioenergetic models.

Conclusion

Although the direct measurement of energy allocation processes remains challenging, the PIE framework offers a robust alternative by leveraging empirical patterns to inform these processes in predictive models. This approach not only allows for dynamic energy allocation but also incorporates uncertainty in allocation processes, enhancing model realism and reliability. By accurately reproducing a variety of observed patterns (40 in total), the model presented here demonstrates its potential for both theoretical and applied ecological research. Despite requiring assumptions and facing inherent limitations, the PIE framework's adaptability makes

it a valuable tool for predicting organism- and population-level responses to environmental changes. Integrating this approach with existing methodologies and applying it to other species, especially with emerging empirical data, promises significant advancements in bioenergetic modeling and our understanding of ecological dynamics. Additionally, applying this framework at the community level could uncover species interactions and energy flows within ecosystems, offering deeper insights into biodiversity and ecosystem responses to changing conditions. Such advancements are crucial for protecting species in the face of ongoing and accelerating environmental change.

Materials and methods

Model description

In this study, we introduce the Pattern-Informed Energetics (PIE) framework — a novel agent-based energy budget modeling approach which considers empirical patterns in a system in driving energy allocation processes. PIE offers a versatile framework for representing species energetics through data-driven energy allocation strategies as a basis for revealing the emergence of individual variation in metabolic, morphological, and life history traits and for predicting the impacts of environmental change. Our approach utilizes recent advancements in animal bioenergetics, simulating the energetics of wildlife populations within a dynamic, spatially-explicit environment. The model is composed of three primary modules, one related to movement behavior of simulated agents, another to energetic processes, and one for the life-history processes of mortality and reproduction. To ensure the realism and accuracy of the model, we parameterized and rigorously tested it using empirical data from the bank vole (*M. glareolus*). However, when sufficient empirical knowledge exists, it would be straightforward to adapt the model for other terrestrial mammal species.

In the subsequent sections, we offer a concise overview of the model. For readers seeking in-depth details, the comprehensive model description can be found in the TRACE document (*54*, *55*), available as a supplemental PDF online. This document

adheres to the Overview, Design concepts, Details (ODD) protocol (*96, 97*), assuring that our model's design, implementation, testing, and application are thoroughly documented and well-aligned with their intended purpose. The model, which was implemented in Netlogo v6.2.0 (https://ccl.northwestern.edu/netlogo/), is open-source and can be downloaded from https://github.com/CaraAGallagher/PIEmodel.

Entities and scales

The model includes two entities: landscape cells and animal agents.

Landscape cells are square grid units which can contain food resources. These cells have a variable resource level, ranging from zero to a maximum value, which was initially calibrated for base simulations and then adjusted for different model scenarios (details provided below). Resource cells undergo replenishment during the animal foraging phase, with the rate of replenishment determined by the resource accumulation rate per timestep and the time elapsed since the last foraging event took place at that location. Similar to the maximum resource value, the resource accumulation rate was initially calibrated for baseline simulations and subsequently modified to align with climate predictions in the various scenarios.

In the model, resources are represented as generic food items not associated with any specific species but linked to vegetation dynamics. These resources' energy density and dry matter are based on empirical data for bank vole forage (Meese, 1969). The proportion of the landscape covered with resource cells was set at 0.75, and the spatial distribution of food resources (*i.e.,* fragmentation level) was controlled using a global variable. Each grid cell spans 10 m x 10 m, a size chosen to allow for realistic population densities, computational feasibility, and the inclusion of multiple landscape cells within an individual's home range. The model's landscape is depicted as consisting of 20x50 cells, encompassing a total area of 100,000 square meters, which resulted in sufficient levels of variability in local vole densities and corresponding resource levels. The model landscape has open boundaries, *i.e.,* it is toroidal and not bounded at the extents.

Animal agents are characterized by their morphometrics, energetics, age, movement speed, and individual trait values, while pregnant and or lactating animals are further characterized by state variables related to reproduction. Morphometric state variables relate primarily to lean and adipose masses and storage levels of animals and their dependent offspring, energetic state variables are used to track the cost of each metabolic process, energy intake values, and storage dynamics, while reproductive state variables characterize the costs of pregnancy and lactation and number, sex, and age of offspring. Only female animals are simulated beyond the weaning stage. Consequently, any individuals born as male are removed from the model at weaning.

The model advances in 30-minute steps, allowing for fine-scale activity patterns and energy budget dynamics to be modeled, while remaining computationally feasible. To simplify the model and focus on the active breeding period, overwintering was omitted. This species exhibits a seasonal reproductive cycle, with winter typically characterized by reduced metabolic rates and limited activity, which have minimal impact on the key processes modeled. Although overwinter breeding has been observed under resource supplementation (*98*), mechanisms linking the initiation of breeding to environmental conditions were not included (e.g., Eccard & Ylönen, 2001), and thus overwinter breeding was not considered here.. As a result, each year begins on day 90 and ends on day 273 to encompass the breeding period. Metabolic calculations are in units of energy per unit time (J 30min^{-1}). Model runs continue either until all animal agents have died or until a specified final timestep, corresponding to 10 years for calibration and 100 years for scenarios. A 5-year burn-in period was sufficient to filter out initial unstable dynamics.

Process overview and scheduling

In each timestep, animals first decide whether to move based on their current satiety and energy balance. Animals that are not satiated have an increasing probability of initiating movement as their energy balance decreases. Once a decision to move is made, animals proceed to randomly select a cell within a specific distance, corresponding to empirical home range radii observed in bank voles (*67, 100–106*) where they intend to forage during that timestep. This movement behavior is

represented implicitly through consumption effects on the selected cell, assuming animals move continuously throughout the 30-minute timestep at an average speed. No territorial dynamics are assumed and animals can overlap in their home ranges. The speed of movement is determined by randomly selecting values from a gamma distribution shaped using empirical data for mean and maximum speeds observed in bank voles (*107*), which influences their transport cost.

All animals then undergo energy budget calculations for each time step, sequentially assessing energy expenditure in the following order: basal maintenance, transport costs, reproduction (if applicable), and lean mass growth.

Maintenance costs are modeled based on body mass following an allometric relationship fit to empirical data for vole respiration.

Animals that remain stationary in a timestep are assumed to be at rest with no associated movement costs. In contrast, foraging animals incur activity costs, which are determined by two distinct processes: the first for calculating postural costs, which are the energetic costs associated with maintaining an upright or particular body position while standing or moving (*108*), and the second for incremental costs of transport (*109*), which are the additional costs required to propel the body forward. Both costs vary allometrically with body mass, but incremental costs are additionally driven by movement speed. Total locomotion costs are determined as the sum of these two processes.

The reproduction procedure involves assessing the independent costs of pregnancy and lactation. Pregnant animals calculate their pregnancy costs based on the energy required to fuel maximum fetal and placental growth (*12, 110, 111*). Nursing animals determine their lactation costs based on the maintenance and maximum potential growth costs of their offspring, taking into consideration inefficiencies associated with milk production and assimilation as well as the reduced thermogenetic capacity of neonates (*112–114*). However, for simplicity, nursing behavior is not explicitly modeled; instead, lactation demands are incurred and allocated on a per-timestep basis, regardless of whether the mother went foraging in a given timestep. Allocation to pregnancy and lactation is modified using the calibrated allocation curves based

on the mother's body mass, with realized neonate and offspring growth depending on allocation in that timestep.

Lean mass deposition occurs throughout an animal's life in the model. It encompasses the growth of structural mass as animals mature and the utilization of protein as a metabolic fuel to cover metabolic costs through stored tissues. To calculate these costs, animals determine the maximum potential lean mass growth based on their current body mass, using growth curves fit to extremely large individuals (*115*). Subsequently, actual lean mass growth is realized following a process similar to that used for reproduction, where allocation to lean mass dynamics is determined by considering the calibrated allocation curve and the animal's current storage level.

Once energy expenditure calculations are complete, animals then attempt to consume food resources from the selected grid cell for foraging. The amount of energy consumed in a timestep varies based on a variety of factors including animal energy expenditure, their stomach capacity, hunger, energy balance, body fat percentage, and the amount of food available on the resource cell. The amount an animal attempts to eat is based on their current energy expenditure and negative energy balance, with stomach dynamics limiting the total capacity for ingestion. Maximum stomach fill and clearance rates are also dynamic and respond to changes in energy demand, particularly during the high demand period of lactation, reflecting documented changes in alimentary capacity in various rodent species (*116–118*). Hunger is represented following duel point intervention theory (*28*), which posits that hunger intensifies at low body fat percentages, driven by the need to ensure survival during periods of illness-induced fasting, while it diminishes at high body fat percentages due to elevated risks of predation. Resource cells encountered by an animal update their resource levels before the first animal consumes resources from that cell in the timestep. If an animal has not fed on that cell for several timesteps, then the cells will replenish their values according to the per timestep resource accumulation rate, up to the maximum resource level. As animals consume food, the cell's resource level decreases proportionally to the amount consumed.

Animals keep track of their energy balance, and any unmet food requirements are recorded so that they can attempt to make up for deficits in following timesteps.

Once both energetic costs and ingested energy are calculated, the overall energy balance is adjusted accordingly.

Based on resulting energy balance, animals update their adipose and lean mass tissue stores. When energy balance is positive, they employ anabolic processes to deposit body tissues. Conversely, when energy balance is negative, catabolic processes break down tissues to mobilize energy for metabolic requirements. The proportion of each tissue deposited or mobilized is determined by the animal's current body condition, guided by Forbes' theory (*32*) and supported by empirical data from three studies on rats (*Rattus norvegicus*) (*119–121*).

Once per day, the model updates the ages of animals and mortality events due to maximum age and starvation can occur. The probability of adults and dependent offspring to starve, as well as the occurrence of abortions, is determined by the animal storage level and the calibrated survival functions. On the last day of the year, overwinter mortality occurs, and resource levels are reset to their maximum values. Conception, birth, and weaning processes are triggered when reaching the relevant day of year, gestation day, or days since mating, respectively.

Calibration

While many parameters used in the model were well-understood and could be based on literature values for bank voles, there were twelve parameters whose values were uncertain and required calibration. This calibration process followed a pattern-oriented modeling approach (*36, 37*) and was carried out in two stages. The first stage aimed at determining the values of two resource cell parameters using empirical population densities. The second stage utilized 16 empirical patterns to determine relationships between storage level and energy allocation to growth, pregnancy, and lactation, as well as between storage level and adult, offspring, and embryo mortality.

To ensure the model simulated realistic animal abundances for the simulated spatial extent, we calibrated parameters determining the maximum level and accumulation rate of resources in each cell. Population densities were then compared with empirical data from bank vole studies, using four articles (*50–53*) with 13 recorded values of mean female population densities (assuming a 1:1 sex ratio) resulting in the median: 14.2 voles per hectare (range 4.4 to 41.4). The parameters were varied over ranges between 40 - 200 g for the maximum resources and 0.005 to 0.025 g per 30 minute timestep for the resource accumulation rate and 25 simulations were run for a 10 year period for each combination of these values. Following the initial 5 year burn-in period, densities were collected weekly from 100 randomly selected suitable sites (total area of one hectare) and the median densities were compared to the empirical data. The combination which minimized the mean absolute deviation from the empirical median value was selected.

Despite extensive knowledge of energy expenditure, the link between body condition and energy allocation to growth, reproduction, and survival remains poorly understood, hindering efforts to model environmental impacts on population dynamics (*39*). Yet direct parameterization remains challenging, if not impossible, for most species due to limited understanding of these relationships. In this study, we used 16 empirical patterns of vole morphometrics, reproduction, and energetics (details in Table S26) to calibrate ten sigmoidal parameters linking animal body condition to growth, pregnancy, lactation, and survival. A Bayesian approximation method, known as rejection approximate Bayesian computation (ABC) (*46*), was employed and the model was executed with 500,000 parameter combinations, with relevant outputs collected for each of the 16 empirical patterns after the burn-in period. The median absolute scaled error was then calculated for each pattern to assess fit for uni- or multivariate patterns, while linear relationship patterns were evaluated using a pass or fail approach. For univariate patterns, error was determined by comparing each point to the empirical observation, with error calculated across all collected values. For multivariate patterns, error was assessed along the relevant variable (e.g., per day in the lactation period for lactation-related patterns Figure 2D-F). The 30 best fitting parameter combinations were retained to select for

well-fitting runs while also considering uncertainty in the posterior distributions (*22*, *46*).

Sensitivity analysis

A comprehensive global sensitivity analysis was conducted on all model parameters to identify their influence on seven model outputs, related to animal morphometrics, reproduction, and population densities, and to quantify the variance contribution attributed to each of the most impactful parameters. Initially, we used the improved Morris' elementary effects method (*122*, *123*) to screen all 60 model parameters, determine sensitivity indexes from the mean of estimated elementary effects, and create a parameter ranking based on their level of influence from the least to the most influential. Next, a variance-based sensitivity analysis following the method of Sobol (2001) was used to estimate first-order and total-effect indices for the ten most influential parameters identified in the Morris screening. The "*sensitivity*" package in R was used in both phases for experiment design and sensitivity index calculations (*125*).

Evaluation

Following the successful calibration of the model, we used the 30 best-fitting parameter sets identified using ABC and compared model outputs to 11 additional patterns to assess its ability to capture various aspects of bank vole energetics, life history, and morphometrics. Details of the 11 patterns, their sources, and values are available in Supplementary Table S33. In this evaluation phase, 150 simulations were conducted. Outputs were collected at the end of the fifth simulation year, with further tracking of surviving animals in the sixth year for survival rates. Model outputs were visually compared to empirical patterns to assess their agreement.

To further assess the model's ability to replicate empirical observations, we simulated a litter manipulation experiment on bank voles under wild conditions (*50*). In this study, the effects of manipulated litter size on weanling number and body mass, subsequent breeding attempts, and maternal survival were assessed over three years (1996–1998) in free-ranging bank voles in central Finland. To replicate the empirical

resource environment, we used the Normalized Difference Vegetation Index (NDVI) as a proxy for resource availability, with data interpolated to a daily resolution from the extended global NDVI3g product (GIMMS) for the years 1990–1999, covering the study period and allowing for six years of burn-in.

The assumption of a linear relationship between NDVI and food availability was adopted as a pragmatic solution in lieu of empirical data defining these dynamics. To operationalize this, the 0–1 NDVI value was converted to a 0–2 modifier of the calibrated parameter controlling the maximum resource level in a resource cell. Under this approach, a value of 1 represented no change to the calibrated value, 0 reduced the maximum food resources to zero, and 2 doubled this value. While this linear assumption could be tested in future studies, it resulted in realistic seasonal dynamics during the evaluation step, supporting its utility for modeling resource availability in this context. We allowed any increases in NDVI to increase the food levels of resource patches once per day equal to the amount increase in maximum, but decreases were only enforced through the use of the maximum resource level as a hard cap.

We closely followed the empirical approach, selecting pregnant females with similar masses (15.7 to 32.4 g) and assigning them to manipulation groups ('Enlarged' + 2 pups, 'Reduced' - 2 pups, or 'Control'). We observed the total abundance of animals and 12 additional patterns related to birth, weaning, and subsequent birth for each selected animal seasonally (13 patterns in total; TRACE Table S34). To account for stochasticity, 100 simulation replicates were conducted, and outputs were analyzed in alignment with the empirical results.

Scenario details

To assess the model's potential for identifying variations in traits and projecting population trajectories over time, we used the model for future projections for the same Konnevesi region from the litter manipulation experiment used for model evaluation, with resource dynamics again driven by NDVI. We collected values for 13 individual traits—related to energetics, morphometrics, and reproduction—as well as population abundance, either seasonally or annually, depending on relevance. We

then predicted future responses at this site under projected changes in temperature and precipitation, again collecting the same trait and population dynamics outputs.

We acknowledge that our predictions are not absolute forecasts due to the exclusion of factors like predation and site-specific details, such as the energy density of locally available food items. Instead, these projections demonstrate the model's capability to reveal the role of resource dynamics in the emergence of population-level variations in traits and dynamics, mediated through individual energetics as driven by the PIE framework.

As a proxy for seasonal resource dynamics, the normalized difference vegetation index (NDVI) was obtained for a 4 km² area centered on the study site's coordinates (62°37'N, 26°17'E) from the Terra MODIS (Moderate Resolution Imaging Spectroradiometer) mission (*58*) (Figure 3B). The product used, MOD13Q1, accessed via the MODISTools package in R (*126*), provided NDVI at a 250 m spatial resolution and 16-day temporal resolution from January 1, 2000, to December 30, 2022. NDVI values were averaged across all spatial cells at the site to capture mean seasonal vegetation dynamics. These NDVI-driven resource dynamics were incorporated into the model in the same way as in the litter manipulation experiment described in the evaluation step.

Projections up to the year 2099 were developed by applying a linear mixed-effects model to the observed NDVI data, using floored values of temperature and precipitation per month as inputs and mean NDVI as the response variable. Our fixed effects included linear and quadratic terms for precipitation (pr and pr^2) and minimum temperature (tasmin and tasmin^2), with a random intercept for the year to account for annual variability. Monthly averages of precipitation and minimum temperature were obtained from three models (CNRM-CM6-1-HR, EC-Earth3-CC, AWI-CM-1-1-MR (*127–129*)) under two emissions scenarios (SSP245, SSP585) and historical levels, as part of the Coupled Model Intercomparison Project Phase 6 (CMIP6) accessed from the Copernicus Climate Data Store (https://cds.climate.copernicus.eu/).

Model fits to the MODIS NDVI data were evaluated and compared against more complex statistical structures, incorporating variables such as incoming solar radiation and lagged temperature and precipitation values (1–12 month intervals), based on their demonstrated benefits in predicting rodent population dynamics (*83*). Because more complex structures did not significantly improve model fit (assessed via AIC and R^2), we proceeded with the simpler structure presented above (Figure 4C & Appendix Figure S30).

To better consider observed within year dynamics in NDVI (Figure 4B), we explored alternative scenarios. In these, we retained the average annual NDVI projected by the statistical model but used a randomly selected year from the observed NDVI data to simulate within-annual changes, adjusted to center around the projected average for that year. This approach preserved the magnitude of within-year variations while aligning with the mean projected value. All projections were interpolated to daily NDVI changes and averaged across the three GCMs, yielding one projection per emissions scenario.

These 3 scenarios (two emissions scenarios, SSP245 and SSP585, and two projection approaches tested for SSP585), each covering 100 simulation years, were run with 500 repetitions to account for stochasticity from ABC parameter combinations and other sources. Six observation days were selected within a year (two in spring (day of year 121 and 152), two in summer (181, 213), and two in fall (244, 272)) to observe values for all relevant agents. Thirteen traits were observed in 2018-2022 (the last five years of the observed data) and in 2094-2098 (the last five years of the projections), while population abundance was collected on each observation day from 2018 to 2099.

Of the trait values, six were collected as the average value for all adult individuals (aside from growth, where all individuals >45 days old were observed) on each observation day: body mass (in g), body condition (% body fat), field metabolic rates (i.e., total metabolic rate excluding production costs), locomotion costs, and energy allocation to reproduction and growth (all in J day^{-1}). Three traits—litter size at weaning, and body mass of neonates and pups at weaning (both in g)—were calculated as averages for events occurring between observation days. Since animals

could give birth or wean between dates, values were assigned to the next scheduled observation day, ensuring all events between observations were included in the calculations. The final four traits—lifetime reproductive success (N pups weaned), age at first birth (days), number of litters per year (N), and age at death (days)—were updated at birth or death, when relevant, and taken as annual averages for all animals that either died during the year or survived until its end.

The outcomes were compared using the statistical software R (*130*) by computing the mean and coefficient of variation for each output across the observed (2018-2022) and projected (2094-2098) periods for each simulation. Within-year dynamics in population abundance were visualized using generalized additive models, while across-year trends and visualized relationships between individual-level traits and population outcomes illustrated with linear models. Pearson correlation coefficients, *r*, were used to assess correlations between pairs of outputs per simulation replicate (171 unique combinations of the mean and CV of 13 traits and six population outcomes), focusing on the magnitude of *r* to determine strength and directionality of relationships.

References

1.	G. Ceballos, P. R. Ehrlich, R. Dirzo, Biological annihilation via the ongoing sixth mass extinction signaled by vertebrate population losses and declines. *Proc Natl Acad Sci USA* **114**, E6089–E6096 (2017).

2.	G. Ceballos, P. R. Ehrlich, Mutilation of the tree of life via mass extinction of animal genera. *Proceedings of the National Academy of Sciences* **120**, e2306987120 (2023).

3.	J. A. Pilowsky, R. K. Colwell, C. Rahbek, D. A. Fordham, Process-explicit models reveal the structure and dynamics of biodiversity patterns. *Science Advances* **8**, eabj2271 (2022).

4.	M. C. Urban, J. M. J. Travis, D. Zurell, P. L. Thompson, N. W. Synes, A. Scarpa, P. R. Peres-Neto, A.-K. Malchow, P. M. A. James, D. Gravel, L. De Meester, C. Brown, G. Bocedi, C. H. Albert, A. Gonzalez, A. P. Hendry, Coding for Life: Designing a Platform for Projecting and Protecting Global Biodiversity. *BioScience* **72**, 91–104 (2022).

5.   M. C. Urban, G. Bocedi, A. P. Hendry, J.-B. Mihoub, G. Peer, A. Singer, J. R. Bridle, L. G. Crozier, L. De Meester, W. Godsoe, A. Gonzalez, J. J. Hellmann, R. D. Holt, A. Huth, K. Johst, C. B. Krug, P. W. Leadley, S. C. F. Palmer, J. H. Pantel, A. Schmitz, P. A. Zollner, J. M. J. Travis, Improving the forecast for biodiversity under climate change. *Science* **353**, aad8466–aad8466 (2016).

6.   C. Barros, Y. Luo, A. M. Chubaty, I. M. S. Eddy, T. Micheletti, C. Boisvenue, D. W. Andison, S. G. Cumming, E. J. B. McIntire, Empowering ecological modellers with a PERFICT workflow: Seamlessly linking data, parameterisation, prediction, validation and visualisation. *Methods Ecol Evol* **14**, 173–188 (2023).

7.   M. C. Dietze, A. Fox, L. M. Beck-Johnson, J. L. Betancourt, M. B. Hooten, C. S. Jarnevich, T. H. Keitt, M. A. Kenney, C. M. Laney, L. G. Larsen, H. W. Loescher, C. K. Lunch, B. C. Pijanowski, J. T. Randerson, E. K. Read, A. T. Tredennick, R. Vargas, K. C. Weathers, E. P. White, Iterative near-term ecological forecasting: Needs, opportunities, and challenges. *Proc. Natl. Acad. Sci. U.S.A.* **115**, 1424–1432 (2018).

8.   N. E. Selin, A. Giang, W. C. Clark, Progress in modeling dynamic systems for sustainable development. *Proc. Natl. Acad. Sci. U.S.A.* **120**, e2216656120 (2023).

9.   S. E. Gilman, M. C. Urban, J. Tewksbury, G. W. Gilchrist, R. D. Holt, A framework for community interactions under climate change. *Trends in Ecology & Evolution* **25**, 325–331 (2010).

10.   V. L. Boult, L. C. Evans, Mechanisms matter: predicting the ecological impacts of global change. *Glob Change Biol*, gcb.15527 (2021).

11.   A. S. A. Johnston, R. J. Boyd, J. W. Watson, A. Paul, L. C. Evans, E. L. Gardner, V. L. Boult, Predicting population responses to environmental change from individual-level mechanisms: towards a standardized mechanistic approach. *Proc. R. Soc. B.* **286**, 20191916 (2019).

12.   R. M. Sibly, V. Grimm, B. T. Martin, A. S. A. Johnston, K. Kułakowska, C. J. Topping, P. Calow, J. Nabe-Nielsen, P. Thorbek, D. L. DeAngelis, Representing the acquisition and use of energy by individuals in agent-based models of animal populations. *Methods Ecol Evol* **4**, 151–161 (2013).

13.   L. Szangolies, C. A. Gallagher, F. Jeltsch, Individual energetics scale up to community coexistence: Movement, metabolism and biodiversity dynamics in fragmented landscapes. *Journal of Animal Ecology* **93**, 1065–1077 (2024).

14.   J. R. Burger, C. Hou, C. A. S. Hall, J. H. Brown, Universal rules of life: metabolic rates, biological times and the equal fitness paradigm. *Ecology Letters* **24**, 1262–1281 (2021).

15.   S. J. Brandl, J. S. Lefcheck, A. E. Bates, D. B. Rasher, T. Norin, Can metabolic traits explain animal community assembly and functioning? *Biological Reviews* **98**, 1–18 (2023).

16. D. Tilman, *Resource Competition and Community Structure* (Princeton University Press, 1982)vol. 296.

17. R. E. Ricklefs, M. Wikelski, The physiology/life-history nexus. *Trends in Ecology & Evolution* **17**, 462–468 (2002).

18. C. R. White, L. A. Alton, C. L. Bywater, E. J. Lombardi, D. J. Marshall, Metabolic scaling is the product of life-history optimization. *Science* **377**, 834–839 (2022).

19. M. Clairbaux, P. Mathewson, W. Porter, J. Fort, H. Strøm, B. Moe, P. Fauchald, S. Descamps, H. H. Helgason, V. S. Bråthen, North Atlantic winter cyclones starve seabirds. *Current biology: CB* **31**, 3964–3971 (2021).

20. G. G. Winberg, Rate of metabolism and food requirements of fishes. *Fish. Res. Bd. Canada Trans. Ser.* **433**, 1–251 (1956).

21. R. Boyd, S. Roy, R. Sibly, R. Thorpe, K. Hyder, A general approach to incorporating spatial and temporal variation in individual-based models of fish populations with application to Atlantic mackerel. *Ecological Modelling* **382**, 9–17 (2018).

22. V. L. Boult, V. Fishlock, T. Quaife, E. Hawkins, C. Moss, P. C. Lee, R. M. Sibly, Human-driven habitat conversion is a more immediate threat to Amboseli elephants than climate change. *Conservat Sci and Prac* **1** (2019).

23. J.-P. Desforges, F. M. van Beest, G. M. Marques, S. H. Pedersen, L. T. Beumer, M. Chimienti, N. M. Schmidt, Quantifying energetic and fitness consequences of seasonal heterothermy in an Arctic ungulate. *Ecology and Evolution* **11**, 338–351 (2021).

24. S. A. L. M. Kooijman, *Dynamic Energy and Mass Budgets in Biological Systems* (Cambridge University Press, 2000).

25. J. Kozłowski, Optimal allocation of resources to growth and reproduction: implications for age and size at maturity. *Trends in ecology & evolution* **7**, 15–19 (1992).

26. J. M. McNamara, A. I. Houston, State-dependent life histories. *Nature* **380**, 215–221 (1996).

27. S. R. Chipps, D. H. Wahl, Bioenergetics Modeling in the 21st Century: Reviewing New Insights and Revisiting Old Constraints. *Transactions of the American Fisheries Society* **137**, 298–313 (2008).

28. J. R. Speakman, If Body Fatness is Under Physiological Regulation, Then How Come We Have an Obesity Epidemic? *Physiology* **29**, 88–98 (2014).

29. J. R. Speakman, K. D. Hall, Models of body weight and fatness regulation. *Philosophical Transactions of the Royal Society B: Biological Sciences* **378**,

20220231 (2023).

30. N. K. Lal, P. Le, S. Aggarwal, A. Zhang, K. Wang, T. Qi, Z. Pang, D. Yang, V. Nudell, G. W. Yeo, A. S. Banks, L. Ye, Xiphoid nucleus of the midline thalamus controls cold-induced food seeking. *Nature* **621**, 138–145 (2023).

31. M. Caloin, Modeling of lipid and protein depletion during total starvation. *American Journal of Physiology-Endocrinology and Metabolism* **287**, E790–E798 (2004).

32. G. B. Forbes, Lean Body Mass-Body Fat Interrelationships in Humans. *Nutrition Reviews* **45**, 225–231 (2009).

33. M. Dammhahn, N. J. Dingemanse, P. T. Niemelä, D. Réale, Pace-of-life syndromes: a framework for the adaptive integration of behaviour, physiology and life history. *Behav Ecol Sociobiol* **72**, 62 (2018).

34. D. Réale, D. Garant, M. M. Humphries, P. Bergeron, V. Careau, P.-O. Montiglio, Personality and the emergence of the pace-of-life syndrome concept at the population level. *Philosophical Transactions of the Royal Society B: Biological Sciences* **365**, 4051–4063 (2010).

35. M. Chimienti, J.-P. Desforges, L. T. Beumer, J. Nabe-Nielsen, F. M. van Beest, N. M. Schmidt, Energetics as common currency for integrating high resolution activity patterns into dynamic energy budget-individual based models. *Ecological Modelling* **434**, 109250 (2020).

36. C. A. Gallagher, M. Chudzinska, A. Larsen-Gray, C. J. Pollock, S. N. Sells, P. J. C. White, U. Berger, From theory to practice in pattern-oriented modelling: identifying and using empirical patterns in predictive models. *Biological Reviews* **96**, 1868–1888 (2021).

37. V. Grimm, S. F. Railsback, Pattern-oriented modelling: a 'multi-scope' for predictive systems ecology. *Phil. Trans. R. Soc. B* **367**, 298–310 (2012).

38. F. Hartig, J. M. Calabrese, B. Reineking, T. Wiegand, A. Huth, Statistical inference for stochastic simulation models - theory and application: Inference for stochastic simulation models. *Ecology Letters* **14**, 816–827 (2011).

39. E. A. McHuron, S. Adamczak, J. P. Y. Arnould, E. Ashe, C. Booth, W. D. Bowen, F. Christiansen, M. Chudzinska, D. P. Costa, A. Fahlman, N. A. Farmer, S. M. E. Fortune, C. A. Gallagher, K. A. Keen, P. T. Madsen, C. R. McMahon, J. Nabe-Nielsen, D. P. Noren, S. R. Noren, E. Pirotta, D. A. S. Rosen, C. N. Speakman, S. Villegas-Amtmann, R. Williams, Key questions in marine mammal bioenergetics. *Conservation Physiology* **10**, coac055 (2022).

40. H. Pontzer, A. McGrosky, Balancing growth, reproduction, maintenance, and activity in evolved energy economies. *Current Biology* **32**, R709–R719 (2022).

41. S. F. Railsback, B. C. Harvey, *Modeling Populations of Adaptive Individuals* (Princeton University Press, 2020; https://www.degruyter.com/document/doi/10.1515/9780691195377/html).

42. R. S. Beltran, K. M. Hernandez, R. Condit, P. W. Robinson, D. E. Crocker, C. Goetsch, A. M. Kilpatrick, D. P. Costa, Physiological tipping points in the relationship between foraging success and lifetime fitness of a long-lived mammal. *Ecology Letters* **26**, 706–716 (2023).

43. J. G. Bright Ross, C. Newman, C. D. Buesching, E. Connolly, S. Nakagawa, D. W. Macdonald, A fat chance of survival: Body condition provides life-history dependent buffering of environmental change in a wild mammal population. *Climate Change Ecology* **2**, 100022 (2021).

44. F. Christiansen, G. A. Víkingsson, M. H. Rasmussen, D. Lusseau, Female body condition affects foetal growth in a capital breeding mysticete. *Funct Ecol* **28**, 579–588 (2014).

45. K. J. Van Benthem, H. Froy, T. Coulson, L. L. Getz, M. K. Oli, A. Ozgul, Trait–demography relationships underlying small mammal population fluctuations. *Journal of Animal Ecology* **86**, 348–358 (2017).

46. E. van der Vaart, A. S. A. Johnston, R. M. Sibly, Predicting how many animals will be where: How to build, calibrate and evaluate individual-based models. *Ecological Modelling* **326**, 113–123 (2016).

47. C. J. Tucker, P. J. Sellers, Satellite remote sensing of primary production. *International Journal of Remote Sensing* **7**, 1395–1416 (1986).

48. E. A. McHuron, S. Adamczak, D. P. Costa, C. Booth, Estimating reproductive costs in marine mammal bioenergetic models: a review of current knowledge and data availability. *Conservation Physiology* **11**, coac080 (2023).

49. E. Pirotta, V. Hin, M. Mangel, L. New, D. P. Costa, A. M. de Roos, J. Harwood, Propensity for Risk in Reproductive Strategy Affects Susceptibility to Anthropogenic Disturbance. *The American Naturalist*, doi: 10.1086/710150 (2020).

50. M. Koivula, E. Koskela, T. Mappes, T. A. Oksanen, Cost of reproduction in the wild: manipulation of reproductive effort in the bank vole. *Ecology* **84**, 398–405 (2003).

51. F. P. Massey, M. J. Smith, X. Lambin, S. E. Hartley, Are silica defences in grasses driving vole population cycles? *Biol. Lett.* **4**, 419–422 (2008).

52. M. Mazurkiewicz, Factors influencing the distribution of the bank vole in forest habitats. *Acta Theriol.* **39**, 113–126 (1994).

53. D. Reil, U. M. Rosenfeld, C. Imholt, S. Schmidt, R. G. Ulrich, J. A. Eccard, J. Jacob,

Puumala hantavirus infections in bank vole populations: host and virus dynamics in Central Europe. *BMC Ecol* **17**, 9 (2017).

54. V. Grimm, J. Augusiak, A. Focks, B. M. Frank, F. Gabsi, A. S. A. Johnston, C. Liu, B. T. Martin, M. Meli, V. Radchuk, P. Thorbek, S. F. Railsback, Towards better modelling and decision support: Documenting model development, testing, and analysis using TRACE. *Ecological Modelling* **280**, 129–139 (2014).

55. A. Schmolke, P. Thorbek, D. L. DeAngelis, V. Grimm, Ecological models supporting environmental decision making: a strategy for the future. *Trends in Ecology & Evolution* **25**, 479–486 (2010).

56. E. Koskela, Offspring growth, survival and reproductive success in the bank vole: a litter size manipulation experiment. *Oecologia* **115**, 379–384 (1998).

57. T. A. Oksanen, P. Jonsson, E. Koskela, T. Mappes, Optimal allocation of reproductive effort: manipulation of offspring number and size in the bank vole. *Proc. R. Soc. Lond. B* **268**, 661–666 (2001).

58. K. Didan, MOD13Q1 MODIS/Terra Vegetation Indices 16-Day L3 Global 250m SIN Grid V061, (2021); https://doi.org/10.5067/MODIS/MOD13Q1.061.

59. E. Pirotta, A review of bioenergetic modelling for marine mammal populations. *Conservation Physiology* **10**, coac036 (2022).

60. K. Rose, K. Holsman, J. Nye, E. Markowitz, T. Banha, N. Bednaršek, J. Bueno-Pardo, D. Deslauriers, E. Fulton, K. Huebert, M. Huret, S. Ito, S. Koenigstein, L. Li, H. Moustahfid, B. Muhling, P. Neubauer, J. Paula, E. Siddon, M. Skogen, P. Spencer, P. Van Denderen, G. Van Der Meeren, M. Peck, Advancing bioenergetics-based modeling to improve climate change projections of marine ecosystems. *Mar. Ecol. Prog. Ser.* **732**, 193–221 (2024).

61. D. I. Bolnick, P. Amarasekare, M. S. Araújo, R. Bürger, J. M. Levine, M. Novak, V. H. W. Rudolf, S. J. Schreiber, M. C. Urban, D. A. Vasseur, Why Intraspecific Trait Variation Matters in Community Ecology. *Trends in Ecology & Evolution* **26**, 183–192 (2011).

62. S. C. Stearns, Trade-Offs in Life-History Evolution. *Functional Ecology* **3**, 259–268 (1989).

63. S. C. Stearns, Life history evolution: successes, limitations, and prospects. *Naturwissenschaften* **87**, 476–486 (2000).

64. J. A. Orr, R. D. Vinebrooke, M. C. Jackson, K. J. Kroeker, R. L. Kordas, C. Mantyka-Pringle, P. J. Van den Brink, F. De Laender, R. Stoks, M. Holmstrup, C. D. Matthaei, W. A. Monk, M. R. Penk, S. Leuzinger, R. B. Schäfer, J. J. Piggott, Towards a unified study of multiple stressors: divisions and common goals across research disciplines. *Proceedings of the Royal Society B: Biological Sciences* **287**, 20200421 (2020).

65. E. Pirotta, L. Thomas, D. P. Costa, A. J. Hall, C. M. Harris, J. Harwood, S. D. Kraus, P. J. O. Miller, M. J. Moore, T. Photopoulou, R. M. Rolland, L. Schwacke, S. E. Simmons, B. L. Southall, P. L. Tyack, Understanding the combined effects of multiple stressors: A new perspective on a longstanding challenge. *Science of The Total Environment* **821**, 153322 (2022).

66. E. Koskela, T. Mappes, H. YloNen, Experimental manipulation of breeding density and litter size: effects on reproductive success in the bank vole. *Journal of Animal Ecology* **68**, 513–521 (1999).

67. T. Mappes, E. Koskela, H. Ylönen, Reproductive costs and litter size in the bank vole. *Proceedings of the Royal Society of London. Series B: Biological Sciences* **261**, 19–24 (1995).

68. J. Damuth, Population density and body size in mammals. *Nature* **290**, 699–700 (1981).

69. J. Damuth, Interspecific allometry of population density in mammals and other animals: the independence of body mass and population energy-use. *Biological Journal of the Linnean Society* **31**, 193–246 (1987).

70. V. B. Scheffer, Body Size with Relation to Population Density in Mammals. *Journal of Mammalogy* **36**, 493–515 (1955).

71. H. Chitty, D. Chitty, "Body weight in relation to population phase in Microtus agrestis" in *Symp. Theriologicum, Brno* (1962)vol. 1960, pp. 77–86.

72. E. Johannesen, H. P. Andreassen, Density-dependent variation in body mass of voles. *Acta Theriol* **53**, 169–173 (2008).

73. M. K. Oli, The Chitty Effect: A Consequence of Dynamic Energy Allocation in a Fluctuating Environment. *Theoretical Population Biology* **56**, 293–300 (1999).

74. J. Sundell, H. Ylönen, M. Haapakoski, Do phase-dependent life history traits in cyclic voles persist in a common environment? *Oecologia* **190**, 399–410 (2019).

75. V. Radchuk, R. A. Ims, H. P. Andreassen, From individuals to population cycles: the role of extrinsic and intrinsic factors in rodent populations. *Ecology* **97**, 720–732 (2016).

76. K. Healy, T. H. G. Ezard, O. R. Jones, R. Salguero-Gómez, Y. M. Buckley, Animal life history is shaped by the pace of life and the distribution of age-specific mortality and reproduction. *Nat Ecol Evol* **3**, 1217–1224 (2019).

77. T. Burton, S. S. Killen, J. D. Armstrong, N. B. Metcalfe, What causes intraspecific variation in resting metabolic rate and what are its ecological consequences? *Proceedings of the Royal Society B: Biological Sciences* **278**, 3465–3473 (2011).

78. S. Jenouvrier, C. Péron, H. Weimerskirch, Extreme climate events and individual

heterogeneity shape life-history traits and population dynamics. *Ecological Monographs* **85**, 605–624 (2015).

79. S. Jenouvrier, M. Desprez, R. Fay, C. Barbraud, H. Weimerskirch, K. Delord, H. Caswell, Climate change and functional traits affect population dynamics of a long-lived seabird. *Journal of Animal Ecology* **87**, 906–920 (2018).

80. G. Manzo, *Agent-Based Models and Causal Inference* (John Wiley & Sons, 2022).

81. W. Ullmann, C. Fischer, K. Pirhofer-Walzl, S. Kramer-Schadt, N. Blaum, Spatiotemporal variability in resources affects herbivore home range formation in structurally contrasting and unpredictable agricultural landscapes. *Landscape Ecol* **33**, 1505–1517 (2018).

82. C. Howard, T. H. E. Mason, S. R. Baillie, J. Border, C. M. Hewson, A. I. Houston, J. W. Pearce-Higgins, S. Bauer, S. G. Willis, P. A. Stephens, Explaining and predicting animal migration under global change. *Diversity and Distributions* **30**, e13797 (2024).

83. K. A. N. K. Karunarathna, K. Wells, N. J. Clark, Modelling nonlinear responses of a desert rodent species to environmental change with hierarchical dynamic generalized additive models. *Ecological Modelling* **490**, 110648 (2024).

84. A. Huete, K. Didan, T. Miura, E. P. Rodriguez, X. Gao, L. G. Ferreira, Overview of the radiometric and biophysical performance of the MODIS vegetation indices. *Remote Sensing of Environment* **83**, 195–213 (2002).

85. V. Eyring, S. Bony, G. A. Meehl, C. A. Senior, B. Stevens, R. J. Stouffer, K. E. Taylor, Overview of the Coupled Model Intercomparison Project Phase 6 (CMIP6) experimental design and organization. *Geosci. Model Dev.* **9**, 1937–1958 (2016).

86. D. Zurell, U. Berger, J. S. Cabral, F. Jeltsch, C. N. Meynard, T. Münkemüller, N. Nehrbass, J. Pagel, B. Reineking, B. Schröder, V. Grimm, The virtual ecologist approach: simulating data and observers. *Oikos* **119**, 622–635 (2010).

87. P. Edelaar, D. I. Bolnick, Appreciating the Multiple Processes Increasing Individual or Population Fitness. *Trends in Ecology & Evolution* **34**, 435–446 (2019).

88. M. T. Wortel, D. Agashe, S. F. Bailey, C. Bank, K. Bisschop, T. Blankers, J. Cairns, E. S. Colizzi, D. Cusseddu, M. M. Desai, B. van Dijk, M. Egas, J. Ellers, A. T. Groot, D. G. Heckel, M. L. Johnson, K. Kraaijeveld, J. Krug, L. Laan, M. Lässig, P. A. Lind, J. Meijer, L. M. Noble, S. Okasha, P. B. Rainey, D. E. Rozen, S. Shitut, S. J. Tans, O. Tenaillon, H. Teotónio, J. A. G. M. de Visser, M. E. Visser, R. M. A. Vroomans, G. D. A. Werner, B. Wertheim, P. S. Pennings, Towards evolutionary predictions: Current promises and challenges. *Evolutionary Applications* **16**, 3–21 (2023).

89. V. Grimm, Pattern-Oriented Modeling of Agent-Based Complex Systems:

Lessons from Ecology. *Science* **310**, 987–991 (2005).

90. N. Mouquet, Y. Lagadeuc, V. Devictor, L. Doyen, A. Duputié, D. Eveillard, D. Faure, E. Garnier, O. Gimenez, P. Huneman, F. Jabot, P. Jarne, D. Joly, R. Julliard, S. Kéfi, G. J. Kergoat, S. Lavorel, L. Le Gall, L. Meslin, S. Morand, X. Morin, H. Morlon, G. Pinay, R. Pradel, F. M. Schurr, W. Thuiller, M. Loreau, Predictive ecology in a changing world. *Journal of Applied Ecology* **52**, 1293–1310 (2015).

91. M. Mangel, Stochastic Dynamic Programming Illuminates the Link Between Environment, Physiology, and Evolution. *Bull Math Biol* **77**, 857–877 (2015).

92. L. G. Halsey, Keeping Slim When Food Is Abundant: What Energy Mechanisms Could Be at Play? *Trends in Ecology & Evolution* **33**, 745–753 (2018).

93. L. G. Halsey, The Mystery of Energy Compensation. *Physiological and Biochemical Zoology*, 716467 (2021).

94. K. L. Laskowski, M. Moiron, P. T. Niemelä, Integrating Behavior in Life-History Theory: Allocation versus Acquisition? *Trends in Ecology & Evolution* **36**, 132–138 (2021).

95. L. Archer, S. Atkinson, A. Pagano, S. Penk, P. Molnár, Lactation performance in polar bears is associated with fasting time and energetic state. *Mar. Ecol. Prog. Ser.* **720**, 175–189 (2023).

96. V. Grimm, U. Berger, F. Bastiansen, S. Eliassen, V. Ginot, J. Giske, J. Goss-Custard, T. Grand, S. K. Heinz, G. Huse, A. Huth, J. U. Jepsen, C. Jørgensen, W. M. Mooij, B. Müller, G. Pe'er, C. Piou, S. F. Railsback, A. M. Robbins, M. M. Robbins, E. Rossmanith, N. Rüger, E. Strand, S. Souissi, R. A. Stillman, R. Vabø, U. Visser, D. L. DeAngelis, A standard protocol for describing individual-based and agent-based models. *Ecological Modelling* **198**, 115–126 (2006).

97. V. Grimm, S. F. Railsback, C. E. Vincenot, U. Berger, C. Gallagher, D. L. DeAngelis, B. Edmonds, J. Ge, J. Giske, J. Groeneveld, A. S. A. Johnston, A. Milles, J. Nabe-Nielsen, J. G. Polhill, V. Radchuk, M.-S. Rohwäder, R. A. Stillman, J. C. Thiele, D. Ayllón, The ODD Protocol for Describing Agent-Based and Other Simulation Models: A Second Update to Improve Clarity, Replication, and Structural Realism. *JASSS* **23**, 7 (2020).

98. R. Andrzejewski, Supplementary food and the winter dynamics of bank vole populations. *Acta Theriol.* **20**, 23–40 (1975).

99. J. A. Eccard, H. Ylönen, Initiation of breeding after winter in bank voles: effects of food and population density. *Can. J. Zool.* **79**, 1743–1753 (2001).

100. G. Bujalska, L. Grüm, Social organization of the bank vole (*Clethrionomys glareolus*, Schreber 1780) and its demographic consequences: a model. *Oecologia* **80**, 70–81 (1989).

101. D. J. Carslake, "Spatial dynamics of cowpox virus infection in wild rodent populations," thesis, The University of Liverpool (United Kingdom) (2003).

102. J. A. Eccard, H. Ylönen, Direct interference or indirect exploitation? An experimental study of fitness costs of interspecific competition in voles. *Oikos* **99**, 580–590 (2002).

103. J. A. Eccard, H. Ylönen, Costs of coexistence along a gradient of competitor densities: an experiment with arvicoline rodents. *J Anim Ecology* **76**, 65–71 (2007).

104. M. Mazurkiewicz, Spatial organization of the population. *Acta Theriol.* **28**, 117–127 (1983).

105. A. Radda, Populationsstudien an Rötelmäusen (Clethrionomys glareolus Schreber, 1780) durch Markierungsfang in Niederösterreich (Studies on Population of the Bank Vole (Clethrionomys glareolus Schreber, 1780) by Mark and Release Trapping in Lower Austria). *Oecologia* **1**, 219–235 (1968).

106. A. Schirmer, A. Herde, J. A. Eccard, M. Dammhahn, Individuals in space: personality-dependent space use, movement and microhabitat use facilitate individual spatial niche specialization. *Oecologia* **189**, 647–660 (2019).

107. U. Maiti, E. T. Sadowska, K. M. Chrzascik, P. Koteja, Experimental evolution of personality traits: open-field exploration in bank voles from a multidirectional selection experiment. *Current Zoology* **65**, 10 (2019).

108. L. G. Halsey, The relationship between energy expenditure and speed during pedestrian locomotion in birds: A morphological basis for the elevated y-intercept? *Comparative Biochemistry and Physiology Part A: Molecular & Integrative Physiology* **165**, 295–298 (2013).

109. H. Pontzer, A unified theory for the energy cost of legged locomotion. *Biol. Lett.* **12**, 20150935 (2016).

110. J. Mu, J. C. Slevin, D. Qu, S. McCormick, S. L. Adamson, In vivo quantification of embryonic and placental growth during gestation in mice using micro-ultrasound. *Reprod Biol Endocrinol* **6**, 34 (2008).

111. R. E. Ricklefs, Embryo growth rates in birds and mammals. *Functional Ecology* **24**, 588–596 (2010).

112. V. L. Boult, T. Quaife, V. Fishlock, C. J. Moss, P. C. Lee, R. M. Sibly, Individual-based modelling of elephant population dynamics using remote sensing to estimate food availability. *Ecological Modelling* **387**, 187–195 (2018).

113. M. Kam, I. S. Khokhlova, A. A. Degen, Partitioning of metabolizable energy intake in sucking altricial and precocial rodent pups. *Journal of Zoology* **269**, 502–505 (2006).

114. P. Koteja, J. Weiner, Mice, Voles and Hamsters: Metabolic Rates and Adaptive Strategies in Muroid Rodents. *Oikos* **66**, 505 (1993).

115. L. Balčiauskienė, Cranial growth of captive bred bank voles (*Clethrionomys glareolus*). *Acta Zoologica Lituanica* **17**, 33–40 (2007).

116. T. L. Derting, B. A. Bogue, Responses of the gut to moderate energy demands in a small herbivore (*Microtus pennsylvanicus*). *Journal of Mammalogy* **74**, 59–68 (1993).

117. K. A. Hammond, M. Konarzewski, R. M. Torres, J. Diamond, Metabolic Ceilings under a Combination of Peak Energy Demands. *Physiological Zoology* **67**, 1479–1506 (1994).

118. Z.-G. Song, D.-H. Wang, Basal metabolic rate and organ size in Brandt's voles (*Lasiopodomys brandtii*): Effects of photoperiod, temperature and diet quality. *Physiology & Behavior* **89**, 704–710 (2006).

119. R. Belkhou, Y. Cherel, A. Heitz, J.-P. Robin, Y. Le Maho, Energy contribution of proteins and lipids during prolonged fasting in the rat. *Nutrition Research* **11**, 365–374 (1991).

120. Y. Cherel, J.-P. Robin, A. Heitz, C. Calgari, Y. le Maho, Relationships between lipid availability and protein utilization during prolonged fasting. *J Comp Physiol B* **162**, 305–313 (1992).

121. M. A. Dunn, S. K. Houtz, E. W. Hartsook, Effects of fasting on muscle protein turnover, the composition of weight loss, and energy balance of obese and nonobese Zucker rats. *The Journal of nutrition* **112**, 1862–1875 (1982).

122. M. D. Morris, Factorial Sampling Plans for Preliminary Computational Experiments. **33**, 15 (1991).

123. F. Campolongo, J. Cariboni, A. Saltelli, An effective screening design for sensitivity analysis of large models. *Environmental Modelling & Software* **22**, 1509–1518 (2007).

124. I. M. Sobol, Global sensitivity indices for nonlinear mathematical models and their Monte Carlo estimates. *Mathematics and Computers in Simulation* **55**, 271–280 (2001).

125. G. Pujol, B. Iooss, A. Janon, sensitivity: Global Sensitivity Analysis of Model Outputs, version R package version 1.28.0 (2022); https://CRAN.R-project.org/package=sensitivity.

126. S. L. Tuck, H. R. P. Phillips, R. E. Hintzen, J. P. W. Scharlemann, A. Purvis, L. N. Hudson, MODISTools – downloading and processing remotely sensed data in R. *Ecology and Evolution* **4**, 4658–4668 (2014).

127. T. Semmler, S. Danilov, T. Rackow, D. Sidorenko, D. Barbi, J. Hegewald, D. Sein, Q. Wang, T. Jung, AWI-CM-1.1-MR model output prepared for CMIP6 CMIP: links to 1pctCO2, abrupt-4xCO2, historical, and piControl simulations, *Earth System Grid Federation* (2018). https://doi.org/10.22033/ESGF/CMIP6.359.

128. A. Voldoire, CNRM-CERFACS CNRM-CM6-1-HR model output prepared for CMIP6 HighResMIP, Earth System Grid Federation (2019); https://doi.org/10.22033/ESGF/CMIP6.1387.

129. R. Döscher, M. Acosta, A. Alessandri, P. Anthoni, T. Arsouze, T. Bergman, R. Bernardello, S. Boussetta, L.-P. Caron, G. Carver, M. Castrillo, F. Catalano, I. Cvijanovic, P. Davini, E. Dekker, F. J. Doblas-Reyes, D. Docquier, P. Echevarria, U. Fladrich, R. Fuentes-Franco, M. Gröger, J. V. Hardenberg, J. Hieronymus, M. P. Karami, J.-P. Keskinen, T. Koenigk, R. Makkonen, F. Massonnet, M. Ménégoz, P. A. Miller, E. Moreno-Chamarro, L. Nieradzik, T. Van Noije, P. Nolan, D. O'Donnell, P. Ollinaho, G. Van Den Oord, P. Ortega, O. T. Prims, A. Ramos, T. Reerink, C. Rousset, Y. Ruprich-Robert, P. Le Sager, T. Schmith, R. Schrödner, F. Serva, V. Sicardi, M. Sloth Madsen, B. Smith, T. Tian, E. Tourigny, P. Uotila, M. Vancoppenolle, S. Wang, D. Wårlind, U. Willén, K. Wyser, S. Yang, X. Yepes-Arbós, Q. Zhang, The EC-Earth3 Earth system model for the Coupled Model Intercomparison Project 6. *Geosci. Model Dev.* **15**, 2973–3020 (2022).

130. R Core Team, R: A language and environment for statistical computing, R Foundation for Statistical Computing (2021); https://www.R-project.org/.

131. S. Díaz, J. Settele, E. S. Brondízio, H. T. Ngo, J. Agard, A. Arneth, P. Balvanera, K. A. Brauman, S. H. M. Butchart, K. M. A. Chan, L. A. Garibaldi, K. Ichii, J. Liu, S. M. Subramanian, G. F. Midgley, P. Miloslavich, Z. Molnár, D. Obura, A. Pfaff, S. Polasky, A. Purvis, J. Razzaque, B. Reyers, R. R. Chowdhury, Y.-J. Shin, I. Visseren-Hamakers, K. J. Willis, C. N. Zayas, Pervasive human-driven decline of life on Earth points to the need for transformative change. *Science* **366**, eaax3100 (2019).

132. G. B. Meese, "Some aspects of energy balance in the Bank vole *Clethrionomys glareolus*," thesis, Durham University (1969).

133. R. M. Sibly, J. H. Brown, A. Kodric-Brown, *Metabolic Ecology: A Scaling Approach* (John Wiley & Sons, 2012).

134. C. A. Gallagher, S. J. Stern, E. Hines, The metabolic cost of swimming and reproduction in harbor porpoises (*Phocoena phocoena*) as predicted by a bioenergetic model: HARBOR PORPOISE ENERGETICS. *Mar Mam Sci* **34**, 875–900 (2018).

135. N. E. I. Nyholm, P. Meurling, Reproduction of the bank vole, Clethrionomys glareolus, in northern and southern Sweden during several seasons and in different phases of the vole population cycle. *Ecography* **2**, 12–20 (1979).

136. D. J. Carslake, "Spatial dynamics of cowpox virus infection in wild rodent

populations," thesis, University of Liverpool (2003).

137. A. Górecki, Metabolic rate and energy budget in the bank vole. *Acta Theriol.* **13**, 341–365 (1968).

138. E. T. Sadowska, C. Stawski, A. Rudolf, G. Dheyongera, K. M. Chrząścik, K. Baliga-Klimczyk, P. Koteja, Evolution of basal metabolic rate in bank voles from a multidirectional selection experiment. *Proceedings of the Royal Society B: Biological Sciences* **282**, 20150025 (2015).

139. M. Grosiak, P. Koteja, U. Bauchinger, E. T. Sadowska, Age-Related Changes in the Thermoregulatory Properties in Bank Voles From a Selection Experiment. *Frontiers in Physiology* **11**, 1408 (2020).

140. M. Kleiber, Metabolic turnover rate: A physiological meaning of the metabolic rate per unit body weight. *Journal of Theoretical Biology* **53**, 199–204 (1975).

141. M. A. Chappell, T. Garland Jr, E. L. Rezende, F. R. Gomes, Voluntary running in deer mice: speed, distance, energy costs and temperature effects. *Journal of Experimental Biology* **207**, 3839–3854 (2004).

142. E. L. Rezende, S. A. Kelly, F. R. Gomes, M. A. Chappell, T. Garland Jr., Effects of Size, Sex, and Voluntary Running Speeds on Costs of Locomotion in Lines of Laboratory Mice Selectively Bred for High Wheel-Running Activity. *Physiological and Biochemical Zoology* **79**, 83–99 (2006).

143. E. M. Dlugosz, M. A. Chappell, D. G. McGillivray, D. A. Syme, T. Garland, Locomotor trade-offs in mice selectively bred for high voluntary wheel running. *Journal of Experimental Biology* **212**, 2612–2618 (2009).

144. K. Schmidt-Nielsen, Locomotion: Energy Cost of Swimming, Flying, and Running. *Science* **177**, 222–228 (1972).

145. C. R. Taylor, N. C. Heglund, G. M. O. Maloiy, Energetics and mechanics of terrestrial locomotion. I. Metabolic energy consumption as a function of speed and body size in birds and mammals. *Journal of Experimental Biology* **97**, 1–21 (1982).

146. F. W. R. Brambell, I. W. Rowlands, III-Reproduction of the Bank Vole (Evotomys glareolus, schreber). I-The oestrous cycle of the female. *Philosophical Transactions of the Royal Society of London. Series B, Biological Sciences* **226**, 71–97 (1936).

147. R. Wiger, Demography of a Cyclic Population of the Bank Vole Clethrionomys glareolus. *Oikos* **33**, 373 (1979).

148. J. O. Nerquaye-Tetteh, J. R. Clarke, Avoidance of used endometrial sites by blastocysts of the bank vole, Clethrionomys glareolus. *Reproduction* **89**, 729–734 (1990).

149. W. Ożdżeński, E. T. Mystkowska, Stages of pregnancy of the bank vole. *Acta Theriologica* **21**, 279–286 (1976).

150. K. Sawicka-Kapusta, Changes in the gross body composition and energy value of the bank voles during their postnatal development. *Acta Theriol.* **19**, 27–54 (1974).

151. A. Fedyk, Gross body composition in postnatal development of the bank vole. I. Growth under laboratory conditions. *Acta Theriol.* **19**, 381–401 (1974).

152. J. Luz, M. A. Griggio, Distribution of Energy between Food-Restricted Dams and Offspring. *Ann Nutr Metab* **40**, 165–174 (1996).

153. H. B. Greizerstein, Placental and Fetal Composition During the Last Trimester of Gestation in the Rat. *Biology of Reproduction* **26**, 847–853 (1982).

154. M. Kam, A. A. Degen, Energetics of Lactation and Growth in the Fat Sand Rat, Psammomys obesus: New Perspectives of Resource Partitioning and the Effect of Litter Size. *Journal of Theoretical Biology* **162**, 353–369 (1993).

155. J. J. Romero, R. Cañas, R. L. Baldwin, L. J. Koong, Lactational Efficiency Complex of Rats: Provisional Model for Interpretation of Energy Balance Data1. *Journal of Dairy Science* **59**, 57–67 (1976).

156. A. Bondi, M. Rechcigl, "Nutrition and Animal Productivity" in *Handbook of Agricultural Productivity* (CRC Press, 1982).

157. S. Brody, *Bioenergetics and Growth* (New York, NY, 1968).

158. G. Livesey, The energy equivalents of ATP and the energy values of food proteins and fats. *Br J Nutr* **51**, 15–28 (1984).

159. J. D. Pullar, A. J. F. Webster, The energy cost of fat and protein deposition in the rat. *Br J Nutr* **37**, 355–363 (1977).

160. M. Gębczyński, Heat economy and the energy cost of growth in the bank vole during the first month of postnatal life. *Acta Theriol.* **20**, 379–434 (1975).

161. L. Hansson, Regional and individual variation in body growth in winter of bank voles Clethrionomys glareolus. *Acta Theriologica* **36** (1991).

162. A. M. Rudolf, M. J. Dańko, E. T. Sadowska, G. Dheyongera, P. Koteja, Age-related changes of physiological performance and survivorship of bank voles selected for high aerobic capacity. *Experimental Gerontology* **98**, 70–79 (2017).

163. C. A. Gallagher, V. Grimm, L. A. Kyhn, C. Chr. Kinze, J. Nabe-Nielsen, Movement and Seasonal Energetics Mediate Vulnerability to Disturbance in Marine Mammal Populations. *The American Naturalist* **197**, 296–311 (2021).

164. F. Kaczmarski, Bioenergetics of Pregnancy and Lactation in the Bank Vole. *Acta Theriologica* **11**, 409–417 (1966).

165. K. Piątkowska, J. Weiner, Maximum rate of energy assimilation in the bank vole. *Acta Theriol.* **32**, 45–50 (1987).

166. W. L. Peacock, J. R. Speakman, Effect of high-fat diet on body mass and energy balance in the bank vole. *Physiology & Behavior* **74**, 65–70 (2001).

167. I. M. Hastings, S. M. Moruppa, L. Bünger, W. G. Hill, Effects of selection on food intake in the adult mouse. *Journal of Animal Breeding and Genetics* **114**, 419–434 (1997).

168. P. C. Even, A. Blais, Increased Cost of Motor Activity and Heat Transfer between Non-Shivering Thermogenesis, Motor Activity, and Thermic Effect of Feeding in Mice Housed at Room Temperature – Implications in Pre-Clinical Studies. *Front. Nutr.* **3** (2016).

169. A. J. Abraham, T. O. Prys-Jones, A. De Cuyper, C. Ridenour, G. P. Hempson, T. Hocking, M. Clauss, C. E. Doughty, Improved estimation of gut passage time considerably affects trait-based dispersal models. *Functional Ecology* **35**, 860–869 (2021).

170. M. Hopkins, J. E. Blundell, "Energy Metabolism and Appetite Control: Separate Roles for Fat-Free Mass and Fat Mass in the Control of Food Intake in Humans" in *Appetite and Food Intake: Central Control*, R. B. S. Harris, Ed. (CRC Press/Taylor & Francis, Boca Raton (FL), ed. 2nd, 2017; http://www.ncbi.nlm.nih.gov/books/NBK453149/).

171. M. DiGirolamo, J. Owens, Water content of rat adipose tissue and isolated adipocytes in relation to cell size. *American Journal of Physiology-Legacy Content* **231**, 1568–1572 (1976).

172. R. F. Reinoso, B. A. Telfer, M. Rowland, Tissue water content in rats measured by desiccation. *Journal of Pharmacological and Toxicological Methods* **38**, 87–92 (1997).

173. A. Buchalczyk, Reproduction, mortality and longevity of the bank vole under laboratory conditions. *Acta Theriologica* **15**, 153–176 (1970).

174. G. Bujalska, "Social System of the Bank Vole, Clethrionomys Glareolus" in *Social Systems and Population Cycles in Voles*, R. H. Tamarin, R. S. Ostfeld, S. R. Pugh, G. Bujalska, Eds. (Birkhäuser, Basel, 1990; https://doi.org/10.1007/978-3-0348-6416-9_15)*Advances in Life Sciences*, pp. 155–167.

175. E. Koskela, T. J. Horne, T. Mappes, H. Ylönen, Does risk of small mustelid predation affect the oestrous cycle in the bank vole,Clethrionomys glareolus? *Animal Behaviour* **51**, 1159–1163 (1996).

176. G. Bujalska, L. Ryszkowski, Estimation of the reproduction of the bank vole under field conditions. *Acta Theriologica* **11**, 351–361 (1966).

177. T. J. Horne, H. Ylönen, Heritabilities of Dominance-Related Traits in Male Bank Voles (clethrionomys Glareolus). *Evolution* **52**, 894–899 (1998).

178. T. A. Oksanen, R. V. Alatalo, T. J. Horne, E. Koskela, J. Mappes, T. Mappes, Maternal effort and male quality in the bank vole, Clethrionomys glareolus. *Proceedings of the Royal Society of London. Series B: Biological Sciences*, doi: 10.1098/rspb.1999.0806 (1999).

179. E. R. Kallio, L. Voutilainen, O. Vapalahti, A. Vaheri, H. Henttonen, E. Koskela, T. Mappes, Endemic Hantavirus Infection Impairs the Winter Survival of Its Rodent Host. *Ecology* **88**, 1911–1916 (2007).

180. Z. Boratyński, E. Koskela, T. Mappes, T. A. Oksanen, Sex-specific selection on energy metabolism – selection coefficients for winter survival. *Journal of Evolutionary Biology* **23**, 1969–1978 (2010).

181. M. Haapakoski, J. Sundell, H. Ylönen, Predation risk and food: opposite effects on overwintering survival and onset of breeding in a boreal rodent. *Journal of Animal Ecology* **81**, 1183–1192 (2012).

182. J. Nabe-Nielsen, F. M. van Beest, V. Grimm, R. M. Sibly, J. Teilmann, P. M. Thompson, Predicting the impacts of anthropogenic disturbances on marine populations. *CONSERVATION LETTERS* **11**, e12563 (2018).

183. J.-P. Desforges, G. M. Marques, L. T. Beumer, M. Chimienti, J. Blake, J. E. Rowell, J. Adamczewski, N. M. Schmidt, F. M. van Beest, Quantification of the full lifecycle bioenergetics of a large mammal in the high Arctic. *Ecological Modelling* **401**, 27–39 (2019).

184. J. H. Brown, J. F. Gillooly, A. P. Allen, V. M. Savage, G. B. West, Toward a metabolic theory of ecology. *Ecology* **85**, 1771–1789 (2004).

185. J. Pinheiro, D. Bates, S. DebRoy, R Core Team, {nlme}: Linear and Nonlinear Mixed Effects Models, (2021); https://CRAN.R-project.org/package=nlme.

186. D. S. Glazier, Beyond the '3/4-power law': variation in the intra-and interspecific scaling of metabolic rate in animals. *Biological Reviews* **80**, 611–662 (2005).

187. L. J. Koong, C. L. Ferrell, Effects of short term nutritional manipulation on organ size and fasting heat production. *Eur J Clin Nutr* **44 Suppl 1**, 73–77 (1990).

188. A. G. Dulloo, L. Girardier, 24 hour energy expenditure several months after weight loss in the underfed rat: evidence for a chronic increase in whole-body metabolic efficiency. *Int J Obes Relat Metab Disord* **17**, 115–123 (1993).

189. P. C. Even, S. Nicolaïdis, Adaptive changes in energy expenditure during mild

and severe feed restriction in the rat. *British Journal of Nutrition* **70**, 421–431 (1993).

190. M. A. Chappell, P. A. Szafrańska, K. Zub, M. Konarzewski, The energy cost of voluntary running in the weasel Mustela nivalis. *Journal of Experimental Biology* **216**, 578–586 (2013).

191. J. Zejda, Litter size in Clethrionomys glareolus Schreber 1780. *Zoologické Listy* **15**, 193–206 (1966).

192. E. Koskela, P. Jonsson, T. Hartikainen, T. Mappes, Limitation of reproductive success by food availability and litter size in the bank vole, Clethrionomys glareolus. *Proc. R. Soc. Lond. B* **265**, 1129–1134 (1998).

193. K. A. Nagy, I. A. Girard, T. K. Brown, Energetics of free-ranging mammals, reptiles, and birds. *Annu. Rev. Nutr.* **19**, 247–277 (1999).

194. T. Mappes, E. Koskela, Genetic Basis of the Trade-Off Between Offspring Number and Quality in the Bank Vole. *Evolution* **58**, 645–650 (2004).

195. Ł. Ołdakowski, Ż. Piotrowska, K. M. Chrząścik, E. T. Sadowska, P. Koteja, J. R. E. Taylor, Is reproduction costly? No increase of oxidative damage in breeding bank voles. *Journal of Experimental Biology* **215**, 1799–1805 (2012).

196. Ł. Ołdakowski, A. Wasiluk, E. T. Sadowska, P. Koteja, J. R. E. Taylor, Reproduction is not costly in terms of oxidative stress. *Journal of Experimental Biology*, jeb.126557 (2015).

197. E. T. Sadowska, E. Król, K. M. Chrzascik, A. M. Rudolf, J. R. Speakman, P. Koteja, Limits to sustained energy intake. XXIII. Does heat dissipation capacity limit the energy budget of lactating bank voles? *Journal of Experimental Biology*, jeb.134437 (2016).

198. T. Sievert, K. Bouma, M. Haapakoski, K. D. Matson, H. Ylönen, Pre- and Postnatal Predator Cues Shape Offspring Anti-predatory Behavior Similarly in the Bank Vole. *Frontiers in Ecology and Evolution* **9** (2021).

199. W. L. Tidhar, J. R. Speakman, An evaluation of four non-destructive methods for predicting body composition in a small rodent. *International Journal of Body Composition Research* **5**, 137–145 (2007).

200. A. Rohatgi, WebPlotDigitizer, version 4.6 (2022); https://automeris.io/WebPlotDigitizer.

201. R. R. Holser, D. E. Crocker, P. W. Robinson, R. Condit, D. P. Costa, Density-dependent effects on reproductive output in a capital breeding carnivore, the northern elephant seal (Mirounga angustirostris). *Proceedings of the Royal Society B: Biological Sciences* **288**, 20211258 (2021).

202. P. Jonsson, J. Agrell, E. Koskela, T. Mappes, Effects of litter size on pup defence and weaning success of neighbouring bank vole females. **80**, 5 (2002).

203. O. Milenkaya, D. H. Catlin, S. Legge, J. R. Walters, Body Condition Indices Predict Reproductive Success but Not Survival in a Sedentary, Tropical Bird. *PLOS ONE* **10**, e0136582 (2015).

204. P. D. DeWitt, D. R. Visscher, M. S. Schuler, R. P. Thiel, Predation risks suppress lifetime fitness in a wild mammal. *Oikos* **128**, 790–797 (2019).

205. N. J. Briscoe, S. D. Morris, P. D. Mathewson, L. B. Buckley, M. Jusup, O. Levy, I. M. D. Maclean, S. Pincebourde, E. A. Riddell, J. A. Roberts, R. Schouten, M. W. Sears, M. R. Kearney, Mechanistic forecasts of species responses to climate change: the promise of biophysical ecology. *Global Change Biology* **n/a**.

206. C. Stawski, P. Koteja, E. T. Sadowska, A Shift in the Thermoregulatory Curve as a Result of Selection for High Activity-Related Aerobic Metabolism. *Frontiers in Physiology* **8**, 1070 (2017).

207. V. Hin, J. Harwood, A. M. de Roos, Density dependence can obscure nonlethal effects of disturbance on life history of medium-sized cetaceans. *PLOS ONE* **16**, e0252677 (2021).

208. T. L. Derting, M. W. Austin, Changes in Gut Capacity with Lactation and Cold Exposure in a Species with Low Rates of Energy Use, the Pine Vole (*Microtus pinetorum*). *Physiological Zoology* **71**, 611–623 (1998).

209. B. P. Kotler, Harvesting Rates and Predatory Risk in Desert Rodents: A Comparison of Two Communities on Different Continents. *Journal of Mammalogy* **65**, 91–96 (1984).

210. J. L. Verdolin, Meta-analysis of foraging and predation risk trade-offs in terrestrial systems. *Behav Ecol Sociobiol* **60**, 457–464 (2006).

211. M. Dammhahn, P. Lange, J. A. Eccard, The landscape of fear has individual layers: an experimental test of among-individual differences in perceived predation risk during foraging. *Oikos* **2022**, e09124 (2022).

212. C. A. Zynel, B. A. Wunder, Limits to food intake by the Prairie Vole: effects of time for digestion. *Functional Ecology* **16**, 58–66 (2002).

213. J. A. Eccard, H. Ylönen, Who Bears the Costs of Interspecific Competition in an Age-Structured Population? *Ecology* **84**, 3284–3293 (2003).

214. M. C. Breedveld, R. Folkertsma, J. A. Eccard, Rodent mothers increase vigilance behaviour when facing infanticide risk. *Sci Rep* **9**, 12054 (2019).

215. L. L. IJsseldijk, S. Hessing, A. Mairo, M. T. I. ten Doeschate, J. Treep, J. van den Broek, G. O. Keijl, U. Siebert, H. Heesterbeek, A. Gröne, M. F. Leopold, Nutritional

status and prey energy density govern reproductive success in a small cetacean. *Sci Rep* **11**, 19201 (2021).

216. J. Salecker, M. Sciaini, K. M. Meyer, K. Wiegand, The nlrx r package: A next-generation framework for reproducible NetLogo model analyses. *Methods in Ecology and Evolution* **10**, 1854–1863 (2019).

217. J. R. Speakman, "The Cost of Living: Field Metabolic Rates of Small Mammals" in *Advances in Ecological Research*, A. H. Fitter, D. G. Raffaelli, Eds. (Academic Press, 1999; https://www.sciencedirect.com/science/article/pii/S0065250408600197)vol. 30, pp. 177–297.

218. K. E. Jones, J. Bielby, M. Cardillo, S. A. Fritz, J. O'Dell, C. D. L. Orme, K. Safi, W. Sechrest, E. H. Boakes, C. Carbone, C. Connolly, M. J. Cutts, J. K. Foster, R. Grenyer, M. Habib, C. A. Plaster, S. A. Price, E. A. Rigby, J. Rist, A. Teacher, O. R. P. Bininda-Emonds, J. L. Gittleman, G. M. Mace, A. Purvis, PanTHERIA: a species-level database of life history, ecology, and geography of extant and recently extinct mammals. *Ecology* **90**, 2648–2648 (2009).

219. D. Ayllón, S. F. Railsback, S. Vincenzi, J. Groeneveld, A. Almodóvar, V. Grimm, InSTREAM-Gen: Modelling eco-evolutionary dynamics of trout populations under anthropogenic environmental change. *Ecological Modelling* **326**, 36–53 (2016).

220. A. Saltelli, P. Annoni, I. Azzini, F. Campolongo, M. Ratto, S. Tarantola, Variance based sensitivity analysis of model output. Design and estimator for the total sensitivity index. *Computer Physics Communications* **181**, 259–270 (2010).

221. J. C. Thiele, W. Kurth, V. Grimm, Facilitating Parameter Estimation and Sensitivity Analysis of Agent-Based Models: A Cookbook Using NetLogo and "R." *JASSS* **17**, 11 (2014).

222. J. S. Millar, G. J. Hickling, Fasting endurance and the evolution of mammalian body size. *Functional Ecology* **4**, 5–12 (1990).

223. R. Carnell, lhs: Latin Hypercube Samples, version R package version 1.1.3 (2021); https://CRAN.R-project.org/package=lhs.

224. E. Tkadlec, J. Zejda, Density-dependent life histories in female bank voles from fluctuating populations. *Journal of Animal Ecology* **67**, 863–873 (1998).

225. W. L. Peacock, E. Król, K. M. Moar, J. S. McLaren, J. G. Mercer, J. R. Speakman, Photoperiodic effects on body mass, energy balance and hypothalamic gene expression in the bank vole. *Journal of Experimental Biology* **207**, 165–177 (2004).

226. J. Rutkowska, E. Koskela, T. Mappes, J. R. Speakman, A trade-off between current and future sex allocation revealed by maternal energy budget in a

small mammal. *Proc. R. Soc. B.* **278**, 2962–2969 (2011).

227. J. Gliwicz, Survival and life span. *Acta Theriologica* **28**, 145–172 (1983).

228. L. Trebatická, T. Ketola, I. Klemme, J. A. Eccard, H. Ylönen, Is reproduction really costly? Energy metabolism of bank vole (Clethrionomys glareolus) females through the reproductive cycle. *Ecoscience* **14**, 306 (2007).

229. C. J. Tucker, J. E. Pinzon, M. E. Brown, D. A. Slayback, E. W. Pak, R. Mahoney, E. F. Vermote, N. El Saleous, An extended AVHRR 8-km NDVI dataset compatible with MODIS and SPOT vegetation NDVI data. *International Journal of Remote Sensing* **26**, 4485–4498 (2005).

230. F. Detsch, gimms: Download and Process GIMMS NDVI3g Data, version 1.2.2 (2023); https://cran.r-project.org/web/packages/gimms/index.html.

231. M. Mazurkiewicz, E. Rajska, Dispersion of young bank voles from their place of birth. *Acta Theriol.* **20**, 71–81 (1975).

Acknowledgements

Supervision: FJ

Writing—original draft: CAG

Writing—review & editing: CAG, VR, MD, FJ

Competing interests: Authors declare that they have no competing interests

Data and materials availability: All data, code, and materials used in the analyses are made available for download on Figshare at: Gallagher, Cara (2025). Pattern-informed energetics: Energy allocation modeling for predicting trait variation and population persistence. figshare. Dataset. https://doi.org/10.6084/m9.figshare.28390238.v1

TRACE Document

This is a TRACE document ("TRAnsparent and Comprehensive model Evaludation"), which provides supporting evidence that our model presented in:

Gallagher et al. *Submitted*. Pattern-informed energetics: Energy allocation modeling for predicting trait variation and population persistence.

was thoughtfully designed, correctly implemented, thoroughly tested, well understood, and appropriately used for its intended purpose.

The rationale of this document follows:

> Schmolke A., Thorbek P., DeAngelis D.L., Grimm V. (2010). Ecological modelling supporting environmental decision making: a strategy for the future. *Trends Ecol. Evol.* 25, 479-486.

and uses the updated standard terminology and document structure in:

> Grimm V., Augusiak J., Focks A., Frank B., Gabsi F., Johnston A.S.A., Liu C., Martin B.T., Meli M., Radchuk V., Thorbek P., Railsback S.F. (2014). Towards better modelling and decision support: documenting model development, testing, and analysis using TRACE. *Ecol. Modell.* 280, 129–139.

and

> Augusiak J., Van den Brink P.J., Grimm V. (2014). Merging validation and evaluation of ecological models to 'evaludation': a review of terminology and a practical approach. *Ecol. Modell.* 280, 117–128.

Maija Karala 2022

Contents

1. Problem formulation

This TRACE element provides supporting information on: The decision-making context in which the model will be used; a precise specification of the question(s) that should be answered with the model, including a specification of necessary model outputs; and a statement of the domain of applicability of the model, including the extent of acceptable extrapolations.

Summary:

> **Climate and land use change have been identified as the major drivers of ecosystem decline in terrestrial systems, and understanding the impacts of these drivers on population dynamics is crucial for effective conservation strategies. Here we present a novel agent-based energy budget modelling approach, called Pattern-Informed Energetics (PIE). This innovative framework incorporates a wide range of morphological and physiological traits of individual animals, allowing population-level traits and densities to emerge from low-level individual foraging success. Notably, the model allows energy allocation strategies to emerge through a high level of empirical grounding, rather than being imposed. By simulating the potential impacts of environmental change on the survival and reproduction of populations, the model can be used to test basic and applied research questions related to species energetics, behavior, and ecology under natural and human-driven dynamics.**

Global declines in ecological systems are being driven at large by land use and climate change (*131*). These factors directly affect the survival of populations by altering environmental conditions, including changes in resource availability. Alterations in resource availability can have far-reaching impacts on the distribution and abundance

of species, mediated through effects on individual fitness and population dynamics. To address this pressing issue, we present an agent-based energy budget modelling approach, called the Pattern-Informed Energetics (PIE) framework, which can flexibly model the energetics of species and allow for the emergence of empirically-driven energy allocation strategies.

Our model incorporates variation in a wide range of morphological and physiological traits of individual animals which give rise to population-level traits and densities that are dependent on the foraging success of individuals. By simulating the energy balance of individuals and populations in dynamic ecosystems, researchers can use our model to investigate the potential impacts of environmental change on the survival and reproduction of populations. Therefore, our model has significant potential for informing conservation strategies and mitigating the impacts of land use and climate change on the natural world.

Changes in environmental conditions have played a critical role in shaping the immense variation in metabolic traits found throughout the animal kingdom. Our modelling framework captures metabolic adaptations that are crucial in determining the energy balance of individuals and populations, thereby influencing their survival and reproductive success. The proposed model can be applied to a wide range of questions concerning the impacts of changes in landscape structure and resource availability on population survival over various spatiotemporal scales, ranging from near- to long-term timescales.

Though the model was developed using a case study focused on bank vole populations (*Myodes glareolus*), it can be readily applied to other terrestrial, homeothermic animals given the availability of relevant data. However, depending on the specific system and research question, certain aspects of the model may require modifications, such as movement behavior or landscape configuration.

The PIE modelling approach represents a valuable tool for predicting the effects of changing environmental conditions on populations, developing effective conservation strategies, and investigating a wide variety of questions related to the energetics, behavior, and ecology of species in the face of environmental change.

2. Model description

This TRACE element provides supporting information on: The model. Provides a detailed written model description. For individual/agent-based and other simulation models, the ODD protocol is recommended as standard format. For complex submodels it should include concise explanations of the underlying rationale. Model users should learn what the model is, how it works, and what guided its design.

Summary:

Here we present the model description following the ODD (Overview, Design concepts and Details) protocol for describing Individual-Based Models (IBMs) (*96, 97*). The model, which was implemented in Netlogo v6.2.0 (https://ccl.northwestern.edu/netlogo/), is open-source and can be downloaded from https://github.com/CaraAGallagher.

2.1. Purpose and patterns

In the animal kingdom, changes in environmental conditions can play a key role in mediating the selection of alternative metabolic phenotypes through their impacts on individual fitness. These variations can contribute to the diversity of energy use and life history traits observed among different species and allow animals to cope with changing conditions, such as occurring with climate change. In this model, we simulate the energetics of wildlife populations in a spatially-explicit and temporally dynamic environment by incorporating recent advancements in our understanding of the processes that shape animal energetics. The model considers trade offs experienced during periods of food limitation, allowing for the assessment of questions related to changes in resource availability, behavioral adaptation, and population persistence. To ensure that the modeled processes are realistic and capture detailed knowledge of the energetics of a specific species, the model has been parameterized and tested against empirical data for the bank vole (*Myodes glareolus*). However, when sufficient empirical knowledge exists, it would be straightforward to adapt the model for any terrestrial mammal species.

Empirical patterns were used in both model calibration and evaluation. For model calibration, 16 patterns were used to evaluate the outcomes of potential values of 10 unknown parameters. These patterns came from a variety of published sources and were selected as they were thought to be driven by the relationships which were being parameterized. See Section 6 for details on model calibration. Twenty four additional patterns were reserved for model evaluation, consisting of datasets which were not considered during earlier model development stages. All patterns and their associated fit criteria are described in Sections 6 and 8 below.

2.2. Entities, state variables, and scales

The model comprises two entities: **landscape cells** and individual **animal agents**.

Landscape cells are square grid cells characterized by their position and whether they contain food resources (*resource-cell*). Cells which do contain food are additionally characterized by their resource level (*resource-level*) and the last timestep when an animal agent consumed their resources (*last-eaten*) (Table S1). Here food represents growth or accumulation of generic food resources, rather than relating to any specific food item, with associated parameters, such as the maximum resource levels (*max-resources*), resource growth rates (*r-growth-ts*), and energy

content (*ED-food*) and dry matter content (*DM-food*) of food stuffs being either calibrated in the case of *max-resources* and *r-growth-ts* (see Section 6) or taken as an average for bank vole food items in (*132*) for *ED-food* and *DM-food*. The proportion of the landscape covered by food cells and landscape fragmentation levels are set at initialization using the sliders *perc-resource-cells* and *fragmentation-level*, respectively, with both values bounded between 0 and 1.

Each grid cell covers 10mx10 m. This cell size was selected as it allowed for the simulation of empirical population densities, while remaining computationally feasible and allowing for individuals to have a number of landscape cells within their home range (see Submodels Section 2.7.1) . The total spatial extent of the landscape is 20x50 grid cells, covering an area of 100,000 m². This landscape size was selected as it resulted in sufficient levels of variability in local vole densities and corresponding resource levels. The model landscape has open boundaries, *i.e.,* it is toroidal and not bounded at the extents.

Animal agents are characterized by 18 base state variables related to their morphometrics, energetics, age, movement speed, and individual trait variation, while pregnant and or lactating animals are further characterized by an additional 17 state variables related to reproduction (Table S1). Morphometric state variables relate primarily to the lean and adipose masses and storage levels of animals and their dependent offspring, energetic state variables are used to track the cost of each metabolic process, energy intake values, and storage dynamics, while reproductive state variables characterize the costs of pregnancy and lactation and number, sex, and age of offspring. All animals above weaning age are represented as female, as such animals which are born male are removed from the model at weaning.

The model proceeds in discrete timesteps of 30 minutes. This interval was selected as it allowed for fine scale activity patterns and energy budget dynamics to be modelled, while remaining computationally feasible for exploring questions demanding long-term projections. When the option to skip the overwinter period is selected, each year begins on day 90 and ends on day 273 to encompass the breeding period. Otherwise, each year consists of 365 days. Metabolic calculations are in units of energy per unit time (J ts-1). Model runs continue until either all animal agents have died or up to a specified final timestep.

Table S1. *State variables used in the model.*

State variable	Code	Description [unit]	Type
Landscape cells			
$U[c]$	*resource-level*	Food resource level of a cell [g]	Float
t_e	*last-eaten*	Timestep where resources were last consumed from cell [unitless]	Integer
Agents			

m	mass	Mass [kg]	Float
m_{LM}	lean-mass	Mass of lean (non-adipose) tissues [kg]	Float
m_{adi}	adipose-mass	Mass of adipose tissues [kg]	Float
age	age	Age in days [days]	Integer
SL	storage-level	Storage level (ratio of adipose stores to total mass) [unitless]	Float
ps	pregnancy-status	Pregnancy status [true or false]	Boolean
ls	lactation-status	Lactation status [true or false]	Boolean
M_B	m-BMR	Basal metabolic rate [J ts-1]	Float
M_L	m-move	Metabolic cost of transport [J ts-1]	Float
M_{LM}	m-growth	Metabolic cost of lean mass deposition [J ts-1]	Float
v	move-speed	Movement speed [m ts-1]	Float
A_d	daily-activity	List tracking if movement occurred in a timestep [unitless]	List
FD	food-debt	Value tracking negative energy balance [J]	Float
EA	energy-assimilated	Energy from food resources [J]	Float
EM	energy-mobilized	Energy from mobilized tissues [J]	Float
SF	stomach-fill	Consumed food held in stomach [g]	List
M_d	daily-m-tot	List tracking daily expenditure of the last 48 timesteps [g]	List
I_d	daily-ingestion	List tracking the amount of food ingested in the last 48 timesteps [g]	List
For pregnant or lactating females:			
n_{emb}	n-emb	Number of embryos [N]	Integer
m_{emb}	mass-emb	Mass of embryo [kg]	Float
m_{pl}	mass-pl	Mass of placental tissue [kg]	Float
m_{gest}	gest-mass	Gestational mass (total mass of embryos and placentae) [kg]	Float
$M_{G,emb}$	m-growth-emb	Metabolic cost of growth of embryo [J ts-1]	Float
M_P	m-preg	Metabolic cost of pregnancy [J ts-1]	Float
ds_{mating}	ds-mating	Days since mating [days]	Float
n_{off}	n-off	Number of offspring [N]	Integer
m_{off}	mass-off	Mass of dependent offspring [kg]	Float
SL_{off}	SL-off	Storage level of offspring [unitless]	Float
$m_{LM,off}$	lean-mass-off	Lean mass of dependent offspring [kg]	Float
sex_{off}	sex-off	Sex of dependent offspring ["male" or "female"]	String
$M_{B,off}$	m-BMR-off	Basal metabolic rate of dependent offspring [J ts-1]	Float
$M_{LM,off}$	m-growth-LM-off	Metabolic cost of lean mass growth of offspring [J ts-1]	Float
M_{Lact}	m-lact	Metabolic cost of lactation [J ts-1]	Float
ds_{birth}	ds-birth	Days since giving birth [days]	Float
$t_{mating,offset}$	t-mating-offset	Offset between -15 and 15 days for variation in breeding season start [days]	Integer

2.3. Process overview and scheduling

At the beginning of each timestep, animals are randomly assessed to determine if they should move (_move_), based on their current satiety and energy balance (see Figure S1). If it is determined that they should move, they do so.

After going through the movement process, animals then go through their energy budget processes (_energy-budget_). First they calculate their energetic costs for the timestep (_energy-costs_), going through each of the metabolic processes, basal maintenance (_basal-maintenance_), cost of transport (_cost-of-transport_), reproduction (_reproduction_), and lean mass growth (_growth-lean-mass_), in that order. After cost calculation, animals update records of total energy use and output monitors (_update-records_).

Animals then proceed to consume resources from their local grid cell (_energy-intake_) if they are available and the animal's current hunger and satiety levels allow for it (see the Submodels section below for a full description of the energy intake procedure). The food levels in each resource cell are dynamically changing and are only updated on the first occasion that an animal encounters a food cell in a given timestep (_resources-grow_). Each food cell keeps track of the last time its resources were consumed (_last-eaten_). During the energy intake procedure, animals encountering a food cell that has not updated its resource levels for that timestep update it based on the time since last eaten and the resource accumulation rates per timestep (_r-growth-ts_), up to the maximum resource level (_max-resources_). After updating resource values, animals consume resources from the cell, and the food level drops accordingly to the amount consumed.

After both energetic costs and ingested energy are determined, the overall energy balance is updated (_energy-allocation_). It is then evaluated whether the animals can meet their current costs based solely on the ingested energy (_energy-assimilated_), or if they need to draw on any body reserves (_energy-mobilized_).

Based on their energy balance, animals update their adipose and lean mass tissue stores (_storage-dynamics_). Anabolic processes result in the accumulation of body tissue for animals with a positive energy balance, while catabolic processes result in tissue breakdown for those that mobilized energy, and the proportion of each tissue deposited or mobilized (_pro-storage-perc_) depends on the current body condition of the animal (_storage-level_). Following the tissue updates (_lean-mass_ & _adipose-mass_), animals then adjust their total body mass (_mass_) and storage levels.

Once a day, in _daily-tasks_, the model updates daily monitors and ages of animals (_age_), and mortality due to old age (_mortality-max-age_) and starvation (_mortality-starvation_) can occur. If it is the last day of the year (_yearly-tasks_), the model resets the year and updates yearly monitors. Additionally, overwinter mortality occurs (_mortality-overwinter_), and resource levels are reset to their maximum values. Finally, if overwintering skipping is enabled (_overwinter-skip?_), animals surviving winter undergo growth to cover the skipped period.
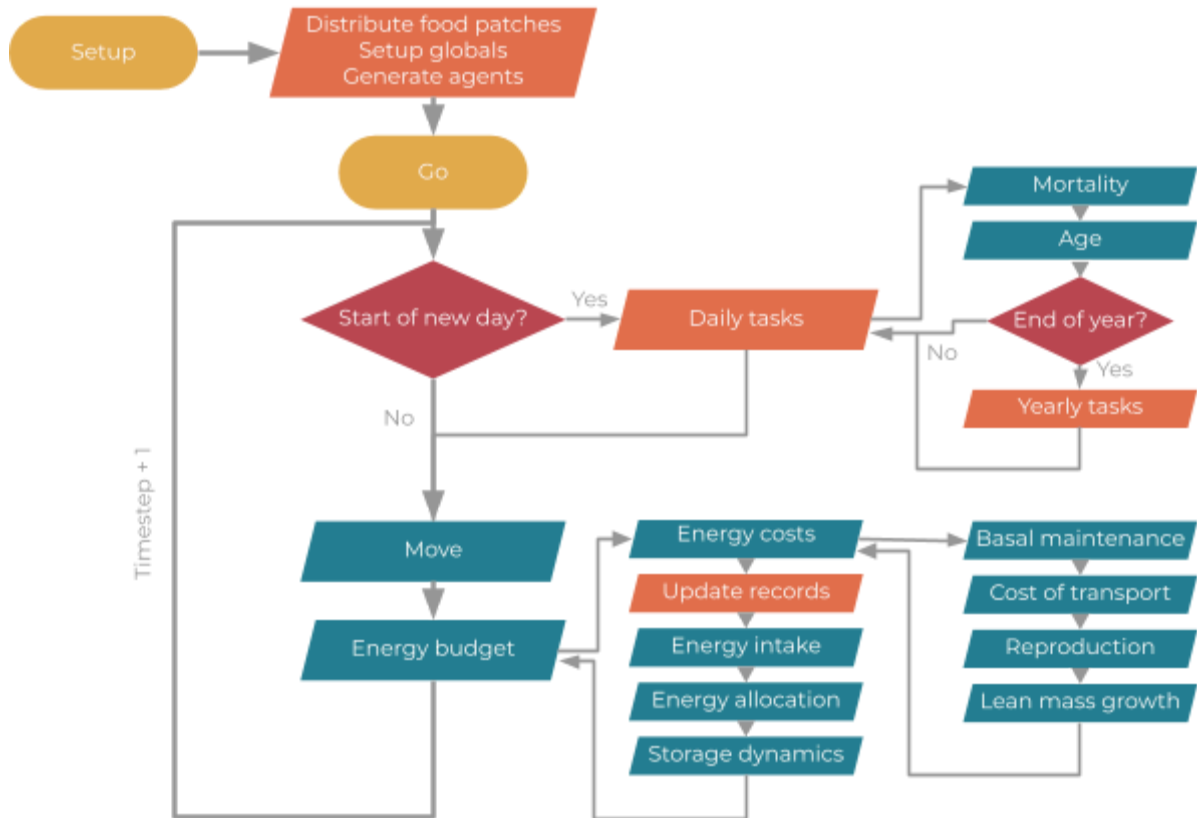
Figure S1. Flowchart of model process execution order. Only adult females are modelled explicitly. Diamond-shaped symbols (in red) indicate decisions made by agents and parallelograms indicate calculations. Blue elements indicate actions taken by animals and orange elements are relevant for both agent and environmental variables. A detailed description of all elements of this flow diagram can be found in the submodel section below.

2.4. Design concepts

2.4.1. Basic principles

To understand the relationships between changes in environmental conditions and population level metabolic traits and fitness, this model is constructed on the foundation of established physiological theory and eco-evolutionary concepts. The central feature of the model is the energy budget, which is shaped by energy allocation dynamics inversely parameterized using empirical data. This comprehensive approach enables the model to capture the intricate interplay between environmental factors, metabolic traits, and population-level outcomes in a biologically realistic and detailed manner.

The modelled energy budgets are based on physiological principles (*12*, *133*) and mathematical models of energy expenditure (*134*). Feedbacks occur between energy budget components such as through links between body condition and energy intake and allocation to growth and reproduction and between energy balance and likelihood of activity in a timestep. The dual intervention point model (*28*) inspired

links between body condition and "hunger" (represented as a modifier of energy intake) such that body condition only modifies hunger at low or high levels, with no influence occurring at intermediate levels. Additionally, the relationship between body condition and the ratio of metabolic fuels catabolized or anabolized is inspired by Forbes' theory (*31, 32*), but parameterized using empirical data from three rat studies (*119–121*).

2.4.2. Emergence

At the population-level, abundance and distributions of metabolic trait values and their outcomes on total energy use, growth, reproduction, and survival all emerge from individual foraging success and resulting fitness-mediated selection. In particular, the key emergent outcomes which were used to evaluate scenarios were adult body mass, age at first birth, basal metabolic rate, interbirth intervals, neonate body masses, litter size, number of litters per year, weaning body mass, activity patterns, average lifespan, and population densities.

Several aspects of the energy budget are informed using imposed metabolic equations. These include the relationships between body condition and energy intake and metabolic fuel use, between body size and movement speed and the costs of movement, and the additive nature of total energy use (see ODD Element 2.7.2).

2.4.3. Adaptation

Individuals adapt their energy allocation based on state-dependent feedback from their environment and body condition. Foraging rates increase when body condition is low and decrease when reserves are sufficient. The decision to embark on a foraging trip is influenced by the current energy balance, with a higher likelihood of foraging as energy balance becomes more negative. Females allocate less energy to reproduction as their reserves decline, leading to higher probabilities of abortion during pregnancy and pup mortality during lactation. Lean mass deposition depends on current condition, while the ratio of metabolic fuels (proteins and lipids) used in catabolic versus anabolic processes also varies with reserves.

2.4.4. Objectives

Animals attempt to maximize their fitness by balancing their energy intake with activity and other metabolic costs, and by adjusting their allocation of available energy to various physiological processes based on their body condition. When their energy intake is insufficient, animals use stored body tissues to cover the costs, and as storage levels decrease, they increasingly rely on protein catabolism, which reduces their metabolic rate. However, if body stores continue to decline, animals

face an increasing risk of mortality. At low body condition, animals prioritize critical survival processes over non-essential ones, such as growth or reproduction, resulting in tradeoffs (Sibly et al., 2013) (see ODD Element 2.7.2 for more details).

2.4.5. Learning

Animals in the model do not learn.

2.4.6. Prediction

Animals in the model do not make predictions.

2.4.7. Sensing

Animals can directly sense their storage levels and energy balance (represented by *food-debt*, see Tables 2.1 and 2.15) and make decisions based on their current nutritional state, *e.g.*, to move, reduce allocation to growth or reproduction, or to alter their energy consumption.

2.4.8. Interaction

Mediating interactions occur in the model through competition for available food resources. Animals can continue to feed on a food cell until its resources are fully exhausted (a *resource-level* of 0), and cells replenish their resources at a set rate (*r-growth-ts*).

2.4.9. Stochasticity

The probability of survival due to starvation (mortality-starvation), the percentage of animal's dying in the overwinter period (mortality-overwinter), the probability of conception (*pregnancy-status* = "true"), the number of embryos implanted (*n-emb*), the initiation of breeding at the start of the season (*t-mating-offset*), the probability of moving in a timestep, and the landscape cell foraged in (see move) are all associated with stochasticity in the model. In all these cases, the variation represented is considered important, as it may have consequences, but its mechanistic basis is unknown or considered not relevant for the purpose of the model.

Additionally, food cells are placed randomly within the landscape (setup-landscape). Each map generation results in a unique landscape containing the specified percentage cover of resource cells (*perc-resource-cells*) which are distributed based on the value of *fragmentation-level*.

2.4.10. Collectives

Mothers and dependent offspring in the model act as collectives. They move and forage as one unit. Though offspring are assumed to be entirely dependent on their mother's milk until weaning when they are created as new entities (see Reproduction in Submodels section 2.7.2.1.3).

2.4.11. Observation

The observed outputs of the model differ between the various model development stages (for details see TRACE Sections 6, 7, and 8).

For calibration, outputs related to 16 empirical patterns were collected from the model during the entirety of the fifth simulation year (to allow for four years of burn-in before collection). Neonate and weaning masses were recorded at birth and weaning events, along with litter size and whether the mother successfully weaned an offspring, relative to the mother's body mass. Once per day animal total and lean body mass by age, lactating mother mass, food intake, and total litter mass in relation to pup age, mother peak food intake, energy use, and milk transfer by litter size, animal body fat percent (either when alive or at death), and field metabolic rate by body mass were recorded.

In the sensitivity analysis, seven model outputs were observed, including body mass of adults, neonates, and weaned offspring, age at first birth, litters per year, litter size at birth, and population density.

For model evaluation, state-dependent field metabolic rates and energy intake (meaning per age class), survival rates, mass-specific basal metabolic rates, litter size, number of litters per year, neonate and weanling body masses, survival, and local population densities were observed.

For scenario testing, we observed 13 individual traits—related to energetics, morphometrics, and reproduction—as well as population abundance, either seasonally or annually, depending on relevance.

2.5. Initialization

Upon initialization, a number of simulated animals are placed randomly in the landscape based on the value of the input parameter *n-animals*. Animals are initialized with identical arbitrary starting values of 0.01 kg *mass*, 20 days of *age*, and a *storage-level* equal to half of the maximum value ($\frac{SL-max}{2}$) (19.9% body fat).

Lean-mass is then calculated as *mass* × (1 - *storage-level*) and *adipose-mass* as *mass* × *storage-level*. The variables *pregnancy-* and *lactation-status* are set to "false".

Lists used for tracking *stomach-fill*, *daily-activity*, *daily-ingestion*, and *daily-m-tot* (energy use) are each initialized as empty lists (*i.e.,* "[]").

The mating period of individuals is set to occur between days 90 and 273 (*50, 57, 135*) and in the default setting (*overwinter-skip?* is set to "true") the day is set to 90. This feature permits the model to skip over the non-breeding period, and consequently, the start and end days of the year are adjusted to five days prior to or after the beginning or conclusion of the mating period, respectively. The number of timesteps occurring per day (*ticks-per-day*) and cell size in meters (*cell-size-m*) are set to 48 and 10, respectively.

Food cells are placed in the landscape randomly in the setup-landscape procedure based on specified input parameters *fragmentation-level* and *perc-resource-cells*, which determine the distribution and total coverage of resources in the landscape, respectively. Landscapes are generated as follows: all grid cells are initialized with *resource-cell* set to "false" and their color (*pcolor*) set to brown. The total number of cells which should become resource cells (*cover*) is then calculated using the total count of cells and the *perc-resource-cells* parameter. Then, while the number of created resource cells is lower than *cover*, a random cell is asked if its *resource-cell* value is equal to "true" and it has any neighboring cells with *resource-cell* set to "false". If so, then it asks one of its neighbors with *resource-cell* set to "false" to become a resource cell (*resource-cell* = "true"). If not, it generates a random float value between 0 and 1 and checks if this value is less than 1 minus the *fragmentation-level* parameter value. If this check returns true, and the cell is not currently a resource cell, it then becomes a resource cell (*resource-cell* = "true"). This occurs until the number of resource cells is equal to *cover*. Then all resource cells set their resource-level to the maximum value (*max-resources*) and set their color to green.

All additional parameters in Table S2 are initialized at their specified values.

Simulation experiments are identical in setup beyond varying parameter values, *e.g.,* running with *fragmentation-level* parameter values of 0.9 versus 0.99.

Table S2. *Model environment parameter definitions and values.*

Symbol	Value	Code	Description [units]
t_d	48	ticks-per-day	Timesteps per day [unitless]
c_m	10	cell-size-m	Cell size [m]
$U[c]_{max}$	140	max-resources	Maximum resources in a resource cell [g]
$c_{\%,rc}$	0.75	perc-resource-cells	Proportion of the map covered by resource cells [Prop]
r_{grow}	0.011	r-growth-ts	Resource accumulation in a timestep [g]
f	0.9	fragmentation-level	Fragmentation level of habitat [unitless]
N	100	n-animals	Number of animals created at initialization [N]

2.6. Input data

In model evaluation and scenario analyses, normalized difference vegetation index (NDVI) data are used to drive within- and between-year variations in resource availability.

2.7. Submodels

The proposed model utilizes a comprehensive approach to examining the relationship between the temporal and spatial variability of environmental resources and the energy balance, survival probabilities, and reproductive success of animals. By incorporating these factors, the model serves as a valuable tool for assessing the population-level impacts of environmental changes at a high temporal and spatial resolution. The movement and energy budget modules of the model have been specifically parameterized for bank voles, yet they possess a level of generality that allows for their adaptation to other terrestrial mammals, provided that adequate data are available for parameterization.

The model is composed of three primary modules, one related to movement behavior of agents (move), another to energetic processes (energy-budget), and one for the life-history processes of mortality and reproduction (demographics) (Figure S2). Each module will be described in its own section, along with relevant parameters and equations, below.
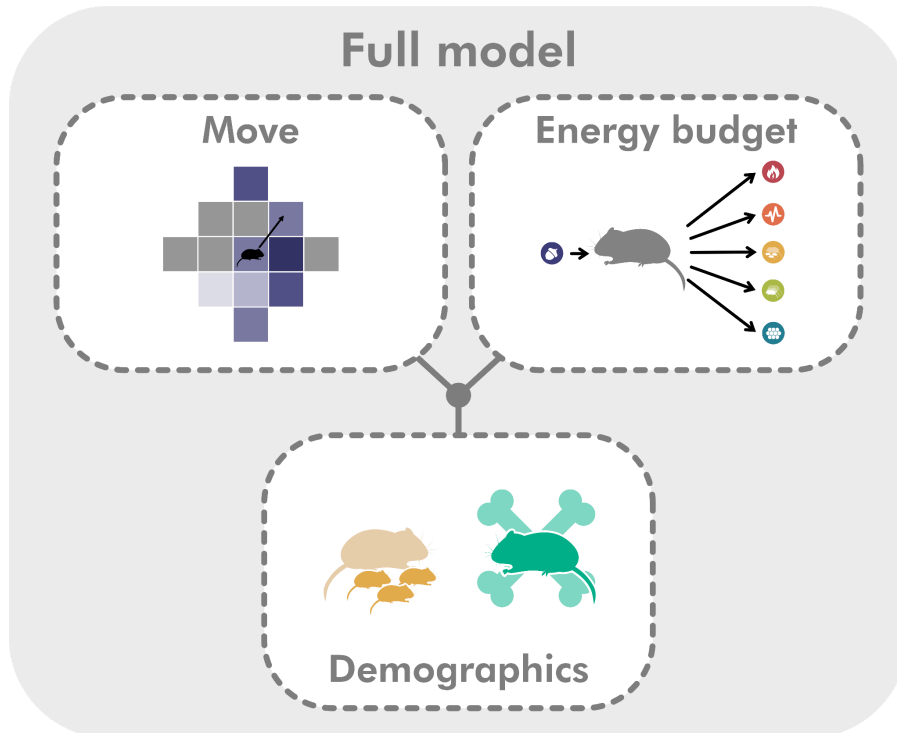
Figure S2. Schematic depicting the model's three distinct modules.

2.7.1. Move (<u>move</u>)

The movement procedure is composed of several steps. First animals determine their probability of moving in a timestep (*move-prob*) based on their energy balance following Eq. 1 (Table S4). This probability is based on the negative energy balance of animals (*food-debt*) compared to daily requirements (represented as the amount of food needed to meet those requirements). Animals then check whether their stomach capacity has been reached (*stomach-fill*) and set their movement probability to zero if this is the case, so that animals with already full stomachs do not engage in foraging bouts. They then roll a random float value with a maximum of one and compare this value to their movement probability. If the random number falls below the movement probability, then the animal will not move in that timestep, setting its movement speed (*move-speed*) to 0 and adding a 0 to the end of its daily activity list (*daily-activity*). If instead the number is greater than the movement probability (which is more likely as the animal's food debt continues to accrue), then the animal will then proceed to engage in a foraging bout. To do this it will first check if it is on its home range core cell (*home-c*) and, if not, move there. Then it will select its *move-speed* for the timestep randomly from a gamma distribution shaped by empirical values of mean and maximum speeds (*speed-mean* & *speed-max*; Table S3). This speed is then converted to meters per half hour and a 1 is added to the end of its daily activity list (*daily-activity*) to indicate that it moved in that timestep. Animals then pull their home range radius (*HRr*) randomly from within the range of

empirical values (*HR-r-min* & *HR-r-max*; Table S3) and randomly pick one cell within their home range radius to forage in for the timestep (*foraging-cell*).

Table S3. *Movement module parameter definitions and values.*

Symbol	Value	Code	Description [units]	Source
v_{mean}	0.166	speed-mean	Mean movement velocity [m s⁻¹]	(*107*)
v_{max}	0.822	speed-max	Maximum movement velocity [m s⁻¹]	
HR_{min}	11.2	HR-r-min	Minimum home range radius [m]	(*67, 100, 102–106, 136*)
HR_{max}	32.2	HR-r-max	Maximum home range radius [m]	

Table S4. *Movement module equations.*

Eq. #	Description [units]	Code	Symbol	Equation	Source
1	Probability of moving in a timestep [Prob ts-1]	move-prob	$P(A)$	$\dfrac{-1}{\frac{\sum M_d}{AE \cdot ED}} \cdot fd + 1$	-

2.7.2. Energy budget (energy-budget)

The energy budget module is a multi-step process that is broken up into several procedures. It includes the four procedures related to calculating energetic costs: *basal-maintenance*, *cost-of-transport*, *reproduction*, and *growth-lean-mass*. Additionally, there is a procedure for energy intake (*energy-intake*), one for allocating energy from assimilated food resources and updating energy balance (*energy-allocation*), and another for determining storage dynamics (*storage-dynamics*). Furthermore, the procedure executing the replenishment of resource cells (*resources-grow*) is also called in this module, as it is triggered by the *energy-intake* procedure.

Animals first calculate their energetic expenditure, with the costs of activity being based on energy balance and allocation to reproduction and growth determined based on body condition, *i.e.,* percent body fat (Figure S3). Storage levels additionally drive potential energy intake through modifiers on attempted intake rates in a timestep following the dual intervention point model (*28*), details below in *storage-dynamics*.

The description below will follow the order in which these processes are executed in the full model (Figure S3). See Table S1 for an overview of the state variables involved in the energy budget module.
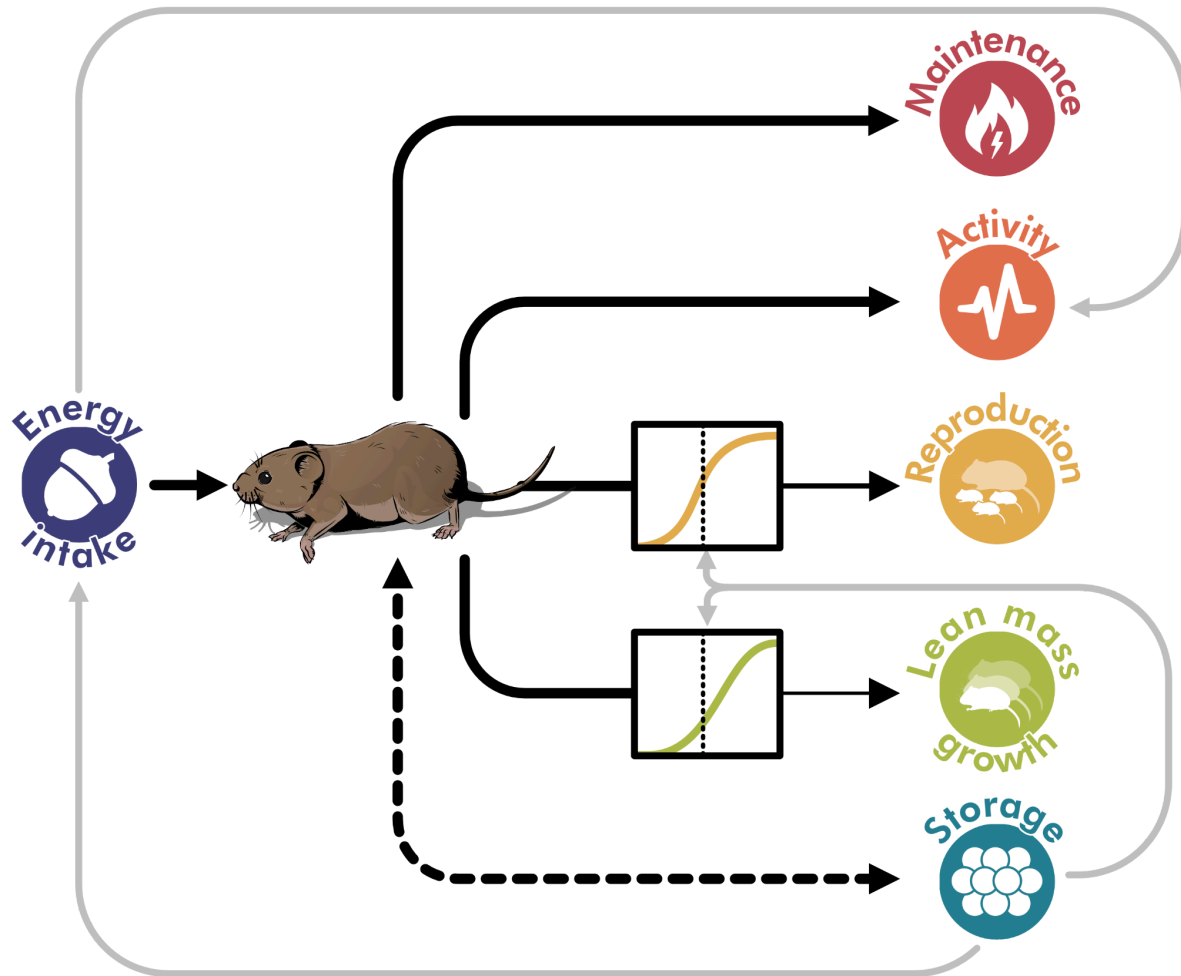
Figure S3. Key processes underlying the energy budget module. Light grey lines indicate interactions between processes.

2.7.2.1. Energy costs

2.7.2.1.1. Basal metabolic rate (BMR) (basal-maintenance)

Maintenance costs are modelled based on body mass following an allometric relationship fit to empirical data for vole respiration (Eqn. 2 in Table S6). See TRACE Section 3 for details on the empirical data used and how parameters were estimated.

Table S2.5. *Basal metabolic rate procedure parameter definitions and values.*

Symbol	Value	Code	Description [units]	Source
B_0	6053.1	B0	Normalization constant [unitless]	*(137–139)*

	γ	0.64	gamma	Allometric scaling exponent [unitless]

Table S6. *Basal metabolic rate procedure equations.*

Eq. #	Description [units]	Code	Symbol	Equation	Source
2	Maintenance costs [J ts-1]	m-BMR	M_B	$B_0 m^\gamma$	*(12, 140)*

2.7.2.1.2. Cost of transport (cost-of-transport)

Animals which do not move in a timestep do not accrue any activity costs (see move module for a description of when animals decide to move). For animals which do move, costs of activity are broken up into two processes: the first for calculating postural costs, which are the energetic costs associated with maintaining a particular body position while standing or moving, and the second for incremental costs of transport, which are the additional costs required to move the body forward. Both costs vary allometrically with body mass, but incremental costs are additionally driven by movement speed. Total costs are determined as the sum of these two processes (see Equation 3 in Table S8). Postural costs were parameterized using empirical data for rodents, while incremental costs follow an allometric relationship (*109*). See TRACE Section 3 for details on the empirical data used and how parameters were estimated.

Table S7. *Cost of transport procedure parameter definitions and values.*

Symbol	Value	Code	Description [units]	Source
B_{pCoT}	4.7	intercept-pcot	Intercept of the postural cost function [J ts-1]	*(141–143)*
γ_{pCoT}	0.63	slope-pcot	Slope of the postural cost function [unitless]	*(141–143)*
B_{iCoT}	10.6	intercept-icot	Intercept of the incremental cost of transport function [J kg^{-1} m^{-1}]	*(109)*
γ_{iCoT}	-0.29	slope-icot	Slope of the incremental cost of transport function [unitless]	*(109)*

Table S8. *Cost of transport procedure equations.*

Eq. #	Description [units]	Code	Symbol	Equation	Source
3	Cost of transport [J ts-1]	m-move	M_{CoT}	$\left(B_{pCoT} m^{\gamma_{pCoT}} + B_{iCoT} m^{\gamma_{iCoT}} \cdot m \cdot v\right) \cdot 1800$	*(144, 145)*

The reproduction procedure can be broken up into the independent costs of pregnancy and lactation. As with all other energetic processes, these procedures are executed every timestep for relevant animals, here those that are pregnant and or lactating. All parameters and equations associated with these two processes can be found in Tables S9 and S10, respectively.

Animals which are pregnant begin the *pregnancy* procedure by first checking whether they have reached the end of the gestation period (if *ds-mating* >= *t-gest*). If so, they then skip the rest of the *pregnancy* procedure and execute *give-birth* (see Section 2.7.3.1.2 below). But if not, animals then check whether the number of days since mating (*ds-mating*) is greater than zero. A value of less than zero represents an implantation delay (*t-0*) which occurs when an animal which already has dependent offspring becomes pregnant. Animals which are in this delayed implantation stage skip the rest of the pregnancy procedure and only advance their *ds-mating* parameter by 30 minutes (the timestep length). Animals which have implanted embryos instead execute all pregnancy related functions, starting with the calculation of the maximum growth of each embryo in the timestep (*max-growth-emb*) based on the current embryo mass (*mass-emb*), the fetal growth constant (*emb-growth-c*), and the asymptotic fetal mass (*emb-mass-inf*) (Equation 4). The parameters *emb-growth-c* and *emb-mass-inf* were determined using empirical data, see TRACE Section 3 for details on the empirical data used and parameter value determination. This mass is then converted to energy required for both fat and protein components (*e-fat* and *e-pro*, respectively) based on the percentage of each component in fetal tissue (*percent-fat-emb* and *percent-pro-emb*) and the energy densities (*ED-fat* and *ED-pro*) and deposition efficiencies (*DE-fat* and *DE-pro*) of fat and protein (Equations 5 and 6). The total energy needed to fuel structural growth (*m-growth-emb*) is then calculated as the sum of *e-fat* and *e-pro* (Equation 7). Since placental tissue also grows alongside embryonic development, animals which have been gestating for more than 9.35 days (the period after which placental mass was no longer negligible for mice in (*110*) calculate their placental growth in a timestep (*max-growth-pl*) based on *ds-mating* (Equation 8). This is then converted to the cost of placental growth (*m-growth-pl*) using the energy density (*ED-pl*) and deposition efficiency (*DE-pl*) of placental tissue (Equation 9). After determining *m-growth-emb* and *m-growth-pl*, the actual amount of energy allocated to pregnancy (as a proportion; *perc-allo-preg*) is then calculated based on the animal's *storage-level* and the calibrated parameters *preg-prob-const* and *preg-prob-mid* (Equation 10, see TRACE Section 6 for allocation curves for each of the 30 selected parameter sets). The total energy allocated to pregnancy is then updated by multiplying the sum of the costs of *m-growth-emb* and *m-growth-pl* by the number of embryos (*n-emb*) and then adjusting this value using *perc-allo-preg* (Equation 11). The embryo, placental, and gestation masses (*mass-emb*, *mass-pl*, and *gest-mass*) are then updated accordingly (Equations 12- 14). At the end of the procedure, the parameter *ds-mating* is advanced by 30 minutes (the length of one timestep).

Animals that are lactating start the _lactation_ procedure by first checking if it is time to _wean_ their offspring (if _ds-birth_ >= _t-nurs_) and, if so, then skip _lactation_ to execute the _wean_ procedure (see Section 2.7.3.1.3 for details). If not, they then check whether the offsprings' total masses, lean masses, or storage levels (_mass-off_, _lean-mass-off_, or _SL-off_) have dropped below zero, in which case _lactation_ should be halted and the _mortality-starvation_ procedure run to ensure that these offspring die. If these cases aren't met, then animals proceed to calculate their lactation costs. These costs can be broken up into two processes, one for calculating offspring BMR costs (_m-BMR-off_) and the second for producing tissue for offspring structural growth (_m-growth-lm-off_). Offspring maintenance costs are calculated similarly to adult costs except here they are modified to represent the reduced thermogenic capacity of neonate rodents (_113, 114_) using the parameter _off-BMR-red_ (Equation 15). The total costs of _m-BMR-off_ are a sum of individual values. Maximum lean mass growth (in kg; _max-growth-lm-off_) is again modelled following the same process as for adults, but here using _lean-mass-off_ as an input (Equation 16). To convert this mass into energy, the percent protein of lean mass tissue (_lean-mass-perc-pro_) is determined based on the age of the offspring (_ds-birth_) following Equation 17, then multiplied by the energy density of protein (_ED-pro_) to get the energy density of lean mass tissue (_ED-lean-mass-off_). Following Equation 18, the total growth costs for lean mass are determined using _max-growth-lm-off_ and _ED-lean-mass-off_ and inefficiencies of growth accounted for using the parameter _off-growth-eff_ (Equation 19). The actual amount of energy allocated to lactation (as a proportion; _perc-allo-lact_) is then calculated based on the animal's _storage-level_ and the calibrated parameters _lact-prob-const_ and _lact-prob-mid_ (Equation 20). This allocation curve differs from others in that the allocation proportion spans between 0 and 2 (as opposed to 0 - 1)(see TRACE Section 6 for allocation curves for each of the 30 selected parameter sets). This is due to the fact that mothers with sufficient energy stores should additionally allocate energy to the development of offspring energy stores (_i.e.,_ body fat) in addition to basic maintenance and lean mass growth costs. After calculating _perc-allo-lact_, animals then estimate their cost of lactation (_m-lact-est_) based on _m-BMR-off_, _m-growth-lm-off_, the number of offspring (_n-off_), and the efficiency of milk production (_milk-prod-eff_) (Equation 21), then adjust this value by _perc-allo-lact_ to calculate their realized lactation costs for the timestep (_m-lact_) (Equation 22). The milk energy that is available to offspring (_milk-energy-output_) is determined by reducing this value by the milk production efficiency (_milk-prod-eff_) (Equation 23). Then based on the amount of energy allocated to lactation relative to offspring costs, animals go through a series of checks following Figure S4. For animals which allocate more than _m-lact-max_ to lactation, their offspring grow maximally (Equation 24) and deposit additional energy into adipose tissue (Equation 25). For those which allocate less than _m-lact-max_ but more than offspring maintenance costs (_m-BMR-off_), then _m-BMR-off_ is covered and offspring grow suboptimally. And for those which allocate less than _m-BMR-off_, the offspring mobilize their own tissues to fulfill maintenance and halt growth for the timestep. At the end of the procedure, offspring mass and storage level (_mass-off_ and _SL-off_) are updated

following Equations 26 and 27, and *ds-birth* is advanced by 30 minutes (one timestep).

Table S9. *Reproduction procedure parameter definitions and values.*

Symbol	Value	Code	Description [units]	Source
Pregnancy				
n_{conc}	[2, 9]	n-emb-range	Range of number of conceived embryos [N]	*(135, 146–148)*
fg	0.112	emb-growth-c	Fetal growth constant [day^{-1}]	*(149)*
$m_{emb,0}$	6.9×10^{-8}	emb-mass-init	Fetal mass at conception [g]	*(149)*
$m_{emb,\infty}$	19.957	emb-mass-inf	Asymptotic fetal mass [g]	*(149)*
$\%_{emb,fat}$	0.38	percent-fat-emb	Fetal body composition-Fat [Prop]	*(150, 151)*
$\%_{emb,pro}$	0.102	percent-pro-emb	Fetal body composition-Protein [Prop]	*(150, 151)*
ED_{pl}	3,249.9	ED-pl	Energy density of placental tissue [J g^{-1}]	*(152)*
DE_{pl}	0.501	DE-pl	Deposition efficiency of placental tissue [Prop]	*(153)*
k_P	-	preg-prob-const	Logistic pregnancy investment steepness constant [unitless]	Calibrated
c_P	-	preg-prob-mid	Logistic pregnancy investment logistic midpoint [unitless]	Calibrated
Lactation				
$\varepsilon_{B,off}$	0.501	off-BMR-red	Relative offspring basal costs multiplier [Prop]	*(113, 114)*
$\varepsilon_{G,off}$	0.880	off-growth-eff	Efficiency of offspring growth [Prop]	*(154)*
ε_{mp}	0.825	milk-prod-eff	Efficiency of producing milk from body stores [Prop]	*(155, 156)*
k_L	-	lact-prob-const	Logistic lactation investment steepness constant [unitless]	Calibrated
c_L	-	lact-prob-mid	Logistic lactation investment logistic midpoint [unitless]	Calibrated

Table S10. *Reproduction procedure equations.*

Eq. #	Description [units]	Code	Symbol	Equation	Source
Pregnancy					
4	Fetal growth rate [g ts-1]	max-growth-emb	Δm_{emb}	$e^{\ln m_{emb}+(\frac{fg}{t_d}\cdot(\ln m_{emb,\infty}-\ln m_{emb}))} - \ln m_{emb}$	*(111)*
5	Energy for fetal fat deposition [J ts-1]	e-fat	e_{fat}	$\dfrac{\frac{\Delta m_{emb}}{1000}\cdot\%_{emb,fat}\cdot ED_{fat}}{\varepsilon_{fat}}$	-

#	Description	Name	Symbol	Formula	Ref
6	Energy for fetal protein deposition [J ts-1]	e-fat	e_{pro}	$\dfrac{\frac{\Delta m_{emb}}{1000} \cdot \%_{emb,pro} \cdot ED_{pro}}{\varepsilon_{pro}}$	-
7	Fetal tissue investment [J ts-1]	m-growth-emb	$M_{emb,t}$	$e_{fat} + e_{pro}$	(112)
8	Placental growth rate [g ts-1]	max-growth-pl	Δm_{pl}	$(-0.542 + 0.079 \cdot ds_{mating} - 0.002 \cdot ds_{mating}^2) - m_{pl}$	(110)
9	Placental tissue investment [J ts-1]	m-growth-pl	$M_{emb,pl}$	$\dfrac{\Delta m_{pl} \cdot ED_{pl}}{DE_{pl}}$	-
10	Allocation to pregnancy based on storage level [unitless]	perc-allo-preg	κ_P	$\dfrac{1}{1 + e^{-k_P\left(\frac{SL}{SL_{max}} - c_P\right)}}$	-
11	Total cost of pregnancy [J ts-1]	m-preg	M_P	$(n_{emb} \cdot (M_{emb,t} + M_{emb,pl})) \cdot \kappa_P$	-
12	Update embryo mass [kg]	mass-emb	m_{emb}	$m_{emb} + (\kappa_P \cdot \Delta m_{emb})$	-
13	Update placental mass [kg]	mass-pl	m_{pl}	$m_{pl} + (\kappa_P \cdot \Delta m_{pl})$	-
14	Update gestational mass [kg]	gest-mass	m_{gest}	$\dfrac{m_{emb} \cdot n_{emb} + m_{pl} \cdot n_{emb}}{1000}$	-
			Lactation		
15	Offspring maintenance costs [J ts-1]	m-BMR-off	$M_{B,off}$	$\displaystyle\sum_{i=off\#}^{n_{off}} B_0 m_{off}{}^{\gamma} \cdot \varepsilon_{B,off} \cdot ITV_{B,off(i)}$	(12, 140)
16	Offspring growth rate [g ts-1]	max-growth-lm-off	$\Delta m_{LM,off}$	$\dfrac{k}{t_d}\left(m_{LM,\infty}{}^{\frac{1}{3}} \cdot m_{LM,off}{}^{\frac{2}{3}} - m_{LM,off}\right)$	(12)
17	Offspring lean mass protein content [unitless]	lean-mass-perc-pro	$\%_{pro,off}$	$0.23(1 - e^{-0.06(ds_{birth}+10.19)})$	(150, 151)
18	Energy density of offspring lean mass [J kg-1]	ED-lean-mass-off	ED_{LM}	$\%_{pro,off} \cdot ED_{pro}$	-
19	Offspring costs of lean mass growth [J ts-1]	m-growth-lm-off	$M_{LM,off}$	$\dfrac{\Delta m_{LM,off} \cdot ED_{LM}}{\varepsilon_{G,off}}$	(112)
20	Allocation to lactation based on storage level [unitless]	perc-allo-lact	κ_L	$\dfrac{1}{1 + e^{-k_L\left(\frac{SL}{SL_{max}} - c_L\right)}} \cdot 2$	-
21	Estimated cost of lactation [J ts-1]	m-lact-est	$M_{Lact,e}$	$\dfrac{M_{B,off} + n_{off} \cdot M_{LM,off}}{\varepsilon_{mp}}$	-
22	Total cost of lactation [J ts-1]	m-lact	M_{Lact}	$M_{Lact,e} \cdot \kappa_L$	-
23	Milk energy output [J ts-1]	milk-energy-output	M_{mp}	$M_{Lact} \cdot \varepsilon_{mp}$	(113)
24	Offspring lean mass [kg]	lean-mass-off	$m_{LM,off}$	$\begin{cases} m_{LM,off} + \Delta m_{LM,off}, & if\, M_{Lact} > M_{Lact,e} \\[2ex] m_{LM,off} + \dfrac{\frac{M_{mp} - M_{B,off}}{n_{off}} \cdot \varepsilon_{G,off}}{ED_{LM}}, & if\, M_{Lact} < M_{Lact,e}\ \&\ M_{mp} > M_{B,off} \\[2ex] m_{LM,off} - \dfrac{\frac{M_{B,off} - M_{mp}}{n_{off}} \cdot \frac{\frac{ED_{pro}}{1000} \cdot \gamma_{mob}}{\frac{ED_{fat}}{1000} \cdot SL_{off} + \frac{ED_{pro}}{1000} \cdot \gamma_{mob}}}{ED_{LM}}, & otherwise \end{cases}$	-
25	Offspring adipose mass [kg]	adipose-mass-off	$m_{adi,off}$	$\begin{cases} m_{off} \cdot SL_{off} + \dfrac{\frac{M_{Lact} - M_{Lact,e}}{n_{off}} \cdot DE_{fat}}{ED_{fat} \cdot (1 - \%_{w,adi})}, & if\, M_{Lact} > M_{Lact,e} \\[2ex] m_{off} \cdot SL_{off}, & if\, M_{Lact} < M_{Lact,e}\ \&\ M_{mp} > M_{B,off} \\[2ex] m_{off} \cdot SL_{off} - \dfrac{\frac{M_{B,off} - M_{mp}}{n_{off}} \cdot \frac{1 - \frac{ED_{pro}}{1000} \cdot \gamma_{mob}}{\frac{ED_{fat}}{1000} \cdot SL_{off} + \frac{ED_{pro}}{1000} \cdot \gamma_{mob}}}{(1 - \%_{w,adi}) \cdot ED_{fat}}, & otherwise \end{cases}$	-
26	Offspring total mass [kg]	mass-off	m_{off}	$m_{LM,off} + m_{adi,off}$	

27	Offspring storage level [unitless]	SL-off	SL_{off}	$\dfrac{m_{adi,off}}{m_{off}}$
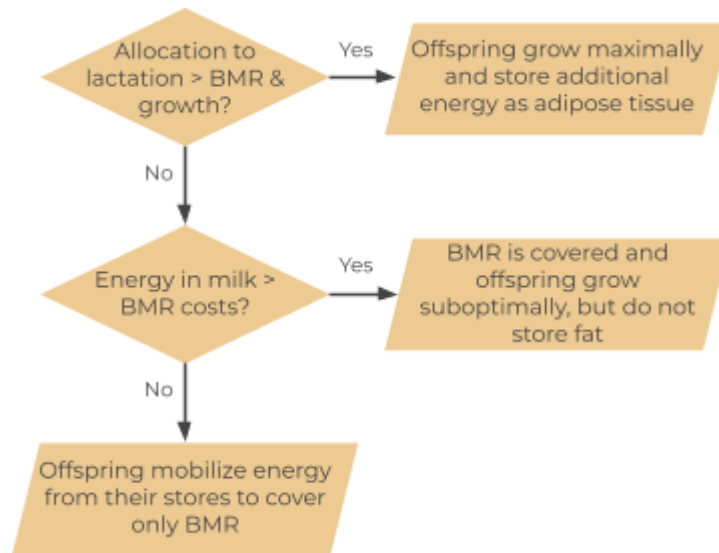
Figure S4. Lactation procedure flowchart for assessing offspring lean mass and adipose deposition based on maternal investment in a timestep.

2.7.2.1.4. Lean mass dynamics (growth-lean-mass)

Lean mass deposition can happen throughout life in the model as animals both grow in structural mass as they mature and use protein as a metabolic fuel when covering metabolic costs using stored tissues (see *storage-dynamics* for details). To estimate lean mass costs, animals first determine the protein content of their lean mass tissue (*lean-mass-perc-pro*) based on their age (Equation 28 in Table S12; Section 3.1.5; Figure S5). They then update the energy content of their tissue (*ED-lean-mass*) using the percent protein from Eqn. 28 and the energy content of protein (*ED-pro*)(Equation 29). Allocation to lean mass deposition (as a proportion; *perc-allo-growth-lm*) is then calculated based on the animal's *storage-level* and the calibrated parameters *growth-lm-prob-const* and *growth-lm-prob-mid* (Equation 30, see TRACE Section 6 for allocation curves for each of the 30 selected parameter sets). Following this step, the lean mass deposition rate (*lean-mass-depo*) is calculated following a Von Bertalanffy growth curve fit to empirical data and modified using *perc-allo-growth-lm* (Equation 31). Finally, the total cost of lean mass deposition (*m-lean-mass*) is then calculated following Equation 32. Any actual addition of lean mass does not occur until the *storage-dynamics* procedure (below).

Table S11. *Lean mass deposition procedure parameter definitions and values.*

Symbol	Value	Code	Description [units]	Source
ED_{pro}	23.5	ED-pro	Protein energy density [kJ g-1]	*(140, 151, 157, 158)*
ε_{fat}	0.735	DE-fat	Deposition efficiency of fat [Prop]	*(159)*
ε_{pro}	0.444	DE-pro	Deposition efficiency of protein [Prop]	*(159)*
k_{LM}	-	growth-lm-prob-const	Logistic lean mass deposition investment steepness constant [unitless]	Calibrated
c_{LM}	-	growth-lm-prob-mid	Logistic lean mass deposition investment logistic midpoint [unitless]	Calibrated
$m_{LM,\infty}$	0.0264	growth-lm-inf	Asymptotic lean mass [kg]	*(115, 150, 151, 160–162)*
k	0.0964	growth-lm-k	Lean mass growth constant [day⁻¹]	*(115, 150, 151, 160–162)*

Table S12. *Lean mass deposition procedure equations.*

Eq. #	Description [units]	Code	Symbol	Equation	Source
28	Lean mass protein content [unitless]	lean-mass-perc-pro	$\%_{pro,LM}$	$0.23(1 - e^{-0.06(age+10.19)})$	*(150, 151)*
29	Energy density of lean mass [J kg-1]	ED-lean-mass	ED_{LM}	$\%_{pro,LM} \cdot EDpro$	-
30	Allocation to lean mass deposition based on storage level [unitless]	perc-allo-growth-lm	κ_{LM}	$\dfrac{1}{1 + e^{-k_{LM}(\frac{SL}{SL_{max}} - c_{LM})}}$	-
31	Lean mass deposition rate [kg ts-1]	lean-mass-depo	Δm_{LM}	$\dfrac{k \cdot \kappa_{LM}}{t_d}((m_{LM,\infty} \cdot \kappa_{LM})^{\frac{1}{3}} \cdot m_{LM}^{\frac{2}{3}} - m_{LM})$	*(12)*
32	Cost of lean mass deposition [J ts-1]	m-lean-mass	M_{LM}	$\dfrac{\Delta m_{LM} \cdot ED_{LM}}{DE_{pro}}$	*(112)*
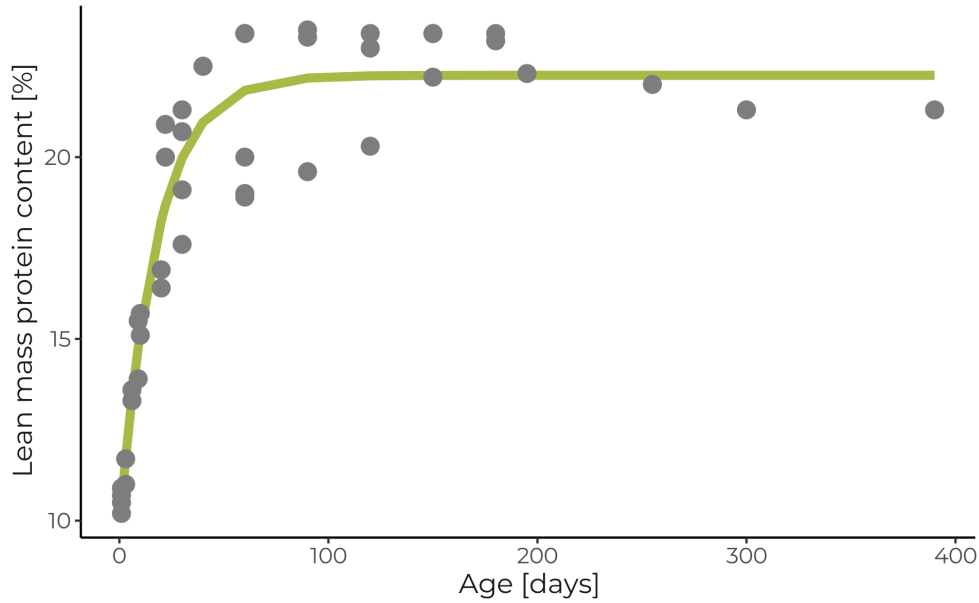
Figure S5. Relationship between age (in days) and the protein content of lean mass tissue (%). Fitted relationship shown in the green line, while grey points represent empirical data (*150, 151*).

2.7.2.2. Update records of total energy use and other monitors (*update-records*)

In this step animals update their total energy use (*M*) as the sum of all metabolic costs calculated in the timestep (Table S13). This value is then added to the list *daily-m-tot* to keep track of costs experienced over the last 48 timesteps (1 day).

Additionally, any outputs used for calibration, sensitivity analysis, or evaluation steps (see TRACE Sections 6 - 8) are collected in this procedure.

Table S13. *Equation used for updating total energy use.*

Eq. #	Description [units]	Code	Symbol	Equation	Source
33	Total energy use [J ts-1]	m-tot	M	$M_{HIF} + M_B + M_{CoT} + M_P + M_{Lact} + M_{LM}$	-

2.7.2.3. Energy intake (*energy-intake*)

The amount of energy consumed in a timestep varies based on a variety of factors including animal energy costs, their stomach capacity, energy balance, and the amount of food available on the resource cell they encounter in a foraging bout.

A series of calculations are performed in this procedure, starting with the determination of variables related to the stomach capacity of animals. First, a modifier (*stomach-mod*) is calculated which augments a base equation for mammal

gut transit time (*stomach-clear-rate*) and maximum stomach fill (*stomach-fill-max*). This modifier is based on the elevation of the metabolic costs of basal metabolic rate, pregnancy, and lactation over the basal maintenance costs of an animal of the same size (Equation 34). This allows animals with elevated costs due either to reproductive constraints or increased maintenance costs to achieve a relatively higher stomach capacity and reduced clearance time, which have both been documented in rodent species (see Section 4). The modifier is then used to calculate *stomach-clear-rate* and *stomach-fill-max* following equations 35 and 36.

Following the determination of stomach capacity and clearance rate, the ingestion rate required to meet energetic requirements for the timestep (*IR-timestep*) is then calculated. To do so, the total energetic requirements (*m-tot*) is reduced by the losses associated with the heat increment of feeding (*m-HIF*). After which, this value is converted to food mass using the assimilation efficiency of food (*AE-food*), heat increment of feeding (as a proportion; *HIF*), and energy density of food items (*ED-food*) (Equation 37). To adjust this value by the current *storage-level* of animals, another modifier is calculated, here called the *IR-mod*. This process is rooted in the dual intervention point model (*28*), which posits that body fat is regulated at two distinct points. Specifically, the hypothesis proposes that animals attempt to increase their fat stores at low body fat percentages, where the potential for surviving periods of fasting due to illness becomes a concern. Conversely, hunger decreases at high body fat percentages, as the risks associated with predation increase dramatically. To implement this hypothesis into the model, first a scaled version of the *storage-level* (*SL-scaled*) is calculated depending on whether the current storage level falls over the upper intervention point (UIP) or below the lower intervention point (LIP) (Equation 38). Here, as a first implementation of dual intervention point theory into an energy budget model, we assumed a symmetrical curve with an unregulated zone centered around the midpoint of potential body fat values, allowing for a tolerance of plus and minus 1.5% body fat. This resulted in a LIP of 18.4% and UIP of 21.4% body fat, though these values can be reparameterized with empirical data when available, potentially leading to asymmetrical curves or variations in the distances between the UIP and LIP. *SL-scaled* is then fed into Equation 39 to determine *IR-mod* for the timestep (see Figure S6 for the resulting relationship of *IR-mod* with *storage-level*).

To allow animals to keep track of their energy balance and make up for lost foraging opportunities (following Gallagher *et al*., 2021), a variable was introduced called *food-debt*. This variable is updated twice during the *energy-intake* procedure, the first time being after the values for *IR-timestep* and *IR-mod* are calculated to determine the total amount of food that an animal would need to eat to meet its energetic and storage requirements. In this step, the product of *IR-timestep* and *IR-mod* is added to the current value of *food-debt* (Equation 40). Animals that are actively foraging at a given timestep (as determined by a non-zero *move-speed*, as described in Sections 2.7.1 and 2.7.2.1.2) will interact with the cell in which they are foraging by asking it to update its *resource-level* via the execution of the

resources-grow procedure (detailed in Section 2.7.2.5). This update is contingent upon the cell having a *resource-level* below the *max-resources* and not having already run the <u>resources-grow</u> procedure during that timestep. They then run a series of comparisons to assess how much food should be consumed (*IR-real*). First, an initial value of *IR-real* is determined to be equal to either the *food-debt*, *resource-level* of the cell, or *IR-max* based on their relative values (Equation 41). This value is then compared to *stomach-fill-max* to ensure that animals do not exceed their stomach capacity (Equation 42). *Food-debt* is then reduced by *IR-real* (Equation 43), *stomach-fill* is updated, and values for metabolizable energy intake (*MEI*), losses associated with the heat increment of feeding (*m-HIF*), and assimilated energy (*energy-assimilated*) are calculated following equations 44, 45, and 46, respectively.

It is important to note that, as currently implemented, the model primarily represents reactive behavior in animals, where they attempt to meet their costs and maintain their body stores. The model does not currently incorporate anticipatory behaviors, such as seasonal hyperphagia, which can be observed in some species. However, this is an area that could be explored in future developments of the model, particularly for applications that require a more detailed understanding of these behaviors.

Table S14. *Energy intake procedure parameter definitions and values.*

Symbol	Value	Code	Description [units]	Source
$\%_{SF}$	0.0507	stomach-fill-perc	Stomach fill as proportion of body mass [Prop]	*(132)*
AE	0.836	AE-food	Assimilation efficiency of food [Prop]	*(132, 164–166)*
HIF	0.228	HIF	Heat increment of feeding as a proportion of ingested energy [Prop]	*(167, 168)*
DM	0.67	DM-food	Dry matter content of foodstuffs [Prop]	*(132)*
ED	12281.1	ED-food	Energy density of foodstuffs [J g-1 wet mass]	*(132)*

Table S15. *Energy intake procedure equations.*

Eq. #	Description [units]	Code	Symbol	Equation	Source
34	Stomach fill modifier [Prop]	stomach-mod	SF_{mod}	$\dfrac{M_B + M_P + M_{Lact}}{M_B}$	-
35	Stomach clear rate [ts-1]	stomach-clear-rate	SF_{clear}	$5.473m^{0.278} \cdot 2((SF_{mod} - 1) \cdot -1 + 1)$	*(169)*(base equation)
36	Maximum stomach fill [g]	stomach-fill-max	SF_{max}	$\dfrac{m \cdot 1000 \cdot \%_{SF}}{DM} \cdot SF_{mod}$	-
37	Total potential ingestion rate for a timestep [g ts-1]	IR-timestep	IR_{ts}	$\dfrac{M - M_{HIF}}{AE \cdot ED \cdot (1 - HIF)}$	*(170)*
38	Scaled storage level from 0 to 1 [unitless]	SL-scaled	SL_{scaled}	$\dfrac{SL}{0.184},$ $\quad if\ SL < 0.184$	Based on theory in *(28)*

39	Ingestion rate modifier based on scaled storage level [unitless]	IR-mod	IR_{mod}	$\dfrac{SL - 0.214}{SL_{max} - 0.214},\quad if\ SL > 0.214$ $(-SL_{scaled} + 1)^3 + 1,\quad if\ SL < 0.184$ $(-SL_{scaled})^3 + 1,\quad if\ SL > 0.214$ $1,\quad otherwise$	Based on theory in (28)
40	Record of unmet food requirements [g]	food-debt	FD	$FD + IR_{ts} \cdot IR_{mod}$	(163)
41	Ingestion rate [g ts-1]	IR-real	IR_{real}	$FD,\quad if\ U[c] > FD < IR_{max}$ $U[c],\quad if\ IR_{max} > U[c] < FD$ $IR_{max},\quad otherwise$	(163)
42	Realized ingestion rate adjusted for stomach fill [g ts-1]	IR-real	IR_{real}	$IR_{real},\quad if\ IR_{real} + \Sigma SF < SF_{max}$ $\Sigma SF - IR_{real},\quad otherwise$	-
43	Update record of unmet food requirements [g]	food-debt	FD	$FD - IR_{real}$	(163)
44	Metabolizable energy intake [J ts-1]	MEI	MEI	$IR_{real} \cdot AE \cdot ED$	-
45	Heat of increment of feeding [J ts-1]	m-HIF	M_{HIF}	$MEI \cdot HIF$	-
46	Assimilated energy [J ts-1]	energy-assimilated	EA	$MEI \cdot (1 - HIF)$	-
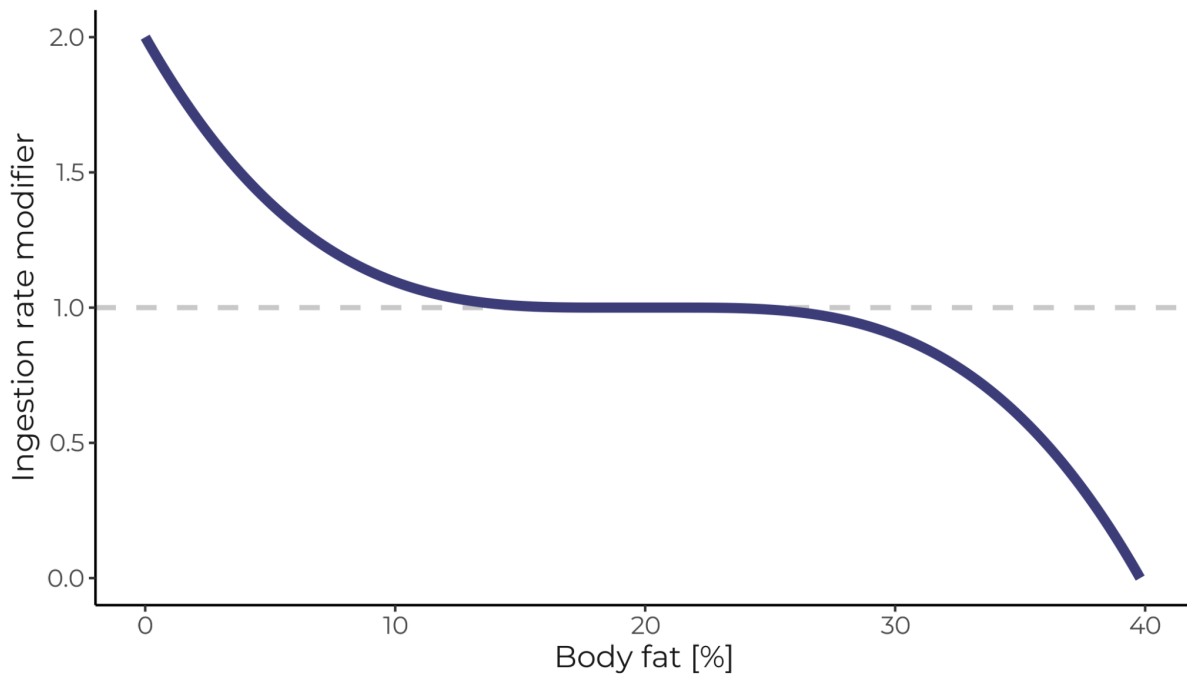
Figure S6. Relationship between body fat (storage-level, %) and the ingestion rate modifier parameter IR-mod (proportion).

2.7.2.4. Energy allocation (energy-allocation)

After costs are estimated in the _energy-budget_ and ingestion determined in _energy-intake,_ these costs are compared here in the _energy-allocation_ procedure to assess the net amount of energy assimilated or mobilized in the timestep

(*energy-assimilated* and *energy-mobilized*, respectively). To do this, animals check whether the value of *energy-assimilated* they calculated in the energy intake step exceeds their total energy expenditure (*m-tot* reduced by the heat increment of feeding, *m-HIF*). If so, they simply reduce their assimilated energy by this value (*energy-assimilated* - (*m-tot* - *m-HIF*)). If not, they use the available assimilated energy and mobilize the remainder by calculating the difference between energy use and intake ((*m-tot* - *m-HIF*) - *energy-assimilated*), resetting *energy-assimilated* to zero, and adding the remainder to *energy-mobilized* to be catabolized from stored tissues in the *storage-dynamics* procedure.

2.7.2.5. Adipose and lean mass dynamics (*storage-dynamics*)

The *storage-dynamics* procedure simulates the dynamics of animal protein and fat stores based on their current *storage-level* and the amount of energy either assimilated or mobilized, as determined by the *energy-allocation* process. The procedure begins by calculating the ratio of metabolic fuels that should be used at the current *storage-level*, referred to as the protein contribution to storage dynamics (*pro-storage-perc*; as described in equation 47). This allows the model to simulate the way animals primarily deposit or mobilize adipose tissue when at high body percentages, while catabolizing or synthesizing progressively more lean mass as stores decline (as illustrated in Figure S7). This procedure is based on Forbes' theory (*32*), which posits that there is a dynamic relationship between protein and fat stores and the way these stores are utilized in response to changes in body composition.

The amount of lean mass mobilized or synthesized is first calculated in terms of energy as the product of either *energy-mobilized* or *energy-assimilated* and *pro-storage-perc* (Equations 48 & 49). Adipose dynamics instead use the inverse of *pro-storage-perc* and are instead determined in units of mass using the parameters for the deposition efficiency and energy density of fat (*DE-fat* and *ED-fat*) and the percent water of adipose tissue (*perc-water-adi*) (Equations 50 & 51). The total change in lean mass stores, called the energy flux from lean mass (*e-diff*), is then calculated by comparing the sum of the energy deposited as lean mass in the *growth-lean-mass* procedure (Equation 32) and the amount of lean mass synthesized due to positive energy balance (determined in *energy-allocation*) to the amount of energy mobilized as lean mass (Equation 52). Then depending on whether this value is negative (a net mobilization of lean mass tissue) or positive (net deposition), animals use the relevant energy content and deposition efficiency parameters to calculate the mass of lean mass either catabolized or deposited (*lean-mass-change*; Equation 53).

Based on the resulting changes in lean and adipose mass, the animal then updates its state variables *lean-mass*, *adipose-mass*, *mass*, and *storage-level* (Equations 54 - 57). A final check is done to ensure that the storage levels and mass of animals do not drop below zero. If they do, then the animal dies.

Table S16. *Adipose and lean mass dynamics procedure parameter definitions and values.*

Symbol	Value	Code	Description [units]	Source
ED_{fat}	39.1	ED-fat	Fat energy density [kJ g-1]	*(151, 157, 158)*
$ED_{c,pro}$	19.1	ED-cpro	Energy density of catabolized protein [kJ g-1]	*(140, 157)*
γ_{mob}	0.015	gamma-mobilize	Fuel partitioning constant [Unitless]	*(119–121)*
$\%_{w,adi}$	0.119	perc-water-adi	Water percent in adipose tissue [Prop]	*(171, 172)*
SL_{max}	0.398	SL-max	Maximum storage level [Prop]	Maximum value in Fedyk 1974 +1SD, adjusted for water content

Table S17. *Adipose and lean mass dynamics procedure equations.*

Eq. #	Description [units]	Code	Symbol	Equation	Source
47	Protein contribution to storage dynamics [unitless]	pro-storage-perc	$\%_{SD,pro}$	$\dfrac{ED_{pro} \cdot \gamma_{mob}}{ED_{fat} \cdot SL + ED_{pro} \cdot \gamma_{mob}}$	*(31)*
48	Lean mass synthesized [J ts-1]	lean-mass-synthesized-energy	$e_{syn,LM}$	$EA \cdot \%_{SD,pro}$	-
49	Lean mass mobilized [J ts-1]	lean-mass-mobilized-energy	$e_{mob,LM}$	$EM \cdot \%_{SD,pro}$	-
50	Adipose synthesized [kg ts-1]	adipose-synthesized	$m_{syn,adi}$	$\dfrac{EA \cdot (1 - \%_{SD,pro}) \cdot DE_{fat}}{ED_{fat} \cdot (1 - \%_{w,adi})}$	-
51	Adipose mobilized [kg ts-1]	adipose-mobilized	$m_{mob,adi}$	$\dfrac{EM \cdot (1 - \%_{SD,pro})}{ED_{fat} \cdot (1 - \%_{w,adi})}$	-
52	Energy flux from lean mass [J ts-1]	e-diff	Δe_{LM}	$e_{syn,LM} + M_{LM} - e_{mob,LM}$	-
53	Realized lean mass flux [kg ts-1]	lean-mass-change	Δm_{LM}	$\dfrac{\Delta e_{LM} \cdot DE_{pro}}{ED_{LM}}, \quad if \Delta e_{LM} > 0$ $\dfrac{\Delta e_{LM}}{\%_{pro} \cdot ED_{c,pro}}, \quad otherwise$	-
54	Update lean mass [kg]	lean-mass	m_{LM}	$m_{LM} + \Delta m_{LM}$	-
55	Update adipose mass [kg]	adipose-mass	m_{adi}	$m_{adi} + m_{syn,adi} - m_{mob,adi}$	-
56	Update total mass [kg]	mass	m	$m_{LM} + m_{adi} + m_{gest}$	-
57	Update storage level [unitless]	storage-level	SL	$\dfrac{m_{adi}}{m - m_{gest}}$	-
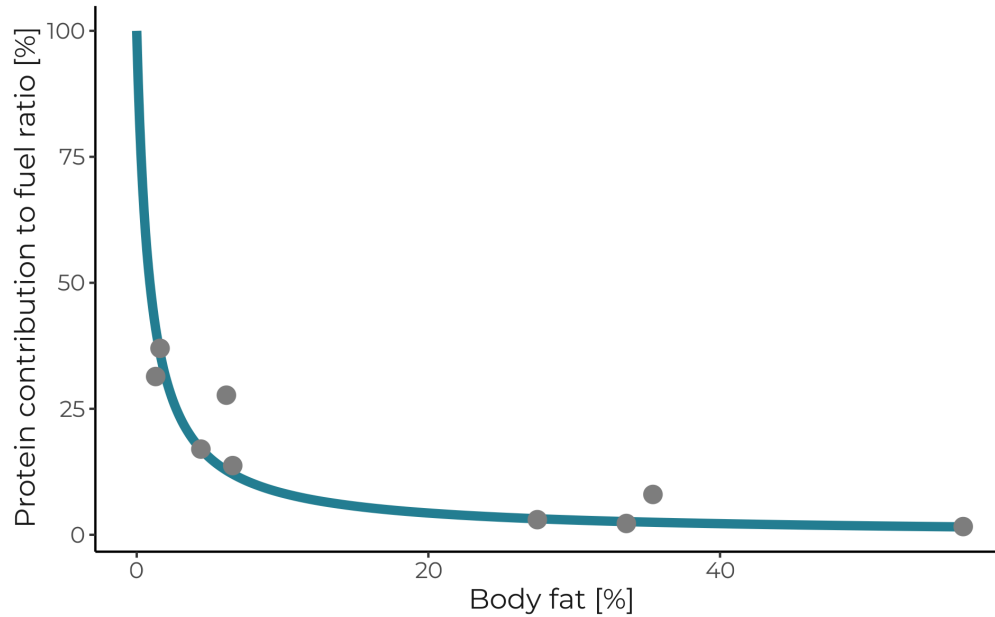
Figure S7. Relationship between body fat (storage-level; %) and the contribution of protein to mobilized or synthesized metabolic fuels (%). Fitted relationship shown in the blue line, while grey points represent empirical data.

2.7.2.5. Resource growth dynamics (resources-grow)

The resources-grow procedure is executed by resource cells, and is triggered by animals foraging on a resource cell during the energy-intake process (see Section 2.7.2.3 above). The procedure begins by estimating the amount of food that should be accumulated (r-growth) based on: 1) the number of timesteps that have passed since the last replenishment of resources, and 2) the parameter determining the amount of resource accumulation per timestep (r-growth-ts). The cell then increases its resource-level by the calculated r-growth value. The procedure concludes by checking if the resource-level would exceed the maximum resources, and if so, it reduces the resource-level to max-resources.

2.7.3. Life-history processes (demographics)

The processes modelled in the life history module (demographics) can be broken up into those which affect reproductive (give-birth and wean) and mortality (mortality-max-age, mortality-starvation, and mortality-overwinter) rates (Figure S8).
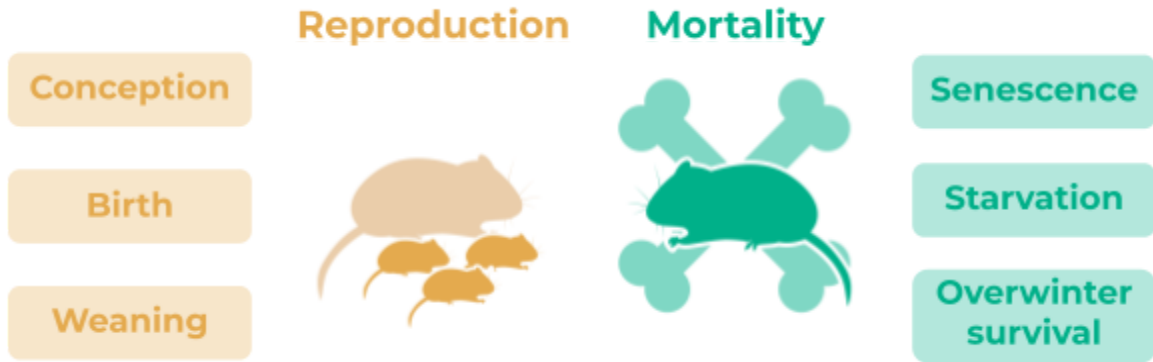
Figure S8. Life history processes driving population demographics.

2.7.3.1. Reproduction

The model includes three procedures, _conceive_, _give-birth_, and _wean_, which simulate life history events related to reproduction. These procedures utilize a set of parameters that pertain to the timing and duration of the reproductive stages of conception, birth, and weaning (as outlined in Table S18).

Table S18. _Life history procedure parameter definitions and values for reproductive processes._

Symbol	Value	Code	Description [units]	Source
t_{mating}	[121, 273]	t-mating	Mating days [day of year]	_(50, 57, 135)_
t_{mature}	45	t-mature	Age of female maturity [days]	_(57, 173, 174)_
$P(O)$	0.22	prob-ovul	Probability of ovulation on a given day [Prob]	_(175)_
t_0	4	t-0	Implantation delay for lactating females [days]	_(146, 176)_
t_{gest}	20	t-gest	Gestation time [days]	_(50, 164, 176)_
t_{nurs}	21	t-nurs	Nursing time [days]	_(57, 164, 177, 178)_

2.7.3.1.1. Conception (_conceive_)

Once per day, animals which are not pregnant check if they should conceive offspring. First they ensure that they are of age (> _t-mature_) and that the day of the year falls within the breeding period (adjusted for the pregnancy and lactation lengths as animals outside of this period should not have dependent offspring). If all conditions are met, animals then pull a random float value which is less than 1 and compare this to the chance of implantation (_prob-ovul_) of 0.22, based on the ovulation cycle of 4.5 days reported for bank voles (_175_). If the random value is less

than *preg-chance*, animals proceed to get pregnant and initialize a suite of state variables for the pregnancy period (Table S19).

Table S19. *State variables updated in the conceive procedure.*

Description [unit]	Code	Updated value
Pregnancy status [true or false]	pregnancy-status	true
Days since mating [days]	ds-mating	0, if lactation-status = false -t-0, if lactation-status = true
Number of embryos [N]	n-emb	U(n-emb-range)
Mass of embryo [g]	mass-emb	emb-mass-init
Mass of placental tissue [g]	mass-pl	0

2.7.3.1.2. Give birth (*give-birth*)

At the start of the pregnancy procedure (see Section 2.7.2.1.3 above), pregnant animals first check if the number of days since mating (*ds-mating*) has reached the gestation length (*t-gest*). If so, these animals then execute the *give-birth* procedure.

In the rare chance that animals already have dependent offspring, they first wean (*wean*) these offspring before giving birth. They then initialize a suite of state variables for the lactation period (Table S20). Animals then finish by calling the *lactation* procedure (Section 2.7.2.1.3 above) to calculate their lactation costs for the timestep.

Table S20. *State variables updated in the give-birth procedure.*

Description [unit]	Code	Updated value
Pregnancy status [true or false]	pregnancy-status	false
Lactation status [true or false]	lactation-status	true
Number of offspring [N]	n-off	n-emb
Number of embryos [N]	n-emb	0
Mass of dependent offspring [kg]	mass-off	mass-emb / 1000
Storage level of offspring [unitless]	SL-off	percent-fat-emb
Mass of embryo [g]	mass-emb	0
Mass of placental tissue [g]	mass-pl	0
Lean mass of dependent offspring [kg]	lean-mass-off	mass-off × (1 - SL-off)
Gestational mass (combined mass of embryos and placentae) [kg]	gest-mass	0
Days since mating [days]	ds-mating	0
Metabolic cost of pregnancy [J ts-1]	m-preg	0

2.7.3.1.3. Wean offspring (*wean*)

At the start of the lactation procedure (see section 2.7.2.1.3 above), animals with dependent offspring first check if the number of days since giving birth (*ds-birth*)

has reached the duration of the nursing period (*t-nurs*). If so, then animals execute the *wean* procedure.

At the start of the procedure, animals set their *lactation-status* to false. They then create a new animal for each offspring (*n-off*) by asking the cell they are on to "sprout" one agent per offspring. Upon creation, each new turtle retains its *mass*, *storage-level*, *adipose-mass*, *lean-mass*, and *age* values (from prior to weaning). The animal then sets its *pregnancy-* and *lactation-status* variables to false and initializes the lists *stomach-fill*, *daily-ingestion*, *daily-activity*, and *daily-m-tot* to empty ("[]"; see Table S1 for variable details). It then selects its home range core cell (*home-c*) by first checking if there are any available resource cells which are not the *home-c* of another animal. If so, the animal randomly selects one of these empty resource cells, if not, then it selects a resource cell at random and sets this cell as its *home-c*.

As the mothers go through this process of weaning their offspring one by one, they reduce their *n-off* value by one until all offspring are sprouted. They then reset their lactation variables to the values in Table S21.

Table S21. *State variables updated in the wean procedure.*

Description [unit]	Code	Updated value
Lactation status [true or false]	lactation-status	false
Days since giving birth [days]	ds-birth	0
Mass of dependent offspring [kg]	mass-off	0
Storage level of offspring [unitless]	SL-off	0
Lean mass of dependent offspring [kg]	lean-mass-off	0
Basal metabolic rate of dependent offspring [J ts-1]	m-BMR-off	0
Metabolic cost of lean mass growth of nursing offspring [J ts-1]	m-growth-lm-off	0
Metabolic cost of lactation [J ts-1]	m-lact	0

2.7.3.2. Mortality

Mortality in the model is simulated through three independent processes: senescence (*mortality-max-age*), starvation (*mortality-starvation*), and overwinter mortality (*mortality-overwinter*). These processes are governed by a set of parameters, which are described in Table S22. In addition, three equations used for determining starvation-related mortality are also provided in Table S23.

Table S22. *Mortality procedure parameter definitions and values.*

Symbol	Value	Code	Description [units]	Source
t_{maxage}	620	t-max-age	Maximum age [days]	*(115, 150, 162, 173)*
k_S	-	surv-prob-const	Logistic survival probability steepness constant [unitless]	Calibrated
c_S	-	surv-prob-mid	Logistic survival probability logistic midpoint [unitless]	Calibrated
$\beta_{mod,emb}$	-	surv-mod-emb	Embryo survival probability modifier [unitless]	Calibrated
$\beta_{mod,off}$	-	surv-mod-off	Offspring survival probability modifier [unitless]	Calibrated
β_W	0.288 [0.2, 0.632]	winter-surv	Female mean overwinter survival probability (range in brackets) [Prop]	*(56, 57, 179–181)*

Table S23. *Mortality procedure equations.*

Eq. #	Description [units]	Code	Symbol	Equation	Source
58	Survival probability [unitless]	surv-prob	β_A	$\dfrac{1}{1 + e^{-k_S(\frac{SL}{SL_{max}} - c_S)}}$	*(182, 183)*
59	Embryo survival probability [unitless]	surv-prob-emb	β_{emb}	$\dfrac{1}{1 + e^{-k_S \cdot (1 + (1 - \beta_{mod,emb}))(\frac{SL}{SL_{max}} - c_S \cdot \beta_{mod,emb})}}$	-
60	Offspring survival probability [unitless]	surv-prob-off	β_{off}	$\dfrac{1}{1 + e^{-k_S \cdot (1 + (1 - \beta_{mod,off}))(\frac{SL}{SL_{max}} - c_S \cdot \beta_{mod,off})}}$	-

2.7.3.2.1. Mortality due to reaching the maximum age (*mortality-max-age*)

This procedure is called once per day as part of the *daily-tasks* procedure. For this, animals simply check if their *age* exceeds the parameter value for maximum age (*t-max-age*), and, if it does, they die. Aging also occurs within the *daily-tasks* procedure.

2.7.3.2.2. Mortality due to starvation (*mortality-starvation*)

The starvation-related mortality procedure (*mortality-starvation*) is called once per day, also within the *daily-tasks* procedure, though a check also occurs at the start of the *lactation* procedure to ensure any offspring which should die do so before the start of the lactation calculations.

This procedure is broken into three parts: one to assess adult mortality, another for determining when abortions occur, and the third for determining dependent offspring death. All follow the same general approach, but differ in their calculation of survival probability and which variables are affected when a death occurs.

For adult mortality, animals first determine their survival probability (*surv-prob*) based on their current *storage-level* and the calibrated parameters *surv-prob-const* and *surv-prob-mid* (see Equation 58 in Table S23). Then animals roll a random-float with a maximum value of 1 and if this value exceeds their *surv-prob* value, they die.

When assessing whether any abortions should occur, animals calculate the embryo survival probability (*surv-embryo-prob*) based on the *storage-level* of the mother and the calibrated parameters s*urv-prob-const*, *surv-prob-mid*, and *surv-mod-embryo* (see Equation 59 in Table S23). They then assess whether each individual embryo should die by rolling a random-float with a maximum value of 1 for each embryo (temporary variable *prob-emb*) and then checking if *prob-emb* exceeds *surv-embryo-prob*. If it does, then that embryo dies and the variables *n-emb* and *gest-mass* are updated accordingly. If by the end of the check, all embryos have died (*n-emb* = 0), then the females set their *pregnancy-status* variable to false and the values of the variables *mass-pl*, *mass-emb*, *ds-mating*, and *m-preg* all to zero.

The process of determining when dependent offspring mortality occurs is similar to that of abortion, except here the survival probability (*surv-prob-off*) depends on the storage level of the offspring itself (*SL-off*) and the calibrated parameters s*urv-prob-const*, *surv-prob-mid*, and *surv-mod-off* (see Equation 60 in Table S23). Again animals roll a survival probability value for each offspring (temporary variable *prob-off*) and compare this to the *surv-prob-off* value. Additionally a check is done to assess whether offspring have a mass, lean mass, or storage level value below zero. If any of these conditions are met, then the offspring dies and the mothers variable *n-off* is updated accordingly. If all offspring die, then the mother ceases nursing and resets lactation related variables to the values in Table S21.

2.7.3.2.3. Overwinter mortality (*mortality-overwinter*)

When the model is set up to skip the winter period (the default setting of *overwinter-skip?* = true), overwinter mortality is triggered on the last day of the year. In this procedure, the observer first selects the year's overwinter mortality value (*yr-overwinter-mortality*) using a random pull from the *winter-surv* range (see Table S22). Then the observer randomly asks a number of animals equal to the population size multiplied by *yr-overwinter-mortality* (rounded) to die.

3. Data evaluation

This TRACE element provides supporting information on: The quality and sources of numerical and qualitative data used to parameterize the model, both directly and inversely via calibration, and of the observed patterns that were used to design the overall model structure. This critical evaluation will allow model users to assess the scope and the uncertainty of the data and knowledge on which the model is based.

Summary:

The model is composed of 60 parameters, primarily concerning the computation of animal energetics. In this section, we outline how certain parameter values were established. We have divided this description into three categories: 1) data employed for parameters acquired during the fitting of equations to empirical observations, 2) data utilized for inverse parameterization or calibration of parameters, and 3) data acquired directly from literature sources to determine parameter values. For comprehensive tables containing parameter values and sources categorized by each model procedure, please refer to Section 2. For additional information on model calibration, please refer to Section 6.

3.1. Data used to fit model equations

The values of parameters driving several relationships in the model were obtained by fitting models to empirical data obtained from peer reviewed literature. This approach was used to inform parameters related to basal metabolic rate, costs of transport, fetal and adult growth, and metabolic fuel use.

3.1.1. Basal metabolic rate

To derive the allometric relationship used to calculate basal metabolic costs (BMR), empirical values of bank vole BMR and body masses (n = 172) were pulled from three publications (*137–139*) and converted to units of Joules per 30 min. We used the basic equation format from the metabolic theory of ecology (*184*):

$$M_B = B_0 m^\gamma$$

to fit four alternative models to the data in R statistical software (*130*) using the *lm* function from the base package "stats" and the *gls* function from the "nlme" package (*185*). Data from control and herbivorous lines were utilized where relevant, as these lines exhibited similar BMR values. We assessed model fit using AIC and determined that a simple *gls* model, fitting log transformed BMR and body mass, provided the best fit (AIC of -491.6) (Figure S9). The interspecific scaling exponents obtained of 0.64 was comparable to the value of 0.618 ± 0.04 found for small (<500 g) rodents in (*186*).
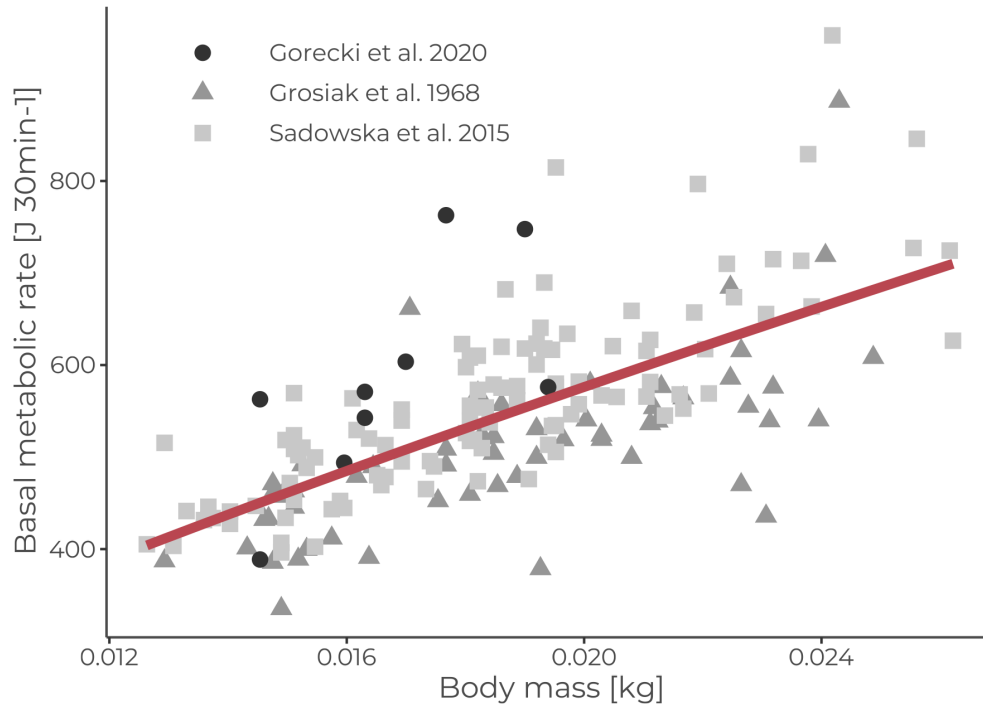
Figure S9. The relationship between body mass and basal metabolic rate. Red line represents the fitted equation used in the model and grey points are empirical values pulled from the three literature sources, with color and shape denoting the exact source for each point.

It's important to consider that using total body mass to estimate basal metabolic rate (BMR) may introduce inaccuracies as it includes adipose tissue, which is relatively metabolically inert. This means that an animal with a higher fat mass may have a higher BMR than it should based on its lean mass, and vice versa for lean animals. However, if the storage levels of the empirical animals are accurately modeled, this shouldn't result in any deviations (see calibration of this pattern in Section 6). Though it's also worth noting that plasticity in BMR could also produce similar patterns (*93, 187–189*), but this is likely driven by different mechanisms.

If values for lean mass, including metabolically active adipose tissues such as brown fat, are available for the empirical animals, it may be better to fit the relationship to these values instead of total body mass. However, in the current implementation, these data were not available.

3.1.2. Cost of transport

To determine the total cost of transport for an animal moving at a specific speed, two cost components need to be considered: postural costs associated with maintaining an elevated posture and incremental costs associated with moving the body forward at that movement speed. Incremental costs were calculated using the universal allometric relationship presented in (*109*). However, since there are no similar

relationships available for postural costs, we estimated these costs using literature values (*141–143*), which presented data for similarly sized rodents (n = 5). We employed the basic equation format shown below and the *gls* function from the "nlme" package (*185*) to estimate parameter values:

$$M_{pCoT} = B_{pCoT}m^{\gamma_{pCoT}}$$

Representing postural costs as mass-dependent aligns with empirical findings (*108, 190*), and, though few, the resulting postural cost parameter values fit the empirical data well (Figure S10).
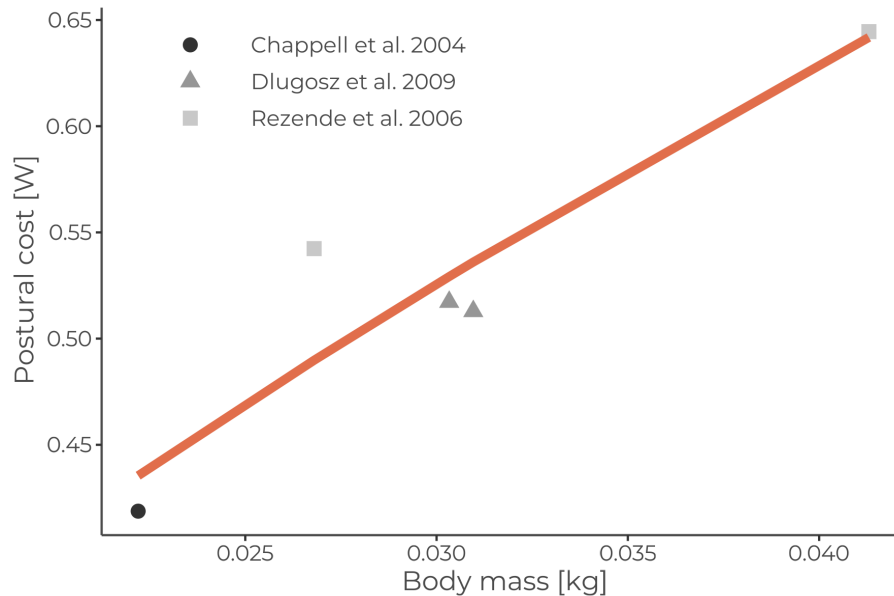
Figure S10. The relationship between body mass and the postural cost of transport (or the costs of maintaining an upright posture). Orange line represents the fitted equation used in the model and grey points are empirical values pulled from the three literature sources, with color and shape denoting the exact source for each point.

Although we would have preferred to use more than the five data points available, the estimated postural costs, along with the calculated basal maintenance and incremental costs, resulted in total metabolic costs of activity that were consistent with empirical patterns (see Figure S16).

3.1.3. Fetal growth curves

To establish the maximum fetal growth rates, we utilized empirical fetal masses from at birth and 10 - 15 days of development (*50, 149*). To ensure that our curve represented maximal growth, which can be reduced with decreasing storage level of the mother (see Section 2), we selected only the highest values for each date from the two literature sources. Subsequently, we fit these maximal values with a Gompertz equation (*111*) (Figure S11).
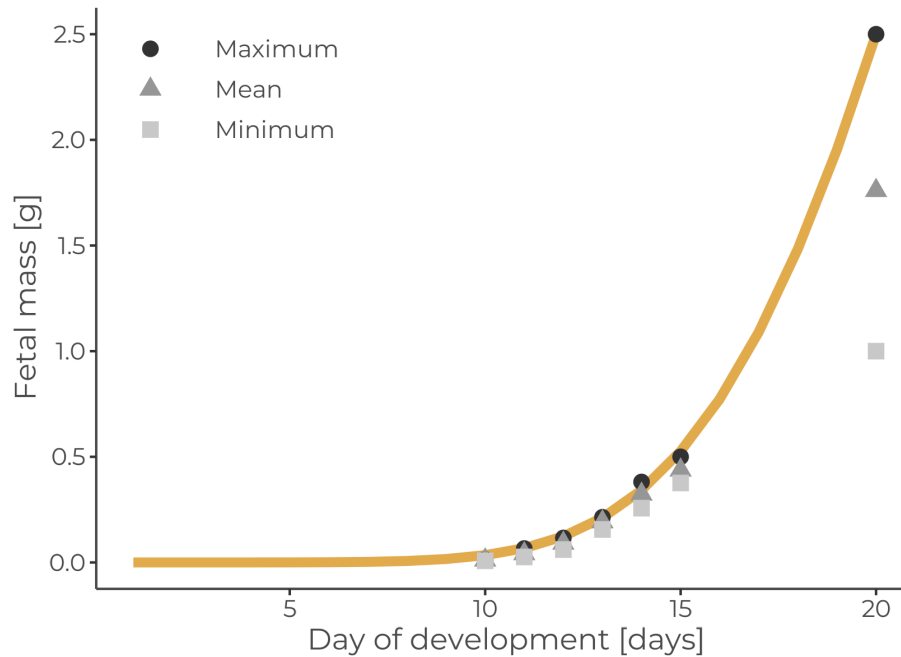
Figure S11. The relationship between the fetal day of development (or day in the gestation period) and fetal masses. Yellow line represents the fitted equation used in the model and grey points are empirical values pulled from Koivula et al. 2003 and Ożdżeński & Mystkowska 1976, with color and shape denoting whether each point corresponds to the maximum, mean, or minimum value reported for that day.

3.1.4. Lean mass growth curves

To determine the parameter values driving the lean mass deposition rates associated with somatic growth, we fitted Von Bertalanffy curves to empirical data of bank vole body mass (*12*). These values were extracted from six literature sources, comprising 134 data points. However, as some of the animals did not have lean mass measurements, we estimated lean mass for these animals based on the relationship between body mass and adiposity in (*150*). We fitted two curves, one to all points, representing the average lean mass growth across all studies, and the other a maximum growth curve, using a subset of animals identified as extremely large in (*115*)(Figure S12). The maximum growth curve drove maximum lean mass growth in model simulations, which was then modified based on storage level (see Section 2), while the average growth curve was used as a calibration pattern (see Section 6).
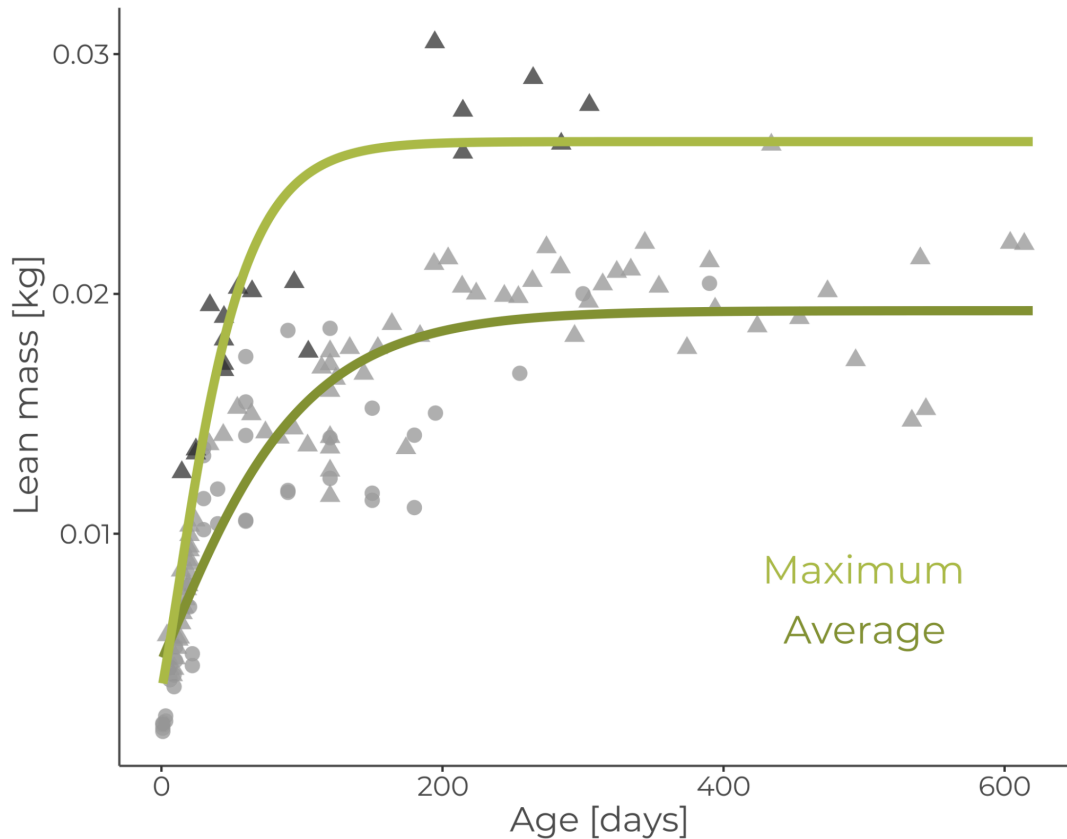
Figure S12. The relationship between age and lean mass. Light green line represents the fitted equation used in the model for maximum growth and the dark green line was used as a pattern for model calibration. Grey points are empirical values pulled from six literature sources. Inferred lean masses are shown as triangles, measured lean masses as circles.

3.1.5. Lean mass percent protein and mobilization

To model lean mass deposition and mobilization, the protein content of lean mass tissue is required. However, this value is known to vary with age in bank voles (*150*, *151*). To represent this relationship, values for protein content of lean mass were taken from two empirical studies (*150*, *151*) and a Von Bertalanffy curve was fit to the dataset. This revealed that protein content increased with age for young animals, then stabilized at values of 22% protein at ~90 days of age (see Figure S5).

Animals typically follow the stages of mammalian starvation, which involve glycogen use (Stage I), switching to primarily fat use as glycogen stores are exhausted (Stage II), and then switching to increased protein catabolism as fat stores decrease (Stage III). Though glycogen dynamics are not represented in this model (due to their low influence on long-term energy balance and the complexity required to implement), the increasing use of lean mass with starvation was estimated following Forbes' theory (*32*). Using Eqn. 8 in (*31*), we fit this relationship to values from three rat studies (*119–121*). To obtain more representative values of protein use, the average storage

levels were used rather than only initial values. This resulted in a curve that was similar to but slightly more conservative with protein use compared to the ones presented in (*31*). This allows the model to simulate the way animals primarily deposit or mobilize adipose tissue when at high body fat percentages, while catabolizing or synthesizing progressively more lean mass as stores decline. The curve was fitted using *nls* in the "stats" package in R (*130*) and produced a gamma value of 0.015 (see Figure S7 for the resulting curve).

3.2. Data used to calibrate uncertain parameters

For all but 12 model parameters, parameterization could be done directly using literature values. For these 12 parameters, calibration was done in two stages. As the calibration process is provided in great detail in section 6, here we will only present the description of the data sets used as patterns for evaluating parameter fits.

For the first calibration step, two parameters related to environmental resource availability and renewal were calibrated using empirical values of bank vole population density. We gathered empirical population densities from multiple studies (*50–53*) that reported mean population densities of bank voles across various sites and years during the spring to autumn period, resulting in a total of 13 values. As the male to female ratios were not provided in these studies and the model focuses only on female animals, we assumed a 1:1 ratio for males and females. The mean empirical female population densities were found to be 17.5 ± 11.8 (SD), with a median density of 14.2 and a range of 4.4 to 41.4 voles per hectare. While we initially aimed to obtain season-specific values to ensure the modelled densities followed described population cycles, we observed large variability in the data across studies, indicating significant inter- and intra-annual fluctuations in population size and spatial heterogeneity in this species (*50–53*).

For the second calibration step, we extensively researched and analyzed 27 literature sources to obtain the necessary data for generating 16 empirical patterns used in Section 6.2. These literature sources included: (*50, 56, 57, 67, 115, 146, 150, 151, 162, 173, 176, 191–199*). The details for each of the patterns can be found in Table S6.3. In many cases, we had to manually extract data from published plots using Automeris WebPlot digitizer v4.5 (*200*). These patterns were used to parameterize sigmoidal functions, which were then described by ten parameters to relate animal body condition to growth, pregnancy, lactation, and adult, offspring, and embryo survival. For additional information on this calibration step, please refer to Section 6.2.

3.3. Data used directly from literature values

For all other parameters, data were available from the literature to directly parameterize each of their values. While the majority of these values were obtained from studies on bank voles, for some parameters we had to refer to closely related

species to locate the necessary data. The sources for these values included other rodent species, particularly rats and mice (*113, 119–121, 141–143, 152–155, 159, 167, 168, 171, 172*). Additionally, three literature sources were relevant to mammals in general (*140, 156, 157*) and one represented a relationship applicable to all animals (*109*). For specific information on where each of these sources was used, please refer to the tables in Section 2.

4. Conceptual model evaluation

This TRACE element provides supporting information on: The simplifying assumptions underlying a model's design, both with regard to empirical knowledge and general, basic principles. This critical evaluation allows model users to understand that model design was not ad hoc but based on carefully scrutinized considerations.

Summary:

In Figure S1, you can find a flowchart that illustrates the conceptual model. In this section, we provide the reasoning behind the following aspects of the model: 1) the development of the energy budget model and allocation strategy, 2) the emphasis on female animals, 3) the representation of basal metabolic rate, 4) the link between energy use and alimentary capacity, 5) the exclusion of predation, and 6) the simplistic representation of animal movement. For more details on the model's simplifying assumptions, refer to Sections 2 and 3.

4.1. Energy budget and allocation

Food availability plays a crucial role in driving population dynamics, and IBMs can incorporate energy budgets to capture this relationship. However, there is currently no consensus on the best approach for modeling energy budgets, as different methods make varying assumptions (*12*), and there has been no direct evaluation of alternative methodologies.

Rather than somewhat arbitrarily selecting between the allocation strategies of the kappa-rule driven Dynamic Energy Budget framework (*24*) or the strict hierarchical structure of the Sibly et al. (2013) approach, we have instead developed a framework which assumes that allocation to non-survival related energetic processes (growth, pregnancy, and lactation) changes dynamically with body condition and which allows this relationship to emerge from grounding the model to empirical data. The parameters that drive this relationship are calibrated using relevant empirical patterns, ensuring that the final allocation strategies produce accurate energetic outputs (see Section 6).

Though body condition may not be the only driver of energy allocation to these processes, other physiological and health-related factors and even experience (*201*) may also play a role. Nonetheless, from an evolutionary perspective, body condition is a crucial indicator of nutritional status. Here, we have employed a logistic function to establish relationships between body condition and energy allocation to reproduction, growth, and survival, as has been observed between reproductive success or mortality and body size or condition-related metrics in bank voles and other animals (*43, 202–204*). However, if other relationships, or even thresholds, align more closely with empirical knowledge for a particular study system, they could also be implemented in this framework.

Additionally, we here assume that during the modelled summer breeding season animals are in their thermoneutral zone and therefore we omit direct representation of thermoregulatory costs. Though these costs could be incorporated either using biophysical or heat loss models (*163, 205*) or observed thermoregulatory curves (*206*) if extending into the winter period or for relevant questions.

Sibly et al. (2013)
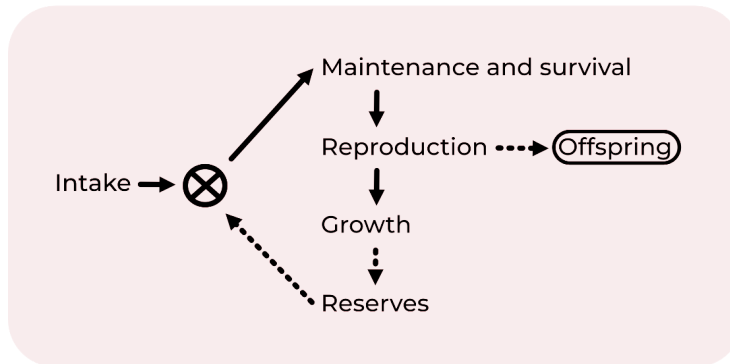
Dynamic Energy Budget (DEB) theory (Kooijman 2000)
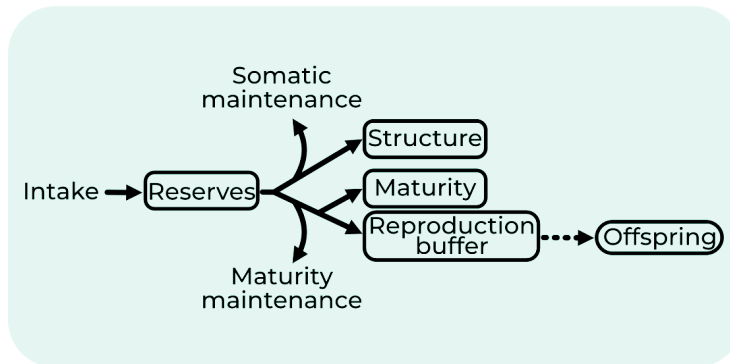
Pattern-Informed Energetics (PIE)
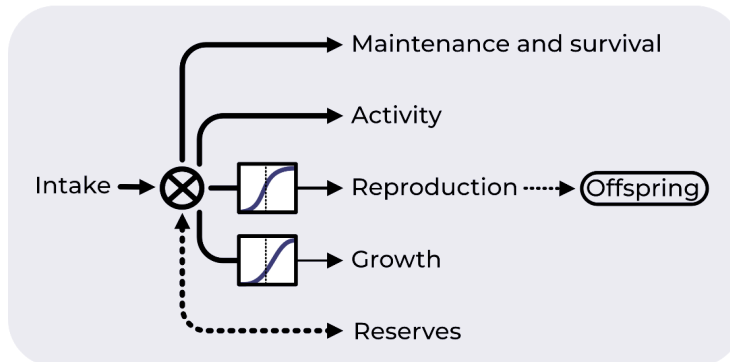
Figure S14. Comparison of energy budget frameworks. The top panel represents the basic framework proposed by Sibly et al. (2013), the middle panel represents the Dynamic Energy Budget framework developed by Kooijman (2000), and the bottom panel represents the updated framework proposed here, in which energy allocation is determined by body-condition driven relationships calibrated to empirical data, represented by the sigmoidal functions connected to reproduction and growth.

Energy intake of animals depends on the food availability of the landscape, energy content of ingested food, food replenishment rates, and spatial distribution of food cells.

Here, in this model implementation, the food in the landscape represents a general food source and does not correspond with any particular species. Instead we used an average energy conversion constant for a unit of food from the diets presented in Meese (1969). However, for more specific inquiries, different diets or qualities can be assessed by incorporating specific resource fields into the model with accompanying energy conversion amounts if known.

The food replenishment rates and maximum resource values of food cells were calibrated to result in population density values consistent with empirical predictions (see Section 6). These parameters were here taken as constants and do not vary seasonally or between resource patches. However, for the purpose of addressing our research questions outlined in Section 1, this simplified representation was sufficient for theoretical testing on long-term scales while also maintaining model tractability. However, for more specific inquiries, it may be necessary to incorporate more detailed representations of landscapes. For example, the seasonality of resources could be implemented, particularly when extending the model to cover the winter season.

In this model, the spatial distribution and number of food cells are incorporated as input parameters rather than representing any real landscape. This allows for testing of the theoretical research questions presented in Section 1.

4.2. Representation of female animals

As a simplifying assumption, only female animals are represented in the model post-weaning. In individual-based population models, it is not uncommon to only represent female animals due to their unique reproductive biology and the need to track population growth. Since, for many species including bank voles, female animals are typically responsible for gestation, lactation, and parental care, they have a more direct impact on population dynamics than males. However, modeling only females can also have limitations, such as not accounting for male-male competition, potential sex-specific differences in behavior and resource use, and intraspecific resource competition, particularly in resource-limited environments (*207*).

4.3. Plasticity in alimentary capacity

During periods of high energy expenditure, such as during lactation or when basal metabolic rate is elevated, the alimentary capacity of some animals may undergo changes to enable processing of increased energy intake. This can involve alterations in gut size or processing time. Changes in alimentary capacity have been documented in various rodent species (*116–118*) and may be particularly relevant for species with the ability to tolerate low ambient temperatures, relatively large litter sizes, short gestation periods, and high rates of postnatal growth (*208*). Importantly, an increase in energy intake without a corresponding increase in processing capability

would lead to a higher number of foraging bouts and consequently, increased predation risk (*209–211*).

To address the need for rodents to increase their alimentary capacity during periods of high energy expenditure, we incorporated variations in both maximum gut fill and processing time (or clearance rate) based on relative energy expenditure (see Section 2.7.2.3). Although the empirical relationship between these metrics is unknown, the relative scaling used produced realistic outcomes for both energy intake (Sections 6 & 8) and activity budgets (Section 5). However, it should be noted that these values are likely to plateau at some point in nature, and the extreme values (maximum and minimum gut size and clearance rate) are currently unknown empirically. Therefore, it is possible that the model may produce unrealistic alimentary capacities in some extreme cases. Once knowledge of these processes is empirically demonstrated, it should be incorporated into the model to ensure the most accurate representation of the adaptive capacity of the gut.

This approach is different from other methods that rely on functional response relationships or daily maximum ingestion rates. In our model, daily consumption emerges as a function of activity patterns, stomach capacity, and energy expenditure. This is supported by empirical evidence of stomach capacity being reached within a 30 minute period (the model timestep) in prairie voles (Zynel & Wunder, 2002).

4.4. Exclusion of predation and competitive effects

Despite its significant role in small rodent population dynamics (*75*), the current version of the model does not account for predation. This omission was a deliberate decision to simplify the model and maintain its tractability. However, as a consequence, the changes in population dynamics and metabolic traits represented in the model may not align with those observed if predation were included. Future iterations of the model could potentially incorporate predation and evaluate its differential effects on individuals based on their activity state. For example, foraging animals may be at a higher risk of predation than resting individuals.

Similarly, interspecific and intraspecific socially-driven competitive effects were not considered, despite existing evidence of these processes affecting bank vole fitness (*213*). This decision was again made to maintain tractability. However, these processes could influence population dynamics and may be included in future developments of the model when applied to questions in this direction.

4.5. Movement representation

Animal movement in the model is represented through a simplistic central place foraging approach (see Section 2.7.1 for movement module details). Each animal departs from a core cell when foraging to visit a single patch located at a realistic distance from their core cell, though this movement is represented only implicitly (*i.e.,*

the animal remains in the core cell but selects and consumes resources from the selected cell). The decision to move is based on the animal's energy balance, and the speed of movement is pulled independently from an empirical distribution. This relatively basic and theoretical representation of animal movement behavior was deemed sufficient for addressing our research questions while still maintaining model tractability. However, for more specific inquiries, a higher level of detail in the representation of movement behaviors may be necessary.

5. Implementation verification

This TRACE element provides supporting information on: (1) whether the computer code for implementing the model has been thoroughly tested for programming errors and (2) whether the implemented model performs as indicated by the model description.

Summary:
> As part of the model development process, the computer code underwent rigorous testing to ensure that each subsequent step was initiated only after the model had successfully passed a wide range of visual and statistical tests. Submodels were visually inspected for performance using the NetLogo graphical user interface (GUI), and model output was exported to compare against empirical relationships. To ensure accuracy, various testing methods were employed to confirm that the model operated as described in the TRACE. The model was further verified by simulating a cohort of animals to test its performance at the individual level over time.

We conducted thorough testing of the model to ensure that each submodel and the model as a whole functioned as expected. Early in the development process, we encoded the basic model in an early version of Netlogo with a homogenous landscape and simplified movements (correlated random walk) to carefully proof the energy budget code. The final NetLogo version of the model underwent systematic inspection using built-in NetLogo features such as monitors, plots, and print statements. Debug code was included throughout the model, controlled by the parameter "debug", which is still present in the final program. Following a unit testing, integration testing, and system testing approach, each energy budget procedure was first independently tested, then tested in combination in the order outlined in Figure S3, eventually testing the entire model as a whole. Some key verification results will be presented in detail below, which demonstrate that the model functions as expected.

5.1. Lean mass growth

To ensure that the growth of lean mass followed the intended allocation process, where animals with higher storage levels increase allocation to lean mass growth and reach larger adult body sizes, we closely monitored the lean masses of animals with predetermined storage levels. To accomplish this, we disabled the mobilization and deposition of lean mass and adipose tissues due to differences in energy balance, thereby ensuring that any observed growth was reflective of the lean mass dynamics procedure (TRACE section 2.7.2.1.4.). Additionally, overwinter skipping was disabled to ensure continuous growth curves. We conducted 30 simulation runs for each of the tested storage levels and calculated the average and standard deviation for each level, as depicted in Figure S15. The output from these simulations was found to be satisfactory, falling within the expected range when compared to the average and maximum growth models derived from empirical data.
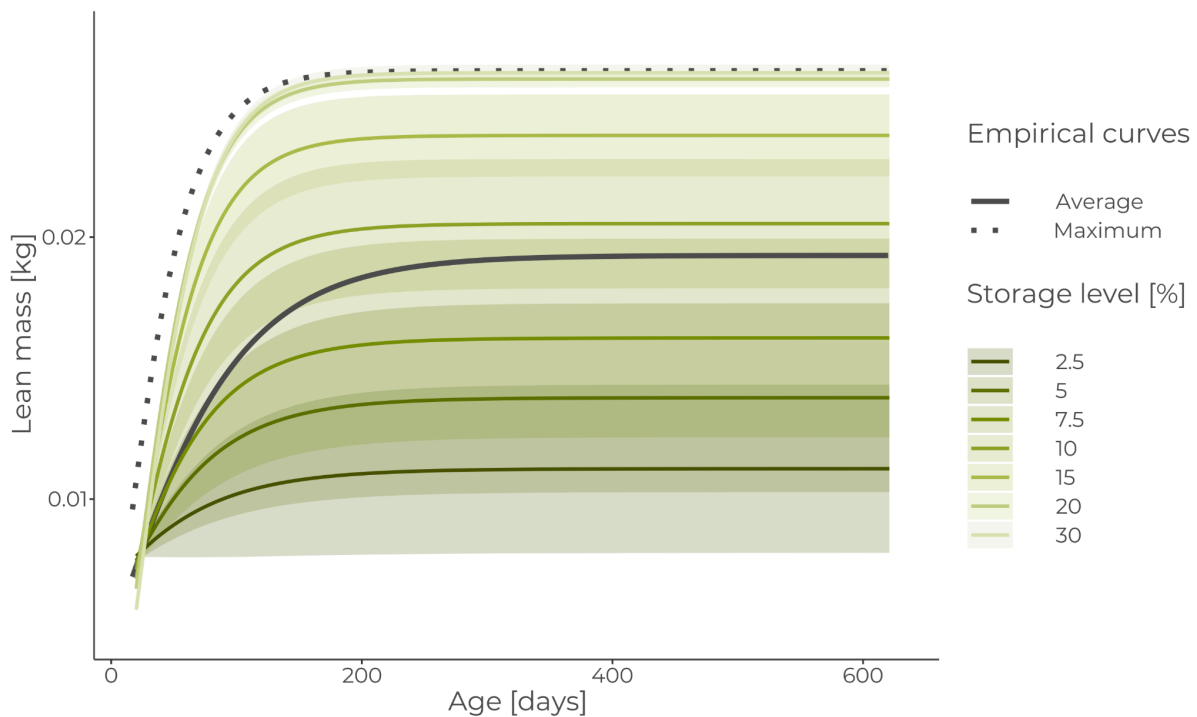
Figure S15. Lean mass growth for animals with predetermined storage levels. The colored lines represent the mean value of the model outputs from 30 simulation runs, while the shaded areas indicate standard deviations. The average and maximum growth curves, derived from empirical data, are shown as large black lines for comparison.

5.2. Activity, cost of transport, and metabolic fuel use

To ensure that the model accurately represented animal activity and the associated costs of transport, several model components were examined in detail. One such component was the metabolic cost of moving at a particular running speed. In the model, animals draw their movement speed from a gamma distribution based on empirical values (for details, see TRACE section 2.7.1). To evaluate whether the

increases in movement costs with running speed were reasonable, we collected data on the costs of activity and basal metabolic rates for all animals once per day for 100 simulation runs. We then compared these outputs to available empirical relationships from other rodent species. The resulting fits fell within the empirical relationships, with variations attributable to differences in animal body mass (Figure S16). These findings confirm that the model provides a reasonable representation of animal energy expenditure during locomotion.
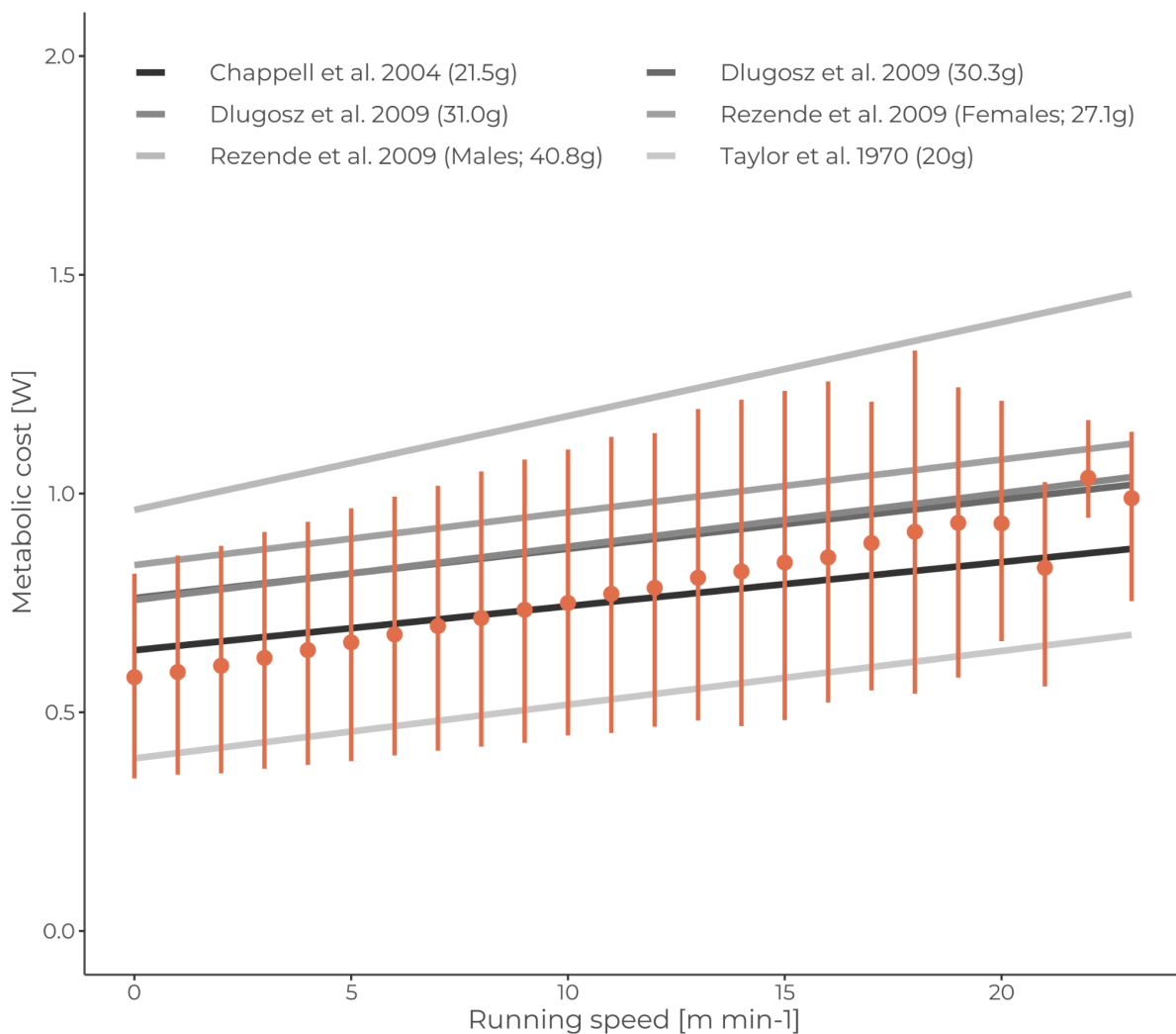
Figure S16. Metabolic costs of activity, measured as the combined costs of movement and basal metabolic rate (in W), for animals moving at various running speeds (in meters per minute). The orange points represent the average costs at each speed and orange lines are 95% confidence intervals for outputs gathered daily from 100 simulation runs. Grey shaded lines show the relationships derived from literature sources, with the empirical animal mass denoted in the figure legend.

Additionally, we assessed the total proportion of the day that voles spent being active. To accomplish this, we recorded the average activity rate of all animals daily, which was calculated based on the previous day's data. Our analysis revealed that, on

average, animals spent approximately 29.5 ± 26.1% of their time moving and foraging, while the rest of the time was spent resting (Figure S17). This value was similar to the percentage of time active found for lactating female voles in (*214*), which reported a range of 19% to 50% (mean 34%), suggesting that modeled voles spend a similar amount of time being active as observed in real-life voles, particularly those in reproductive states similar to those represented in the model outputs.
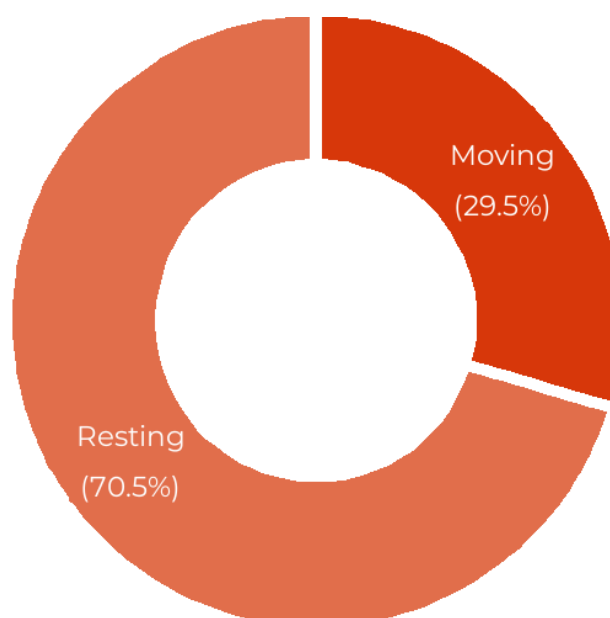
Figure S17. Average percentage of time spent either moving (dark orange) or resting (light orange) in outputs from 100 simulations. The data represent the average behavior of all animals in simulation year 5 and highlight the relative proportion of time spent foraging versus in rest.

To verify that animals were mobilizing a metabolic fuel ratio that was appropriate for their current storage level, we collected data on the mass of mobilized lean and adipose tissue for all animals daily in simulation year 5. Our analysis showed that the mass of adipose tissue mobilized outweighed that of lean mass until storage levels dropped below approximately 7% (Figure S18). Below this point, the proportion of lean mass mobilized increased relative to adipose tissue, which is consistent with the intended model process and reflects the inefficiency of catabolizing lean mass tissue.
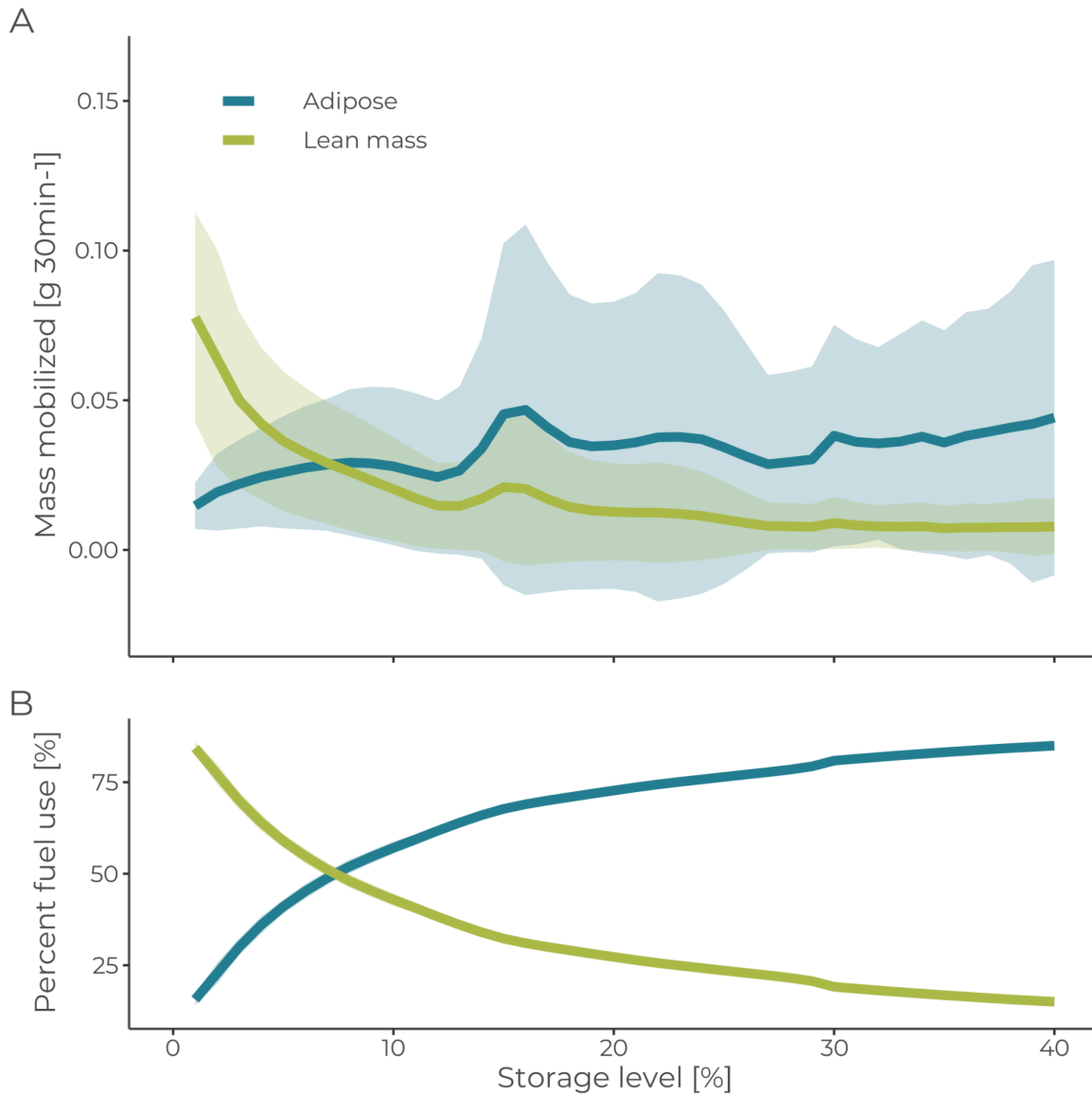
Figure S18. Average mass mobilized (A) and proportion of metabolic fuels used (B) (in terms of mass) by animals as a function of their storage level. Green lines represent mobilization of lean mass tissue, while blue lines represent adipose catabolism. The filled regions depict plus or minus one standard deviation from the mean. Outputs were averaged over 100 simulation runs.

5.3. Cohort follow

To further verify the model, a subset of animals consisting of the offspring of the first ten reproducing females in simulation year 5 were tracked from birth until the end of the simulation year (ending at the overwinter skipped period) for 100 simulation replicates. This cohort analysis allowed us to monitor changes in structural and total body mass, survivorship, and total energetic costs over time (see Figure S19), and

revealed key aspects of the energy budget. Specifically, the added mass associated with gestational periods can be seen as two distinct peaks in Figure S19A, and were accompanied by an increase in lean mass, likely due to elevated energy consumption during this period. Each of these peaks was then followed by a slight decline in lean body mass, attributed to the high energetic demands of lactation. These early-born animals had, on average, two successful litters during the simulation year (Figure S19C) and exhibited high early survival rates (Figure S19B) which declined after reaching reproductive maturity (aligning with periods of population peaks; see Figure S20). Additionally, the reduced costs experienced by dependent offspring and the increases in the heat increment of feeding (HIF) associated with the lactation period could be observed (Figure S19). An interesting output was an increase in activity costs towards the end of the simulation year. This coincided with the strongest period of survivorship decline and represents increased competition during this period. Overall this cohort analysis allowed for a visual inspection of the energy budget over time and confirmed that key aspects of the energy budget and demographic modules functioned as intended.
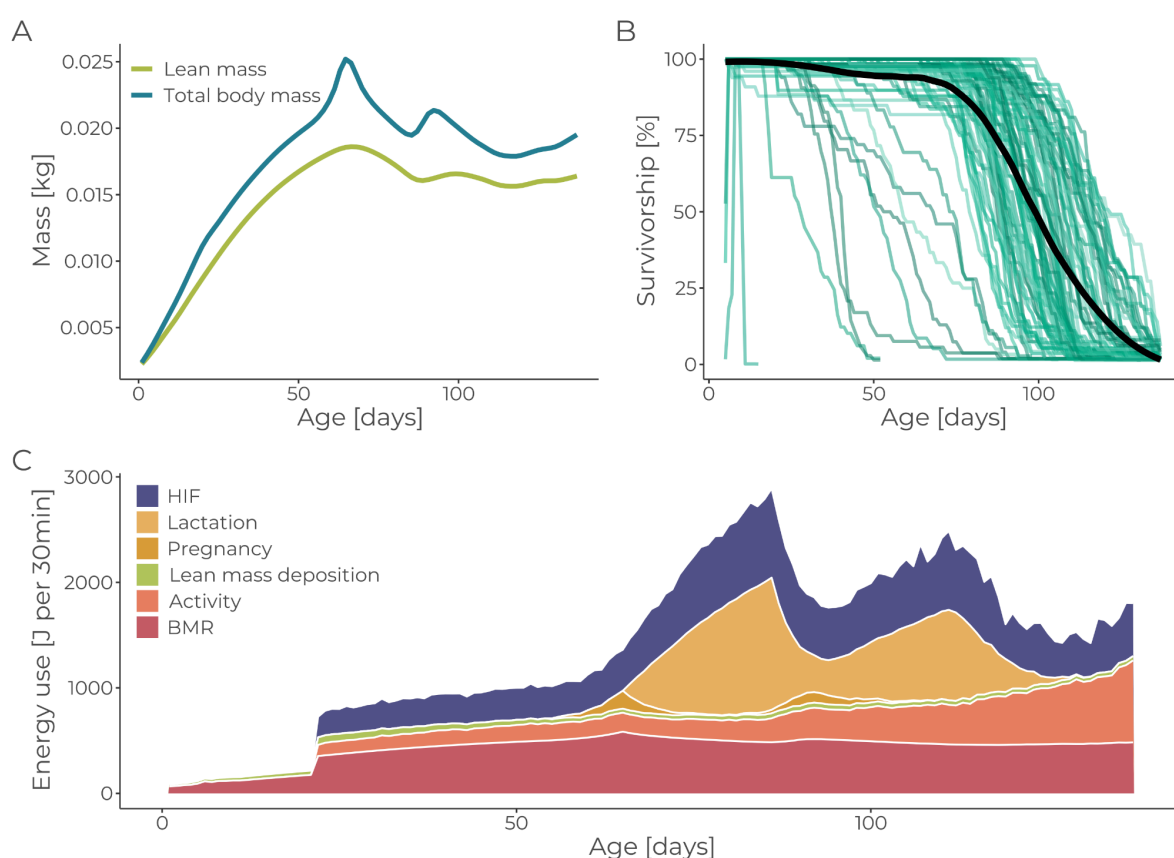
Figure S19. Various outputs of a cohort of voles tracked for one simulation year, including (A) the average lean and total body mass at the age of surviving voles, (B) survivorship, and (C) the average energetic costs of surviving voles broken down into individual energetic costs. All outputs are based on 100 simulations in which the offspring of the first ten reproducing females were tracked from birth. In panel B, individual colored lines represent the outputs from individual runs, while the thicker black line

depicts the average survivorship across all runs. In C, inefficiencies associated with milk digestion are not depicted.

6. Model output verification

This TRACE element provides supporting information on: (1) how well model output matches observations and (2) how much calibration and effects of environmental drivers were involved in obtaining good fits of model output and data.

Summary:

The model's uncertain parameters were calibrated through a two-stage approach that employed empirical patterns of the bank vole species and the approximate Bayesian computation method. In the first calibration step, we ensured that resource parameters produced realistic population densities. For the second calibration, we focused on energy allocation parameters and used 16 empirical patterns to assess model fit. The final model output was in good agreement with the empirical data.

While many parameters used in the model were well-understood and could be based on literature values for bank voles, there were twelve parameters whose values were uncertain and required calibration. This calibration process was carried out in two stages. The first stage was aimed at determining the values of two resource cell parameters, based on empirical population densities (6.1. Density calibration). The second stage utilized 16 empirical patterns to establish the relationship between storage level and energy allocation to growth, pregnancy, and lactation, as well as between storage level and adult, offspring, and embryo mortality (6.2. Energy allocation and survival). Each step will be detailed separately below. Base values were used for landscape configuration (see Table S24).

6.1. Density calibration

To first ensure that the model included a realistic number of animals for the represented spatial extent, the resource parameters *max-resources-base* and *r-growth-ts* were calibrated and the resulting population densities were compared with available empirical data for bank voles. Empirical population densities were obtained from four articles (*50–53*) which recorded the mean population density of bank voles, spring to autumn, across multiple sites and years, producing a total of 13 values. A 1:1 male to female ratio was assumed, as the relative ratios for male and female voles were not reported, and the model only represents female animals. This resulted in mean empirical female population densities of 17.5 ± 11.8 (SD), a median density of 14.2, and a range of 4.4 to 41.4 voles per hectare.

To enable the reproduction of empirical patterns we followed a "virtual ecologist" approach (*86*), where a patch-set was introduced, called *dens-cells*, which consisted

of 100 randomly selected suitable habitat cells (*resource-cells*) covering 1 hectare in total. Only *resource-cells* were selected to ensure that the simulated "trapping sites" would not be placed in unsuitable habitats, as would be the case in empirical studies. The population densities per hectare were then estimated for each parameter combination by summing the number of animals located on the *dens-cells*. The parameter *max-resources-base* was varied between 40 and 200 g in increments of 20, and *r-growth-ts* was varied between 0.005 and 0.025 g in increments of 0.002, after a preliminary exploration of values that produced stable populations without crashing or growing beyond the empirical values. Simulations were run for 10 years, with 25 repetitions for each parameter combination, and the first 5 years were discarded as burn-in. The population densities were collected weekly on the *dens-cells*, within the simulation period and the period covered by the literature records (between days 121 and 278 of the year). All density values were then compared to the median value of 14.2 female voles per hectare from the empirical data, and the absolute value of any deviations from the median were averaged for all timesteps for each parameter combination (Table S24). The combination that best fit the data (minimized the average difference) was a *max-resources-base* of 140 g and a *r-growth-ts* value of 0.011 g per timestep (Figure S20).

Table S24. *Results for the best fitting 10 parameter combinations in the calibration of the maximum resource level, maxR, and the resource accumulation per timestep, rGrow. The selected values are shown in bold.*

max-resources-base	r-growth-ts	Mean	Median	Standard deviation	Mean absolute deviation
140	**0.011**	14.4	10	13.7	0.186
120	0.013	13.9	9	12.7	0.267
140	0.009	13.9	9	13.6	0.289
100	0.015	13.7	10	11.6	0.454
180	0.007	14.7	8	17.1	0.464
160	0.009	14.7	8	15.8	0.488
120	0.015	14.8	10	12.9	0.55
80	0.017	13.6	10	10.9	0.554
100	0.017	14.8	10	12.2	0.555
60	0.021	13.6	11	9.71	0.578
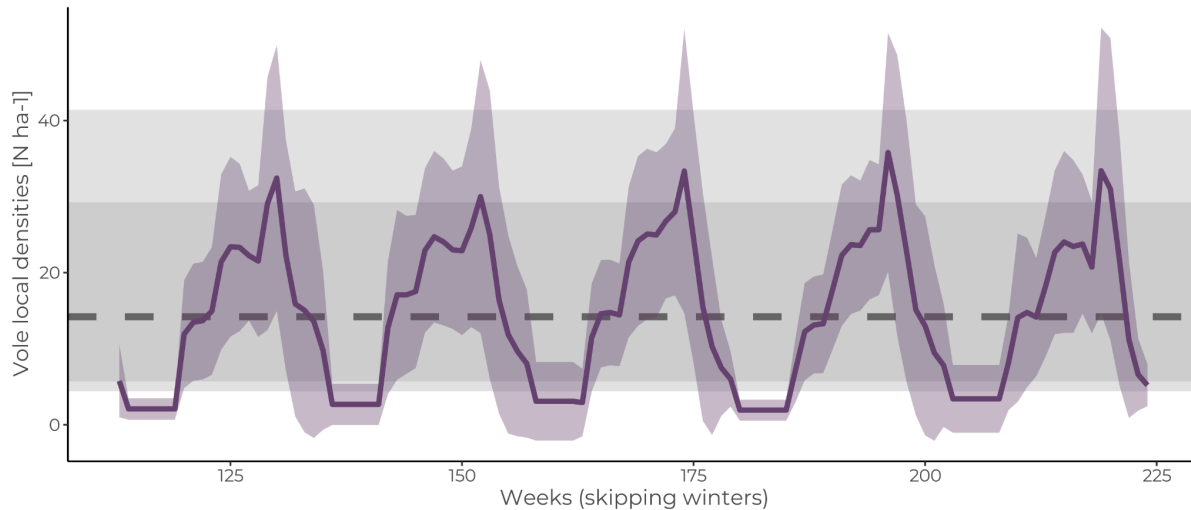
Figure S20. **Population density of voles** (not including dependent offspring) over five simulation years in 25 replicate runs from the accepted parameter combination in the calibration step. Mean density from model outputs is represented by the purple-colored line and the standard deviation depicted using the filled area. The mean value of the empirical data plus and minus its standard deviation is shown in the dark grey rectangle, while the full range of empirical values is shown in light grey. The dashed grey line indicates the median value in the empirical data.

6.2. Energy allocation and survival calibration

Despite the abundance of knowledge regarding parameters associated with energy expenditure in various species, the interplay between body condition and its impact on energy allocation for growth, reproduction, and mortality remains largely elusive (*39*). Understanding these relationships is pivotal for accurately describing the dynamics of populations and linking environmental changes to their impacts, and as such, they are crucial parameters in bioenergetic models. However, due to the limited understanding of these relationships, direct parameterization remains a challenge. In light of this, many bioenergetic studies have resorted to incorporating rough estimates of body condition in emaciated animals as threshold values to determine the failure of reproduction or the occurrence of mortality. However, there is a scarcity of evidence to support the existence of such threshold values, and nonlinear relationships, rather than stepwise or threshold based relationships, have been supported by observations of increased reproductive success, offspring growth, and survival with increasing body size and condition (*43, 44, 202, 215*). In view of this knowledge, in the present study, we aimed to calibrate sigmoidal functions described by 10 parameters to relate animal body condition to growth, pregnancy, lactation, and adult, offspring, and embryo survival: the growth slope and midpoint (*growth-lm-prob-const* & *growth-lm-prob-mid*), pregnancy slope and midpoint (*preg-prob-const* & *preg-prob-mid*), lactation slope and midpoint (*lact-prob-const* & *lact-prob-mid*), and survival slope, midpoint, and modifiers for embryo and offspring survival (*surv-prob-const*, *surv-prob-mid*, *surv-mod-emb*, & *surv-mod-off*).

A Bayesian approximation method, known as rejection approximate Bayesian computation (ABC) (*46*), was employed to calibrate these ten parameters. The method followed a pattern-oriented modelling approach (*36, 37*), utilizing 16 empirical patterns as a basis for comparison. To sample the parameter space, the R package *nlrx* (*216*) was used. We followed a Latin hypercube sampling strategy and drew from uniform prior distributions with minimum and maximum specified in Table S25. The model was then executed with 500,000 parameter combinations, with relevant outputs collected for each of the 16 empirical patterns, as detailed in Table S26.

Table S25. *Ranges of values used to generate the parameter space for the energy budget calibration.*

Parameter name	Minimum	Maximum
growth-lm-prob-const	10	50
growth-lm-prob-mid	0	0.2
preg-prob-const	10	50
preg-prob-mid	0	0.2
lact-prob-const	10	50
lact-prob-mid	0	0.2
surv-prob-const	20	120
surv-prob-mid	0	0.1
surv-mod-embryo	0	2
surv-mod-off	0	2

Table S26. *Empirical patterns used for calibrating the energy budget module. All outputs collected in simulation year 5. The "Value" column indicates whether the patterns were represented by a range (denoted as "R") or a single value (denoted as "SV") for comparison to model outputs.*

Pattern description	When collected	Value	Fit threshold	Source
1. Fetal mass at birth	At birth	R: Range between 1 - 2.5 g	0	(*50*)
2. Birth mass by litter size	At birth	SV: Negative relationship	0	(*194*)
3. Total body mass by age	Once per month	SV: von Bertalanffy curve per age in days	0.36	(*115, 150, 151, 160–162*)
4. Lean mass by age	Once per month	SV: von Bertalanffy curve per age in days	0.36	(*115, 150, 151, 160–162*)
5. Lactating mother mass by pup age	Daily between lactation days 0 to 15	SV: Mean values per day	0.265	(*197*)
6. Lactating mother food intake by pup age	Daily between lactation days 0 to 15	SV: Mean values per day	0.36	(*197*)
7. Total litter mass by pup age	Daily between lactation days 0 to 15	SV: Mean values per day	0.36	(*197*)
8. Mother peak food intake by litter size	Once on lactation day 15	SV: Trendline per litter size	0.36	(*197*)
9. Mother peak energy use by litter size	Once on lactation day 15	SV: Trendline per litter size	0.36	(*197*)
10. Mother peak milk	Once on lactation	SV: Trendline per litter size	0.36	(*197*)

transfer by litter size	day 15			
11. Pup mass at weaning by litter size	At weaning	SV: Negative relationship	0	*(56, 57, 198)*
12. Litter size at birth	At birth	R: Between 3.6 - 6.1 offspring	0.36	*(50, 146, 164, 173, 176, 191, 197)*
13. Litter size at weaning	At birth	R: Between 1.28 - 5.28 offspring	0.36	*(50, 56, 67, 164, 192, 195, 196)*
15. Range of percent body fat	Once per month	R: Between 3 - 29% body fat	0	*(150, 151, 199)*
16. Percent body fat of animals at death	At death	R: Below 3% body fat	0	*(150, 151, 199)*
17. Field metabolic rate by body mass	Once per month	SV: Average of two allometric relationships per body mass	0.36	*(193, 217)*

To evaluate the fit of each parameter combination, outputs were collected after the fifth year of simulation at specific intervals, as indicated in Table S26. The median absolute scaled error was then calculated for each pattern by comparing the output to either a single value or a range (as indicated by "R" or "SV" in the Value column in Table S26). If the pattern had a single value target, the absolute scaled error was calculated by taking the difference between the output and the target value:

$$\left| \frac{output - pattern}{pattern} \right|$$

If the pattern was represented by a range, the output was considered to fit the pattern if it fell within the range and was assigned a value of 0. If the output was outside of the range, the absolute scaled error was computed based on the range itself:

$$\left| \frac{output - pattern\ upper\ limit}{pattern\ upper\ limit - pattern\ lower\ limit} \right|, \quad if\ output > pattern\ upper\ limit$$

$$\left| \frac{pattern\ lower\ limit - output}{pattern\ upper\ limit - pattern\ lower\ limit} \right|, \quad if\ output < pattern\ lower\ limit$$

The median value across all points was used to represent the overall fit of the simulation for each pattern. Linear relationship patterns (2 and 11) were evaluated differently, with a negative slope being considered a pass (0) and a positive slope being considered a fail (1). The outputs were filtered based on maximum values for each pattern fit, as specified in Table S26. These values were selected because they resulted in the best fit to the data, with some adjustments made for patterns that needed to be constrained to 0 (patterns 1, 2, 11, 14, and 15) or which required slightly lower thresholds to best fit (pattern 5) (Figure S21).
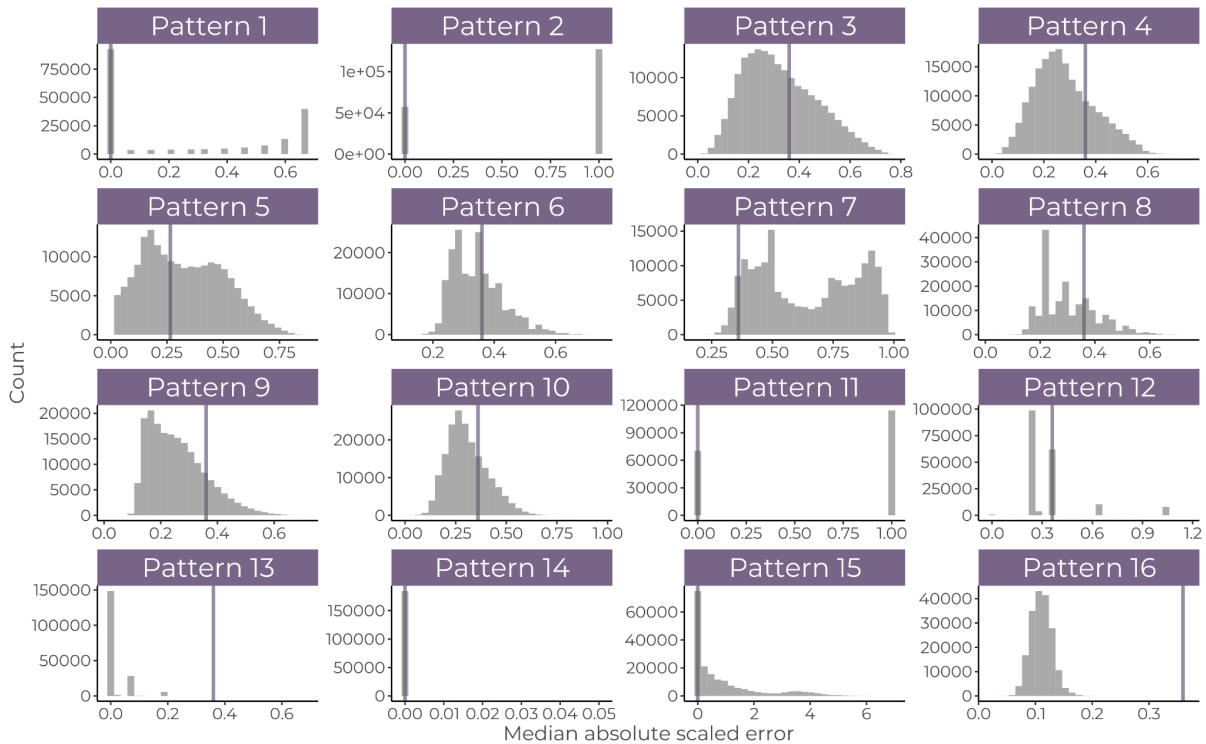
Figure S21. **Resulting fits for each pattern in all completed runs of the calibration step**, with the fits represented in grey and the acceptance threshold for each pattern shown as a purple line.

The parameter combinations resulting from model calibration were found to fit the empirical patterns quite well, with only a few minor discrepancies. These discrepancies can be attributed to conflicts between the patterns themselves, particularly in the case of lactating mother body mass by pup age (pattern 5; Figure S22D) and total body mass by age (pattern 3; Figure S22B). The laboratory animals used for pattern 5 had a considerably higher average body mass than those used for pattern 3, which made it difficult to fit both patterns tightly without sacrificing one or the other. Despite this, the resulting fit is a good compromise, as it fits both patterns fairly well and ultimately corresponds to the mean body mass from the PanTHERIA database (*218*) used for model evaluation (see Section 8 below). However, this discrepancy did result in slightly lower values for mother food intake and energy use, as these patterns were also obtained from the same literature source (Figure S22, Panels G & H). Nevertheless, these values were in accordance when adjusted for mass and were deemed to be acceptable fits.
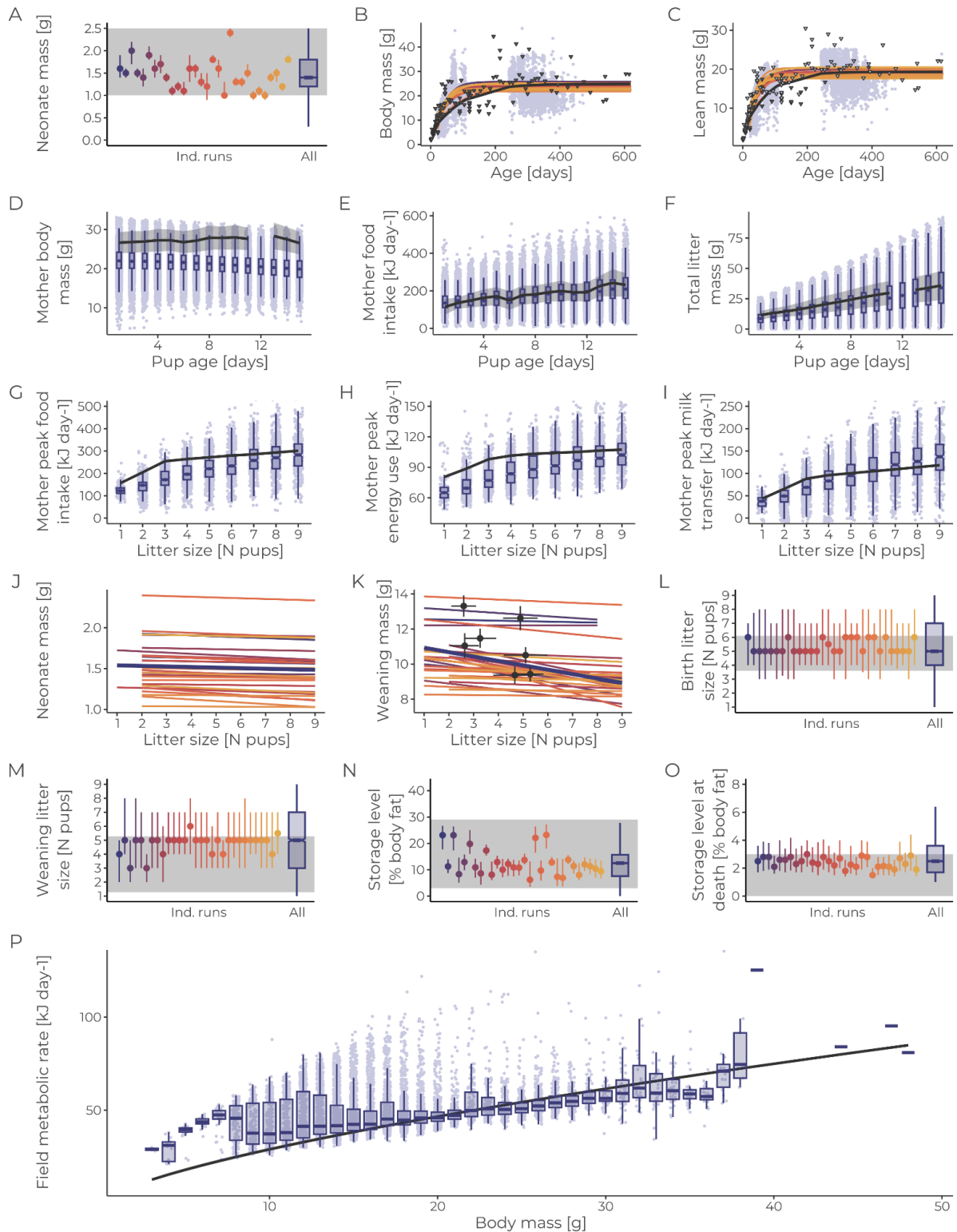
Figure S22. Comparison of model predictions for the 30 best fitting parameter combinations with the 16 empirical patterns used for calibration (depicted in black or grey) for (A) neonate mass, (B) total and (C) lean body mass with age, mother (D) body mass, (E) food intake, and (F) total litter mass with pup age, mother peak (G) food intake, (H) energy use, and (I) milk transfer with litter size, (J) neonate

and (K) weanling mass by litter size, litter size at (L) birth and (M) weaning, storage level of (N) living and (O) dead animals, and (P) field metabolic rate by body mass. The figure shows outputs from individual parameter sets using unique colors and combined results are shown in purple. For panels A, D, E, F, L, M, N, and O, the grey rectangle denotes the range of empirical values used to assess pattern fit, while the purple box plot shows the model results for all accepted parameter combinations, and colored point ranges are medians and 95% CIs for each individual parameter set. For panels B, C, G, H, I, and P, the empirical values are represented by the solid black line. For panels J and K, fit was defined qualitatively as a negative relationship, and as such, only illustrative points (mean ± s.e.) from two independent empirical studies (*56*, *57*) are shown in K. In panels B and C and J and K, the colored lines denote von Bertalanffy and linear relationships fit to outputs from each of the individual parameter sets. Additionally, in panels B and C, dark grey triangles represent measured empirical values, and light grey triangles are inferred (see Data evaluation). Light purple points in B-I and P represent individual data points from the model.

When observing the posterior distributions for the selected parameter sets, the parameter space was considerably reduced for all except three parameters, *growth-lm-const*, *preg-prob-const*, and *lact-prob-const* (Figure S23). Though, when correlations between parameters were assessed, it became clear that these parameters were each fairly positively correlated with their corresponding midpoint parameters (Figure S24).
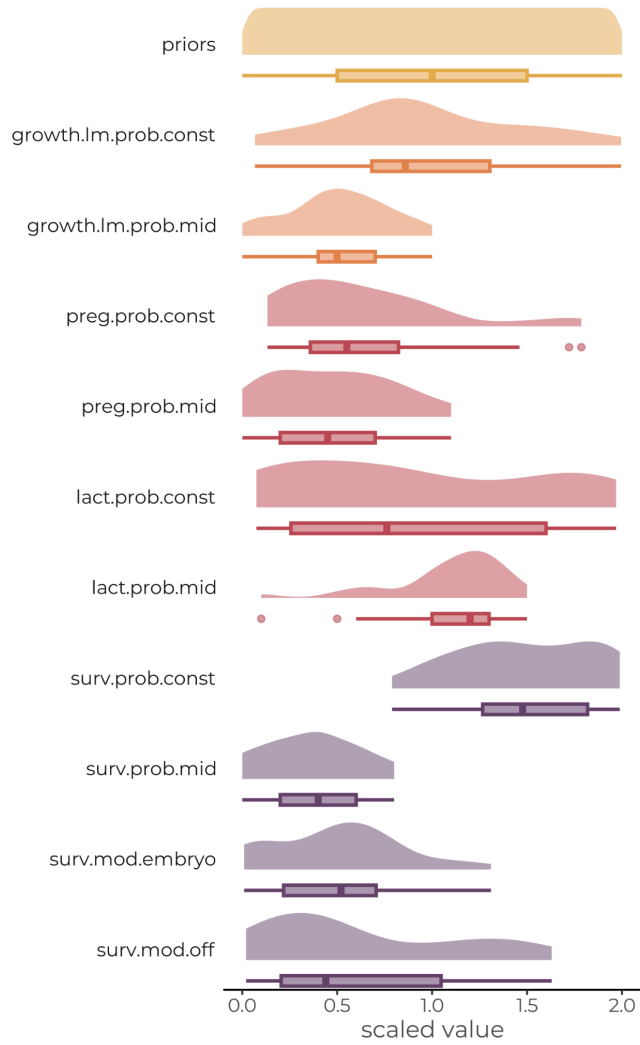
Figure S23. **Resulting density curves of parameter values after calibration of the model using approximate Bayesian computation.** Each parameter has been scaled between 0 and 2 for ease of comparison, and the uniform prior distributions for are shown at the top of the plot. The colored curves and corresponding boxplots represent the posterior distribution for each calibrated parameter.
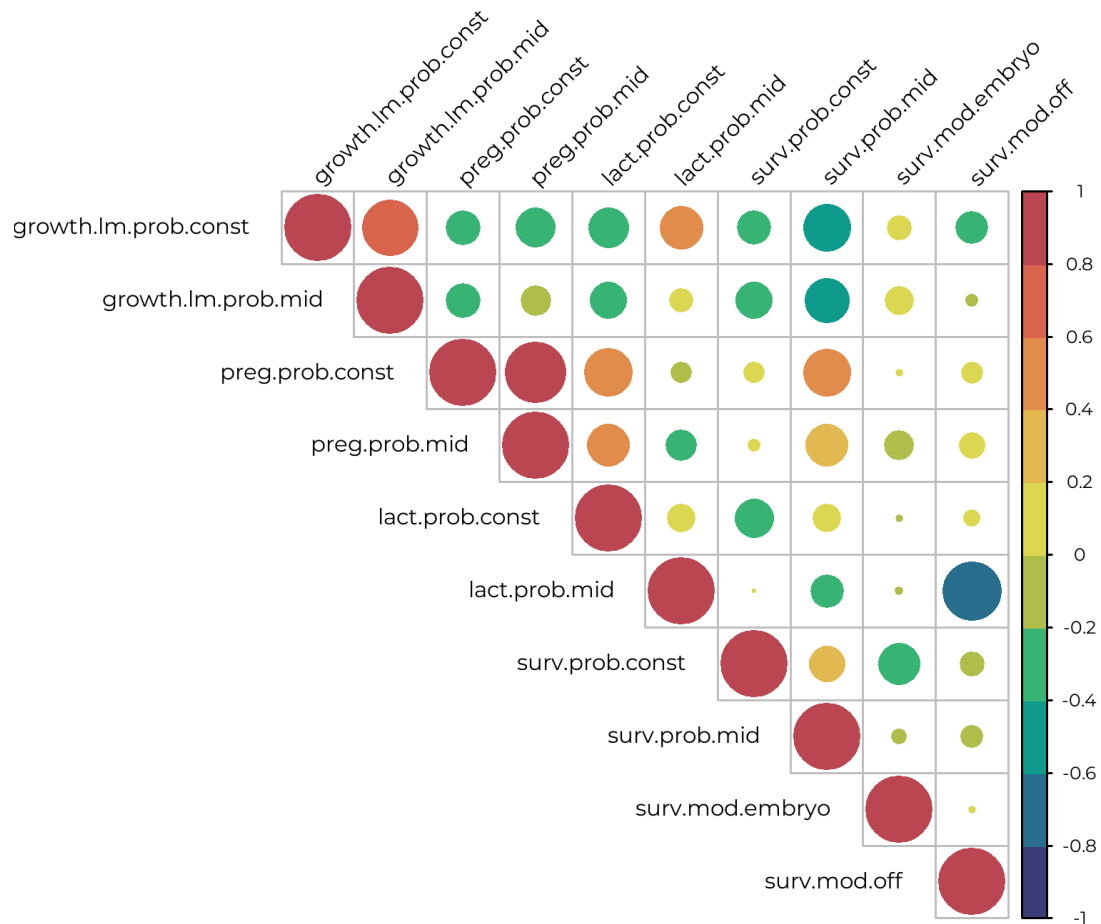
Figure S24. **Correlation between calibrated parameters in the model**, where each cell in the matrix represents the correlation coefficient between two parameters. The color and intensity of the cell indicate the strength and direction of the correlation, with warmer colors representing positive correlations and cooler colors representing negative correlations. The size of the circle in each cell denotes the magnitude of the correlation coefficient.

As a final check, the population density values for each of the parameter sets were compared to the mean and median (± 1SD) of the empirical density values (see section 6.1. Density calibration above) (Figure S25). While the average values were a bit low compared to the empirical values, they fell well within the reported range and as such were accepted.
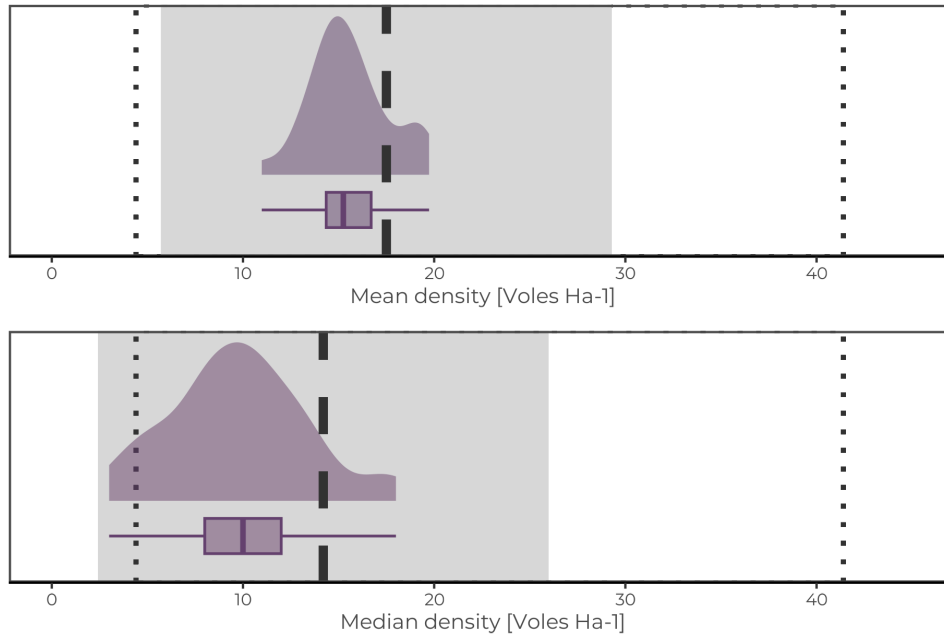
Figure S25. **Population density outputs (in female voles per hectare) for mean (top) and median (bottom) densities** for the 30 best-fitting parameter sets. The large dashed black line denotes the empirical literature value for each metric, while the grey region indicates this value plus or minus the standard deviation of literature values. The thin dotted lines represent the minimum and maximum observed values. The density curve depicts the relative density of model outputs.

The selected parameter combinations resulted in the 30 relationships seen in Figure S26. Each of these parameter sets was utilized independently in model simulations, with the curves varying among simulation runs to consider uncertainty in the model results.
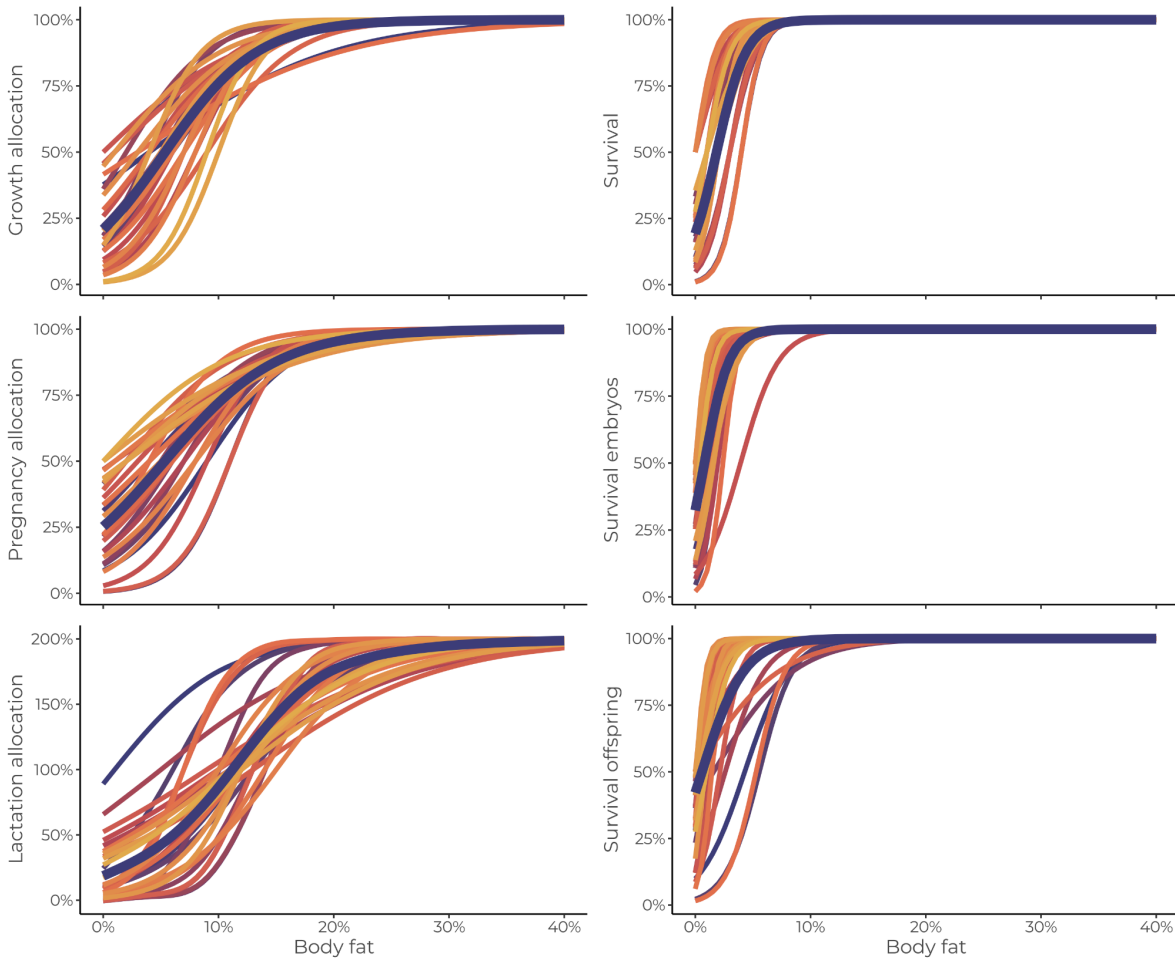
Figure S26. Relationships resulting from the calibration step of the model, depicting the 30 best-fitting parameter sets. These curves illustrate the association between body fat percentage and allocation to growth (top left), pregnancy (middle left), lactation (bottom left), and the probability of adult (top right), embryo (middle right), and offspring (bottom right) survival. The thick purple line represents the average across outputs. Each curve is utilized directly in a model simulation, with the curves varying between simulations to introduce uncertainty in model predictions.

Having completed the calibration process, we affirm that the model was effectively fit to the data with regards to population densities and the relationships between body condition and vital rates, thus demonstrating that energy utilization in the modeled animals closely aligns with that observed in their wild and captive counterparts.

7. Model analysis and application

This TRACE element provides supporting information on: (1) how sensitive model

output is to changes in model parameters (sensitivity analysis), and (2) how well the emergence of model output has been understood.

Summary:
> **We conducted a two-part global sensitivity analysis to identify the most influential parameters to the outputs of seven modelled metrics, which related to animal morphometrics, reproduction, and population densities. Initially, we used the Morris method to screen all model parameters and create a parameter ranking based on their level of influence from the least to the most influential. Next, we performed a variance decomposition analysis using the Sobol method to identify the contribution of the ten most influential parameters to the variance in model outputs. We were able to clearly identify key parameters for some output metrics, while for others, variance resulted from the interaction of various factors in the model.**

Following (*219*) (see associated TRACE document section 7), we performed a comprehensive global sensitivity analysis on the parameters of our model to determine which parameters had the greatest influence on the model outcomes and to quantify the variance contribution attributed to each of the most impactful parameters. The sensitivity analysis was executed in two phases, beginning with a screening of all 60 parameters of the model. During this phase, the values of the parameters were varied over five levels, with the central value being the value used in the calibrated model. The parameters were then ranked based on their effect on seven model outputs, which included body mass of adults, neonates, and weaned offspring, age at first birth, litters per year, litter size at birth, and population density. These outputs were selected due to their representation of different levels of organization, ranging from individual-level to population-level variables, and their utilization in evaluating the model and scenarios derived from the PanTHERIA database (*218*).

The second phase of the sensitivity analysis involved the application of a full variance decomposition technique (*124, 220*) on the same outputs for the ten parameters that were determined to be the most influential during the Morris screening. Both phases of the sensitivity analysis were executed by running the model for three years and collecting the mean of all outputs at the conclusion of this three-year period.

For the screening of parameters, we employed the improved version of Morris' elementary effects method (*122, 123*) and utilized the mean of the distribution of the estimated elementary effects to calculate a sensitivity index for each parameter. In regards to variance decomposition, we followed the advanced techniques of Sobol et al. (2001) and Saltelli et al. (2010) to estimate the first-order and total-effect indices of each of the ten most influential parameters. Both phases of the sensitivity analysis were facilitated using the *sensitivity* package (*125*) in R to design the experiments and calculate sensitivity indexes.

7.1. Screening of influential parameters

The initial step in evaluating the sensitivity of the model parameters was the application of the improved Morris Elementary Effects Screening Method (*122, 123*). This approach, which is based on individually randomized one-factor-at-a-time designs (*221*), has been deemed an efficient method for identifying influential parameters in IBMs. The method entails estimation of the relative effects of changes in the values of the input parameters, referred to as "elementary effects," and subsequent statistical analysis to determine their relative importance to the model output. In accordance with the TRACE methodology presented by Ayllón et al. (2016), the sensitivity measure was estimated as the mean of the distribution of the absolute values of the elementary effects, which serves as a proxy for the total sensitivity index.

Each of the 60 model parameters were varied over five levels, with the central value corresponding to the value used in the final calibrated model (as detailed in Table S27). The parameters were subject to a maximum increase or decrease of 20%. The number of tested settings is determined by the product of the number of elementary effects computed per parameter and the number of parameters, plus one. In this case, with 50 elementary effects selected, the total number of model runs was calculated as 50 × (60 + 1) = 3050.

Table. S27. *The parameter values used in the Morris screening global sensitivity analysis. Full parameter details can be found in the corresponding module in TRACE Section 2. Central values from calibrated parameters (denoted with *) were selected as the average value of each parameter in the selected parameter sets.*

Parameter code	Lower extreme	Lower median	Central value	Upper median	Upper extreme
Landscape parameters:					
perc-resource-cells	0.6	0.675	0.75	0.825	0.9
max-resources-base	112	126	140	154	168
r-growth-ts	0.0088	0.0099	0.011	0.0121	0.0132
fragmentation-level	0.64	0.72	0.8	0.88	0.96
n-animals	80	90	100	110	120
Move parameters:					
speed-mean	0.1328	0.1494	0.166	0.1826	0.1992
speed-max	0.6576	0.7398	0.822	0.9042	0.9864
HR-r-min	9.04	10.17	11.3	12.43	13.56
HR-r-max	26.56	29.88	33.2	36.52	39.84
Energy budget parameters:					
B0	4842.48	5447.79	6053.1	6658.41	7263.72
gamma	0.512	0.576	0.64	0.704	0.768
intercept-pcot	3.76	4.23	4.7	5.17	5.64
slope-pcot	0.504	0.567	0.63	0.693	0.756
intercept-icot	8.48	9.54	10.6	11.66	12.72
slope-icot	-0.232	-0.261	-0.29	-0.319	-0.348

n-emb-mid	4.4	4.95	5.5	6.05	6.6
emb-growth-c	0.0896	0.1008	0.112	0.1232	0.1344
emb-mass-init	5.52E-08	6.21E-08	6.90E-08	7.59E-08	8.28E-08
emb-mass-inf	15.9656	17.9613	19.957	21.9527	23.9484
percent-fat-emb	0.0304	0.0342	0.038	0.0418	0.0456
percent-pro-emb	0.0816	0.0918	0.102	0.1122	0.1224
ED-pl	2599.92	2924.91	3,249.90	3574.89	3899.88
DE-pl	0.4008	0.4509	0.501	0.5511	0.6012
preg-prob-const*	18.2984	20.5857	22.873	25.1603	27.4476
preg-prob-mid*	0.0384	0.0432	0.048	0.0528	0.0576
off-BMR-red	0.4008	0.4509	0.501	0.5511	0.6012
off-growth-eff	0.704	0.792	0.88	0.968	1.056
milk-prod-eff	66	74.25	82.5	90.75	99
lact-prob-const*	22.6224	25.4502	28.278	31.1058	33.9336
lact-prob-mid*	0.0872	0.0981	0.109	0.1199	0.1308
ED-pro	18.8	21.15	23.5	25.85	28.2
DE-fat	0.588	0.6615	0.735	0.8085	0.882
DE-pro	0.3552	0.3996	0.444	0.4884	0.5328
growth-lm-prob-const*	23.2408	26.1459	29.051	31.9561	34.8612
growth-lm-prob-mid*	0.0408	0.0459	0.051	0.0561	0.0612
growth-lm-inf	0.02112	0.02376	0.0264	0.02904	0.03168
growth-lm-k	0.07712	0.08676	0.0964	0.10604	0.11568
stomach-fill-perc	0.04056	0.04563	0.0507	0.05577	0.06084
AE-food	0.6688	0.7524	0.836	0.9196	1.0032
HIF	0.1824	0.2052	0.228	0.2508	0.2736
DM-food	0.536	0.603	0.67	0.737	0.804
ED-food	9824.88	11052.99	12281.1	13509.21	14737.32
ED-fat	31.28	35.19	39.1	43.01	46.92
ED-cpro	15.28	17.19	19.1	21.01	22.92
gamma-mobilize	0.012	0.0135	0.015	0.0165	0.018
perc-water-adi	0.0952	0.1071	0.119	0.1309	0.1428
SL-max	0.3184	0.3582	0.398	0.4378	0.4776
Life history parameters:					
t-mating-start	96.8	108.9	121	133.1	145.2
t-mating-end	218.4	245.7	273	300.3	327.6
t-mature	36	40.5	45	49.5	54
prob-ovul	0.176	0.198	0.22	0.242	0.264
t-0	3.2	3.6	4	4.4	4.8
t-gest	16	18	20	22	24
t-nurs	16.8	18.9	21	23.1	25.2
t-max-age	496	558	620	682	744

surv-prob-const*	75.7344	85.2012	94.668	104.1348	113.6016
surv-prob-mid*	0.0144	0.0162	0.018	0.0198	0.0216
surv-mod-emb*	0.4016	0.4518	0.502	0.5522	0.6024
surv-mod-off*	0.5064	0.5697	0.633	0.6963	0.7596
winter-surv-mid	0.3328	0.3744	0.416	0.4576	0.4992

The Morris screening revealed that, for the simulated conditions, one parameter, the deposition efficiency of fat (DE-fat), was the most influential on all output patterns (Table S28). When using a value of 40% of the maximum value found as a threshold, three outputs were predominantly influenced by this parameter (Table S28). Additionally, again using a threshold of 40%, 45 of the parameters were found to be influential on the number of litters per year. However, closer inspection of the outputs revealed that this result was not indicative of a high number of parameters being highly influential, but rather that these parameters were equally but only slightly influential. The 10 parameters found to be the most sensitive to the simulated conditions, based on the sum of the outputs (excluding litters per year) in Table S27, and their potential mechanisms of influence on the model are outlined in Table S29. In the same table, methods for obtaining values for these parameters for reapplication of the model are suggested. Special care should be taken in calibrating or parameterizing these parameters, as well as any others found to be influential, in the absence of well-known empirical measurements.

Table S28. Morris method results from the complete sensitivity analysis of the model displayed as a percentage of maximum sensitivity (represented by the * index) found at the end of simulation year three for each of the seven model outputs of focus: body mass of adults, neonates, and weaned offspring, age at first birth, litters per year, litter size at birth, and population density. Sensitivity values over 40% of the maximum are shown in bold. Any parameter which had a sensitivity value of over 40% is shown in bold. Parameters with the strongest influence which were ID'd for the following Sobol analysis are shown in blue.

Parameter code	Adult body mass	Neonate body mass	Weaning body mass	Age at first birth	Litters per year	Litter size at birth	Population density
perc-resource-cells	12.8	2.4	6.7	19.4	**52.2**	11.8	26.8
max-resources-base	14.5	3.6	6.0	29.2	**43.7**	15.8	26.7
r-growth-ts	7.6	1.4	2.3	17.9	**52.8**	11.4	20.3
fragmentation-level	16.7	5.6	7.5	21.9	36.7	11.6	18.7
n-animals	7.6	1.8	2.4	9.3	33.3	6.5	15.8
speed-mean	12.1	3.0	6.3	18.3	**51.1**	16.7	38.5
speed-max	12.2	4.2	6.1	27.3	34.9	12.2	17.7
HR-r-min	12.8	1.8	3.4	32.2	**65.2**	14.4	24.9
HR-r-max	14.8	5.6	6.0	**43.0**	32.4	16.4	14.1
B0	18.1	1.6	5.0	17.9	**41.8**	9.3	24.4
gamma	25.3	9.6	18.5	39.3	**63.9**	20.5	36.5
intercept-pcot	17.8	2.0	4.0	31.3	**49.9**	8.8	18.2
slope-pcot	27.6	5.4	11.5	32.6	**79.5**	18.8	39.0
intercept-icot	22.8	2.1	2.3	33.3	**70.1**	17.0	19.2
slope-icot	6.8	1.0	1.3	13.2	33.3	8.2	18.5
n-emb-mid	19.6	1.0	1.9	16.2	28.3	23.1	25.9

emb-growth-c	37.9	**56.7**	25.6	**42.8**	81.6	25.7	19.8
emb-mass-init	25.6	11.4	10.5	33.9	**63.6**	24.0	23.3
emb-mass-inf	17.0	14.6	5.2	21.0	30.5	6.0	25.3
percent-fat-emb	7.2	3.9	2.0	23.2	**48.0**	13.2	27.5
percent-pro-emb	29.8	12.8	10.9	25.5	**40.8**	17.7	17.2
ED-pl	7.2	1.0	1.9	19.1	**55.5**	9.4	22.5
DE-pl	17.0	3.2	6.4	20.6	**47.1**	15.8	22.0
preg-prob-const	28.2	6.0	6.0	19.8	**50.6**	9.2	26.0
preg-prob-mid	9.8	3.2	2.4	21.3	**45.4**	9.8	23.3
off-BMR-red	26.7	2.6	8.4	18.3	**42.0**	10.3	19.8
off-growth-eff	7.6	1.7	6.1	7.8	27.1	5.0	22.8
milk-prod-eff	13.1	2.0	7.6	14.8	25.9	9.3	26.2
lact-prob-const	20.9	3.0	6.4	13.2	**67.8**	13.1	18.6
lact-prob-mid	12.7	3.1	7.3	38.3	**57.7**	14.5	35.0
ED-pro	28.0	2.2	8.4	30.5	**75.8**	9.9	21.8
DE-fat	**100.0**	**100.0**	**100.0**	**100.0**	**100.0**	**100.0**	**100.0**
DE-pro	12.7	2.9	3.8	16.3	**45.8**	9.6	26.0
growth-lm-prob-const	19.5	2.1	3.5	23.7	**61.2**	11.7	19.6
growth-lm-prob-mid	24.8	1.6	2.7	17.0	35.5	7.7	26.0
growth-lm-inf	**40.0**	3.6	11.1	24.4	**56.0**	9.7	25.6
growth-lm-k	21.8	3.3	18.9	28.5	**47.1**	13.9	18.6
stomach-fill-perc	35.3	7.6	10.0	27.7	32.0	15.4	24.0
AE-food	30.3	13.5	8.3	23.8	**64.3**	15.8	36.0
HIF	29.2	15.8	19.7	29.2	**59.8**	12.3	25.7
DM-food	16.1	3.4	8.0	26.0	**51.8**	12.7	21.0
ED-food	17.7	2.7	4.1	16.8	30.1	7.3	35.6
ED-fat	28.7	1.8	6.8	24.3	**64.4**	11.9	28.3
EC-pro	38.9	7.0	6.9	30.0	**77.4**	17.9	23.3
gamma-mobilize	12.6	1.3	1.6	19.7	**49.0**	4.5	24.0
perc-water-adi	19.9	11.9	8.8	32.5	**57.1**	16.3	21.8
max-SL	33.7	11.2	15.6	**42.3**	78.4	23.6	33.1
t-mating-start	34.4	6.3	8.2	**53.3**	72.2	29.2	20.7
t-mating-end	28.7	3.4	5.6	**66.4**	43.3	10.3	33.8
t-mature	7.0	2.5	3.3	29.6	**47.5**	14.2	21.8
prob-ovul	16.4	1.4	2.4	12.0	34.8	5.1	22.1
t-0	15.9	8.2	11.0	24.3	**45.0**	13.5	21.4
t-gest	30.8	**67.4**	27.1	21.4	**56.8**	5.6	21.5
t-nurs	10.7	4.7	18.2	34.9	**73.6**	17.0	24.6
t-max-age	31.2	7.4	4.5	**45.9**	66.0	19.6	25.5
surv-prob-const	13.5	1.6	3.5	26.8	**75.3**	11.5	29.2
surv-prob-mid	11.4	2.8	2.3	29.1	34.9	9.6	21.0
surv-mod-emb	15.4	9.7	6.3	21.3	**50.1**	11.3	17.6
surv-mod-off	8.3	2.0	3.5	14.3	**50.2**	6.0	16.4
winter-surv-mid	14.1	5.2	7.1	31.4	29.9	8.6	28.4

Table S29. Parameter sensitivity ranking as a percentage of the maximum sensitivity value of the 25 most influential parameters identified for each of the model outputs. Sensitivity values over 40% of the maximum are shown in bold.

Parameter code	Adult body mass	Parameter code	Neonate body mass	Parameter code	Weaning body mass	Parameter code	Age at first birth	Parameter code	Litters per year	Parameter code	Litter size at birth	Parameter code	Population density
DE-fat	**100.0**	DE-fat	100.0	DE-fat	100.0	**DE-fat**	**100.0**	DE-fat	100.0	**DE-fat**	**100.0**	DE-fat	**100.0**
growth-lm-inf	**40.0**	**t-gest**	**67.4**	t-gest	27.1	**t-mating-end**	**66.4**	emb-growth-c	81.6	t-mating-start	29.2	slope-pcot	39.0
EC-pro	38.9	**emb-growth-c**	**56.7**	emb-growth-c	25.6	**t-mating-start**	**53.3**	slope-pcot	79.5	emb-growth-c	25.7	speed-mean	38.5
emb-growth-c	37.9	HIF	15.8	HIF	19.7	**t-max-age**	**45.9**	max-SL	78.4	emb-mass-init	24.0	gamma	36.5
stomach-fill-perc	35.3	emb-mass-inf	14.6	growth-lm-k	18.9	**HR-r-max**	**43.0**	EC-pro	77.4	max-SL	23.6	AE-food	36.0
t-mating-start	34.4	AE-food	13.5	gamma	18.5	**emb-growth-c**	**42.8**	ED-pro	75.8	n-emb-mid	23.1	ED-food	35.6
max-SL	33.7	percent-pro-emb	12.8	t-nurs	18.2	**max-SL**	**42.3**	surv-prob-const	75.3	gamma	20.5	lact-prob-mid	35.0
t-max-age	31.2	perc-water-adi	11.9	max-SL	15.6	gamma	39.3	**t-nurs**	**73.6**	t-max-age	19.6	t-mating-end	33.8
t-gest	30.8	emb-mass-init	11.4	slope-pcot	11.5	lact-prob-mid	38.3	**t-mating-start**	**72.2**	slope-pcot	18.8	max-SL	33.1
AE-food	30.3	max-SL	11.2	growth-lm-inf	11.1	t-nurs	34.9	**intercept-icot**	**70.1**	EC-pro	17.9	surv-prob-const	29.2
percent-pro-emb	29.8	surv-mod-emb	9.7	t-0	11.0	emb-mass-init	33.9	**lact-prob-const**	**67.8**	percent-pro-emb	17.7	winter-surv-mid	28.4
HIF	29.2	gamma	9.6	percent-pro-emb	10.9	intercept-icot	33.3	**t-max-age**	**66.0**	t-nurs	17.0	ED-fat	28.3
ED-fat	28.7	t-0	8.2	emb-mass-init	10.5	slope-pcot	32.6	**HR-r-min**	**65.2**	intercept-icot	17.0	percent-fat-emb	27.5
t-mating-end	28.7	stomach-fill-perc	7.6	stomach-fill-perc	10.0	perc-water-adi	32.5	**ED-fat**	**64.4**	speed-mean	16.7	perc-resource-cells	26.8
preg-prob-const	28.2	t-max-age	7.4	perc-water-adi	8.8	HR-r-min	32.2	**AE-food**	**64.3**	HR-r-max	16.4	max-resources-base	26.7
ED-pro	28.0	EC-pro	7.0	ED-pro	8.4	winter-surv-mid	31.4	**gamma**	**63.9**	perc-water-adi	16.3	milk-prod-eff	26.2
slope-pcot	27.6	t-mating-start	6.3	off-BMR-red	8.4	intercept-pcot	31.3	**emb-mass-init**	**63.6**	max-resources-base	15.8	DE-pro	26.0

off-BMR-red	26.7	preg-prob-const	6.0	AE-food	8.3	ED-pro	30.5	**growth-lm-prob-const**	**61.2**	DE-pl	15.8	preg-prob-const	26.0
emb-mass-init	25.6	HR-r-max	5.6	t-mating-start	8.2	EC-pro	30.0	**HIF**	**59.8**	AE-food	15.8	growth-lm-prob-mid	26.0
gamma	25.3	fragmentation-level	5.6	DM-food	8.0	t-mature	29.6	**lact-prob-mid**	**57.7**	stomach-fill-perc	15.4	n-emb-mid	25.9
growth-lm-prob-mid	24.8	slope-pcot	5.4	milk-prod-eff	7.6	max-resources-base	29.2	**perc-water-adi**	**57.1**	lact-prob-mid	14.5	HIF	25.7
intercept-icot	22.8	winter-surv-mid	5.2	fragmentation-level	7.5	HIF	29.2	**t-gest**	**56.8**	HR-r-min	14.4	growth-lm-inf	25.6
growth-lm-k	21.8	t-nurs	4.7	lact-prob-mid	7.3	surv-prob-mid	29.1	**growth-lm-inf**	**56.0**	t-mature	14.2	t-max-age	25.5
lact-prob-const	20.9	speed-max	4.2	winter-surv-mid	7.1	growth-lm-k	28.5	**ED-pl**	**55.5**	growth-lm-k	13.9	emb-mass-inf	25.3
perc-water-adi	19.9	percent-fat-emb	3.9	EC-pro	6.9	stomach-fill-perc	27.7	**r-growth-ts**	**52.8**	t-0	13.5	HR-r-min	24.9

Two parameters which relate to basal metabolic rate and transport costs of animals, *gamma* and *slope-pcot,* had a substantial effect on the model's outputs. *Gamma* determines the exponent of the allometric relationship between body mass and basal metabolic rate, while *slope-pcot* represents the exponent of the relationship between body mass and postural costs of transport - the energy required to maintain an upright posture associated with standing or moving. These parameters dictate the relative metabolic costs that animals incur based on their body size. Although the debate on the existence of universal scaling exponents is very much ongoing, at least in regard to maintenance costs, here and in many cases data may exist for the study species and closely related species to parameterize these parameters directly.

The parameter *emb-growth-c*, which represents the fetal growth constant, was found to have a strong impact on various model outputs, including the neonate body mass, age at first birth, and the number of litters per year. Since this parameter determines the maximum rate of fetal growth and thus the cost of embryonic tissue production, its influence on neonate mass outputs and, subsequently, on offspring survival and reproductive costs is expected. Fetal masses were available in this study, and similar data should be obtainable for many other mammalian species. When available, empirical values should be used, but neonate masses and literature-based relationships could be used to estimate this parameter when data are not available.

Two parameters related to the storage dynamics submodel were found to be highly influential on model outputs. These two parameters were the maximum storage level (*SL-max*) and energy density of fat (*ED-fat*). They affect an animal's ability to store energy and access it during times of food scarcity, thereby influencing storage levels, energy allocation to growth and reproduction, and ultimately survival. Although empirical data on the storage levels of animals can be readily obtained for many species, determining the maximum storage levels can be more challenging. Though allometric relationships may be useful when data are unavailable (*222*). Furthermore, the deposition efficiencies of fat are not well-understood, and values are only available for a few species, mainly rodents. It is important to note that while the *DE-fat* values were derived from rodent species, specific empirical data for bank voles was unavailable, and the extent of variability between species for this parameter is unknown.

Additionally, one parameter influencing the energetic costs of digestion, or the heat increment of feeding, *HIF*, was identified as being relatively influential.
This parameter controls the amount of energy generated as waste heat when digesting food resources, and therefore determines the amount of energy available from ingested food which is available for other physiological processes such as growth, reproduction, and maintenance. In nature, the heat increment of feeding is influenced by various factors such as diet composition, food quantity, and environmental conditions, and it can vary significantly among different mammal species. Therefore, it may not be well understood for all mammals, and empirical measurements may not be available for many species. In some cases, values from similar species may be used, or the parameter may be calibrated following a pattern-oriented modelling approach.

Finally, four parameters related to animal demographics were found to have a significant impact on model outputs: the start and end of the mating period (*t-mating-start* & *t-mating-end*), the gestation period (*t-gest*), and the maximum age (*t-max-age*). These parameters control the timing of demographic events and therefore affect reproductive and mortality rates in the model. Altering the start and end of the mating period changes the length of time available for reproduction, allowing for more or fewer litters per year. The gestation period influences the time spent gestating and size of offspring at birth and therefore the costs associated with pregnancy, lactation, and offspring survival. Finally, the maximum age determines the longest time individuals can survive before succumbing to senescence. However, these parameters are generally well-understood and can be obtained directly from empirical studies for many species.

Table S30. Parameters which were found to have the highest influence on model outputs (calculated as the summation of their sensitivity indices for all model outputs aside from the number of litters per year) in the global sensitivity analysis ranked in order of decreasing influence.

Parameter code	Sensitivity considerations
gamma	This parameter determines the exponent of the relationship between the body mass of animals and their basal maintenance costs. Values for this parameter can be obtained from empirical data, when available. See Section 3 for how this was done in this parameterization.
slope-pcot	This parameter represents the exponent of the relationship between the body mass and the postural cost of transport, which, for some species of mammals, empirical estimates exist or are obtainable. Values from empirical measurements should be used here and, when available, though in this case values needed to be obtained from other small rodents. See Section 3 for how this was done in this parameterization.
emb-growth-c	This parameter represents the fetal growth constant, which, for many species of mammals, empirical data exist to determine its value. The growth constant determines the maximum rate at which neonate mass is deposited during fetal development, while actual deposition rates depend on mother allocation to pregnancy. Values from empirical measurements should be used here. See Section 3 for details on this parameterization.
DE-fat	The energy density of catabolized protein differs from the "true" energy content of protein from its heat of combustion due to urinary losses occuring with the process of catabolism. This parameter converts energy to mass whenever animals catabolize stored lean mass tissue. While empirical values exist for some species, data was not available for bank voles, and the extent of variability between mammals for these parameters remains unknown. Empirical values should be used here, ideally for the species which the model represents.
HIF	This parameter controls the heat increment of feeding, or the energetic costs associated with digestion, in the model. While estimates may be available for some mammal species, it is likely to be unknown for many others. Moreover, in reality, this parameter is influenced by diet. In the absence of empirical measurements, values from similar species may be used as a substitute (as done here). Alternatively, this parameter can be calibrated.
max-SL	This parameter controls the maximum body fat percentage of animals in the model. This parameter is obtainable for many species and values from empirical

t-mating-start	This parameter sets the start of the breeding season in the model and, when overwinter skipping is enabled, determines the first simulated day of the year (five days before the beginning of the mating season). The breeding season is typically known for many mammal species, so it is recommended to obtain values for this parameter from empirical data, where possible.
t-mating-end	This parameter sets the end of the breeding season in the model and, when overwinter skipping is enabled, determines the last simulated day of the year (five days after the end of the mating season). The breeding season is typically known for many mammal species, so it is recommended to obtain values for this parameter from empirical data, where possible.
t-gest	This parameter represents the length of the gestation period in the model. The values of this parameter are fairly well known in mammal species and, as such, empirical data should be used when available.
t-max-age	This parameter represents the maximum age of animals in the model. The values of this parameter are fairly well known in mammal species and, as such, empirical data should be used when available. Alternatively allometric and or phylogenetic relationships may be available for use when species-specific values are unknown.

(Note: the table's first row continues text from the previous page:)

measurements should be used. Additionally, existing allometric relationships may be used when empirical values are not available.

7.2. Prioritization of parameters

For the ten parameters found to be the most highly influential on the selected model outputs (all except for the Number of litters per year) using the Morris method for the current simulation conditions we applied a variance-based sensitivity analysis following the method of Sobol (2001). For assessing parameter sensitivity, we again used the seven model outputs: body masses of adults, neonates, and weaned offspring, age at first birth, litters per year, litter size at birth, and population density. We ran this analysis to estimate the effect of these highly influential parameters on the variance of model outputs and to assess the contribution arising from interactions between these parameters on model output variance. This analysis was run using the sensitivity package in R (*125*) and the input parameter combinations were designed using two latin hypercube sampling matrices (*lhs* package in R; (*223*) with values constrained between the extreme low and extreme high values determined for each of the parameters as used previously in the Morris method (Table S27). As outputs were not centered, we used the *soboljansen* function to design the sensitivity analysis. A total of 6000 model runs were performed, with a sampling matrix size of 500 and ten parameters sampled, calculated as m × (p + 2) where m is the size of the Monte Carlo sampling matrix and p is the number of parameters sampled.

When looking at the first-order indices, the results showed that the *DE-fat* parameter had the greatest impact on the variance of adult, neonate, and weaning body masses as well the litter size at birth and population density, while *SL-max* had the largest impact on the variance of the age at first birth and *gamma* had the largest impact on the number of litters per year (Table S31).

Table S31. Results of the first-order indices of the Sobol sensitivity analysis for the ten parameters identified as the most influential on model outputs using the Morris method. The contribution to the variance in seven model outputs was determined for each parameter (mean ± standard error for 1000 bootstrap iterations). Indices found with values greater than 15% are shown in bold.

Parameter code	Adult body mass	Neonate body mass	Weaning body mass	Age at first birth	Litters per year	Litter size at birth	Population density
gamma	0.089 (0.11)	-0.036 (0.084)	0.017 (0.057)	-0.059 (0.084)	**0.167** (0.135)	0.121 (0.061)	0.109 (0.065)
slope-pcot	0.107 (0.101)	-0.059 (0.088)	-0.009 (0.057)	-0.041 (0.083)	0.004 (0.144)	0.095 (0.059)	0.012 (0.065)
emb-growth-c	0.073 (0.088)	**0.182** (0.085)	0.03 (0.058)	-0.075 (0.091)	0.112 (0.135)	0.078 (0.059)	0.02 (0.066)
DE-fat	**0.463** (0.078)	**0.21** (0.073)	**0.699** (0.023)	-0.121 (0.113)	0.104 (0.173)	**0.581** (0.055)	**0.508** (0.039)
HIF	0.106 (0.107)	-0.025 (0.083)	0.036 (0.056)	0.01 (0.089)	0.043 (0.16)	0.146 (0.062)	0.049 (0.066)
SL-max	0.116 (0.107)	-0.038 (0.086)	-0.003 (0.057)	**-0.173** (0.102)	-0.069 (0.185)	0.125 (0.064)	-0.011 (0.069)
t-mating-start	-0.024 (0.103)	-0.052 (0.088)	0.002 (0.054)	-0.068 (0.091)	0.121 (0.143)	0.059 (0.06)	-0.007 (0.066)
t-mating-end	0.073 (0.111)	-0.06 (0.088)	0.007 (0.055)	0.021 (0.087)	0.034 (0.158)	0.074 (0.058)	-0.005 (0.07)
t-gest	0.122 (0.093)	**0.191** (0.094)	0.042 (0.058)	-0.08 (0.079)	0.104 (0.155)	0.085 (0.063)	0.005 (0.064)
t-max-age	0.04 (0.108)	-0.062 (0.089)	-0.004 (0.055)	-0.067 (0.078)	-0.012 (0.142)	0.09 (0.059)	0.023 (0.062)

To gain a more comprehensive understanding of the influence of input parameters on the model output variance, we additionally evaluated the total-effect indices. These indices provide insight into the combined effect of a parameter, taking into account its interactions with all other input parameters. The low sum of first order sensitivity indices indicates that the impact of parameter interactions on the variance of model outputs cannot be ignored and must be taken into consideration in this analysis.

The results of the total-effects analysis showed that *DE-fat* had a large impact on all model outputs when indirect effects were taken into account (Table S32). Additionally, *SL-max* was also found to be important for the age at first birth, the number of litters per year, and the litter size at birth. The parameters *slope-pcot, t-mating-start,* and *t-max-age* were found to have both low first-order indices and low total-effect indices, suggesting that these parameters may have a weak or negligible effect on these model outputs (Figure S27). While variance in three of the outputs, adult body mass, weaning body mass, and population density was primarily driven by one parameter, *DE-fat*, age at first birth and the number of litters per year had relatively high sensitivity indices for all of the input parameters. This indicates that interactions between parameters and processes play a crucial role in driving the variance of these outputs and, accordingly, minimal impacts were observed for changes in each parameter individually for these two outputs (Figure S27).

Table S32. Results of the total-effect indices of the Sobol sensitivity analysis for the ten parameters identified as the most influential on model outputs using the Morris method. The contribution to the variance in seven model outputs was determined for each parameter (mean ± standard error for 1000 bootstrap iterations). Indices found with values greater than 40% are shown in bold.

Parameter code	Adult body mass	Neonate body mass	Weaning body mass	Age at first birth	Litters per year	Litter size at birth	Population density
gamma	0.241 (0.041)	0.02 (0.005)	0.037 (0.004)	**0.423** (0.065)	**0.447** (0.062)	0.224 (0.036)	0.225 (0.022)
slope-pcot	0.219 (0.042)	0.01 (0.003)	0.024 (0.006)	0.306 (0.047)	0.386 (0.074)	0.14 (0.029)	0.124 (0.018)
emb-growth-c	0.12 (0.03)	0.366 (0.04)	0.083 (0.008)	0.388 (0.06)	0.344 (0.052)	0.183 (0.033)	0.104 (0.012)
DE-fat	**0.755** (0.086)	**0.529** (0.062)	**0.865** (0.056)	**0.811** (0.066)	**0.923** (0.1)	**0.923** (0.06)	**0.826** (0.06)
HIF	0.288 (0.041)	0.068 (0.012)	0.108 (0.013)	**0.403** (0.05)	**0.561** (0.079)	0.319 (0.044)	0.224 (0.028)
SL-max	0.289 (0.049)	0.049 (0.01)	0.077 (0.01)	**0.705** (0.076)	**0.842** (0.11)	**0.407** (0.045)	0.234 (0.032)
t-mating-start	0.185 (0.045)	0.01 (0.004)	0.01 (0.003)	0.375 (0.06)	0.383 (0.066)	0.123 (0.027)	0.105 (0.014)
t-mating-end	0.269 (0.05)	0.014 (0.004)	0.02 (0.005)	**0.694** (0.07)	**0.504** (0.085)	0.177 (0.033)	0.152 (0.016)
t-gest	0.149 (0.029)	**0.404** (0.038)	0.094 (0.009)	0.38 (0.055)	**0.571** (0.08)	0.22 (0.037)	0.104 (0.014)
t-max-age	0.253 (0.048)	0.008 (0.003)	0.012 (0.004)	0.275 (0.053)	0.303 (0.063)	0.13 (0.028)	0.067 (0.008)
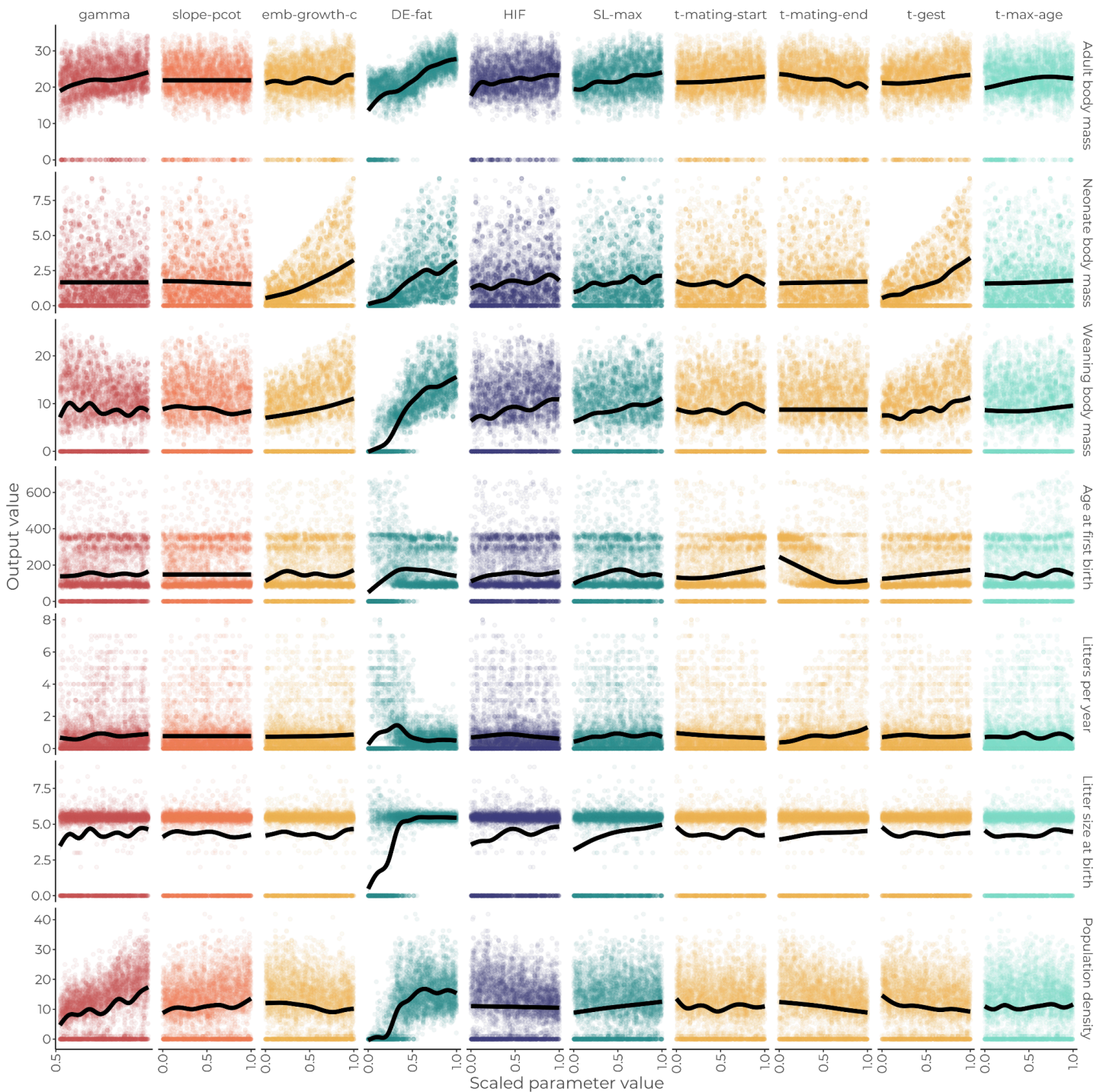
Figure S27. Impacts on seven key model outputs (rows) by the ten parameters (columns) varied in the Sobol sensitivity analysis. Parameter values were scaled between 0 and 1 using their minimum and maximum values and results are presented for each of the 6000 simulation runs. Black lines represent GAMs fit to the outputs. The three body mass related outputs (Adult body mass, Neonate body maxx, and Weaning body mass) are in units of grams, Age at first birth is in days, and Litters per year, Litter size at birth, and Population density are all counts (N). The colors of individual points represent the submodel to which that parameter belongs, with red for maintenance, orange for activity, yellow for reproduction, dark blue for storage, purple for energy intake, and light blue for mortality.

8. Model output corroboration

This TRACE element provides supporting information on: How model predictions compare to independent data and patterns that were not used, and preferably not even known, while the model was developed, parameterized, and verified. By documenting model output corroboration, model users learn about evidence, which, in addition to model output verification, indicates that the model is structurally realistic so that its predictions can be trusted to some degree.

Summary:

Following the calibration process, the model was subjected to a thorough two phase evaluation utilizing independent data pertaining to bank vole energetics, mortality, morphometrics, life history, and population densities. The first phase focused on diverse energetic and trait patterns found across literature. The outcomes of this evaluation demonstrated that the model predictions were in good agreement with the empirical patterns. For the second phase, we replicated an empirical bank vole litter manipulation experiment in the wild to assess the model's accuracy in reflecting observations when applied to a specific system. The model successfully reproduced key patterns, including seasonal fluctuations in population density, weaning mass, and survival dynamics, closely aligning with empirical results for most metrics. While some discrepancies were noted, such as overestimation of litter size at weaning and deviations in neonate body mass in late summer, overall, we were satisfied with the model's performance in capturing complex reproductive and survival trends both across reproductive status (litter size) and season. Based on this, the model was deemed appropriate for utilization in scenario simulations.

8.1. Initial evaluation against diverse patterns

After successfully calibrating the model, we evaluated it against 11 additional patterns to assess its ability to capture various aspects of bank vole energetics, life history, and morphometrics. The objective was to ensure that the model outputs were in agreement with values for bank voles in several energetic studies and in the PanTHERIA database (*218*). The 11 patterns and their associated sources and values can be found in Table S33.

For this evaluation step, 150 simulations were run (5 repetitions per parameter set; see Section 6 for details), and outputs were collected in simulation year 5 (with additional tracking of surviving animals in year 6 for pattern 19). The interval with which each output was collected can be found in Table S33.

Almost all of the evaluation patterns displayed good model fits, with a few minor deviations (Figure S281). There was a slight discrepancy in the mortality pattern between days 50-200 (Figure S28C), which was likely due to the inclusion of overwinter skipping and the one-time application of overwinter mortality, though the model accurately captured early and late survival percentages. The age at first birth also posed a challenge in evaluation as animals born early in the breeding season mature quickly enough to breed within that season, while others only breed if

they survive to the spring of the following year (Figure S28E), which follows empirical knowledge of this species (*224*). This made it difficult to accurately evaluate pattern fit. Nevertheless, the majority of animals breed in the year of their birth, with a median age at first breeding of 68 days, compared to the empirical value of 83.22 days, while the mean (± 1 SD) was 111.1 ± 88.7 days. Despite the difficulties posed by the gap between the breeding seasons, the overlap between these values were taken as close enough to consider the fit sufficient.

Table S33. *Empirical patterns used in initial model evaluation. All outputs collected in simulation year 5.*

Pattern	When collected	Value	Source
17. State-dependent field metabolic rate	Once per week	Mean with error (in kJ day) for 2 states: Reproducing & Nonreproducing	(*137, 197, 199, 225, 226*)
18. State-dependent food consumption	Once per week	Mean with error for 4 states: Juvenile, Nonreproducing, Pregnant, & Lactating	(*132, 164–166, 197*)
19. Survival rates	At death	Survivorship curve covering 16 months	(*227*)
20. Adult body mass	Once per week	20.73 g	(*218*)
21. Age at first birth	At birth	83.22 days	(*218*)
22. Mass-specific basal metabolic rate	Once per week	26.25 J g^{-1} 30min^{-1}	(*218*)
23. Litter size	At birth	4.31 offspring	(*218*)
24. Litters per year	Once at end of year	3.5 litters year^{-1}	(*218*)
25. Neonate body mass	At birth	1.83 g	(*218*)
26. Weaning body mass	At weaning	9.43 g	(*218*)
27. Population density	Once per day	18.5 females ha^{-1}	(*218*)

Similarly, evaluating the model fit for the numbers of litters born per female per year posed a bit of a challenge (Figure S28H). While females born in the previous season which had a full breeding season to reproduce had 4.2 ± 0.5 litters per year, compared to the empirical value of 3.5, females born within a breeding season only had the opportunity to have 1-2 litters with most not breeding at all (55.1%) (a mean number of litters of 0.6 ± 0.8). While it is likely that the value in the PanTHERIA database corresponds to the potential of an animal breeding over the entire breeding season (similar to other records of "up to" 4 or 5 litters per year (*174, 228*), it is unclear under exactly which conditions this value was collected under. As such, we decided to use a minimum age of 130 days to primarily include animals which had nearly the entire breeding season to reproduce for further analyses (2.5 ± 1.0, mean ± 1 SD). Furthermore, the mass-specific basal metabolic rates in the model were slightly lower than the reported values in the database (Figure S28F), though the difference was minimal even on a daily scale (a reduction of 0.3 g of food per day). The BMR calculations in the model were based on data from multiple animals and studies (see Section 3, Data evaluation, for details), while the value in the database represents a single value from an unknown number of individuals, thus some variance is expected.

While use of the PanTHERIA database led to some some overlap with the types of patterns used in the calibration section (litter size at birth, neonate mass, and population density), the patterns used here from PanTHERIA represent distinct datasets from those used to generate the calibration patterns. The results of this evaluation indicated that the model fits were generally quite satisfactory.
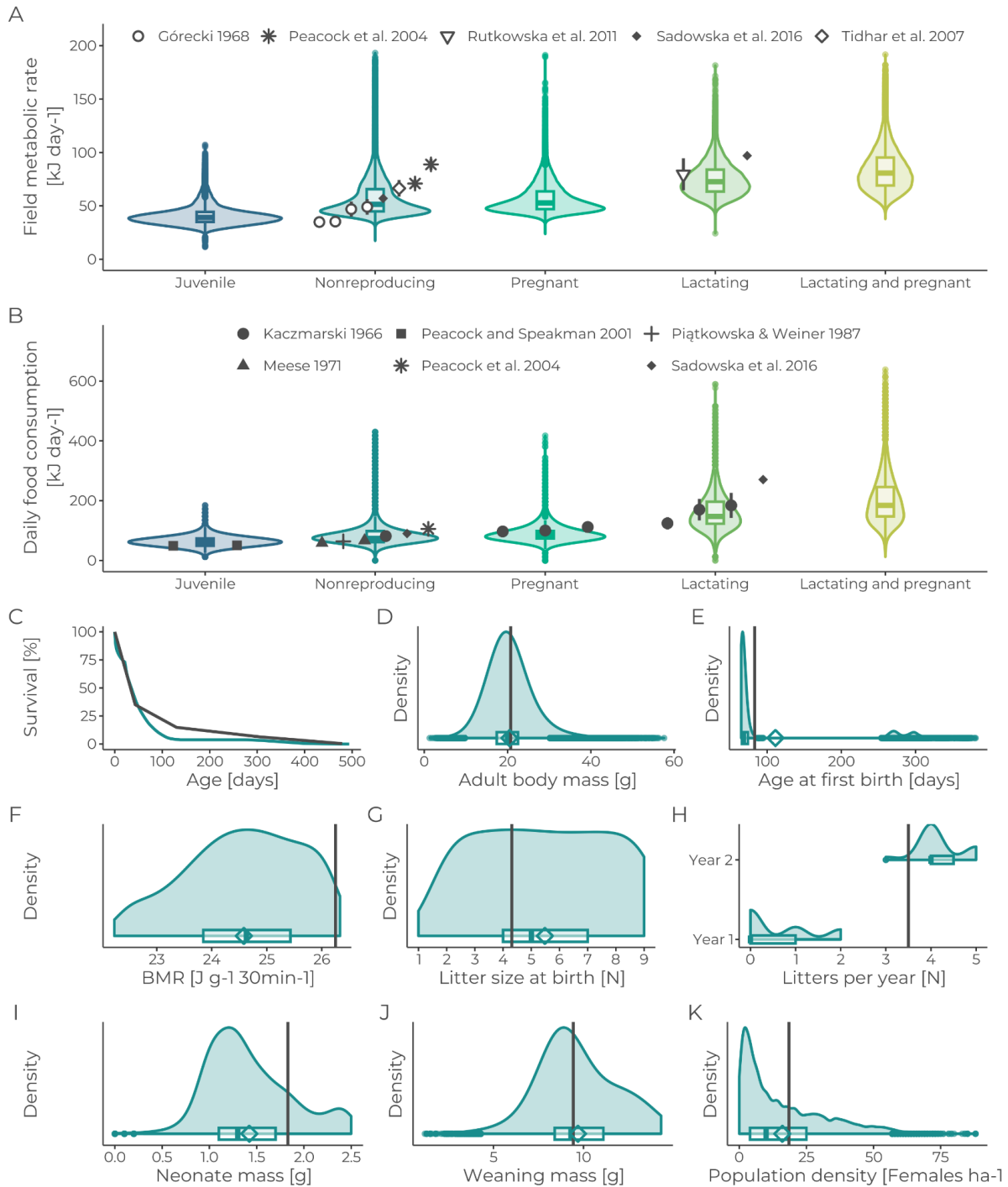
Figure S28. **Comparison of model predictions (depicted in blue) with eleven empirical patterns** (depicted in grey) for various traits, including (A) state-dependent field metabolic rates, (B) state-dependent food consumption, (C) survivorship curve, (D) adult body mass, (E) age at first birth, (F) mass-specific metabolic rate, (G) litter size at birth, (H) number of litters per year, (I) neonate mass, (J)

weanling mass, and (K) population density. For (A) and (B), the points represent the mean values, and whiskers represent the error estimates from the studies. For (D) through (F), dashed lines represent the single value estimates from the PanTHERIA database. Blue diamonds represent the mean value from the model outputs, and the filled area represents the density curve. Model outputs are presented from 150 simulation replicates.

8.3. Replication of empirical litter manipulation experiment

To further evaluate the model's ability to reproduce empirical observations, we replicated the conditions and evaluated key outputs of a litter manipulation experiment conducted on bank voles under wild conditions (*50*). Litter manipulation experiments represent a classic approach in small mammal reproductive studies, where litter sizes of females which have recently given birth are experimentally increased or decreased. Such studies have been used to assess the costs and trade-offs associated with reproduction across various species and settings, from laboratory environments to outdoor enclosures and the wild (*50*, *56*, *57*).

In the selected study, the effects of manipulated litter size on weanling number and body mass, characteristics of subsequent breeding attempts, and maternal survival were assessed over three years in free-ranging bank voles in Konnevesi, central Finland. Empirical values were manually extracted from published plots using Automeris WebPlot digitizer v4.5 (*200*).

To replicate the study conditions and sampling design, several adjustments were made to the model. The mating period was set from day 130 to day 279 of the simulation year, and the maximum number of embryos at birth was increased from 9 to 10 to better match the study's findings. To mimic the empirical resource environment, the Normalized Difference Vegetation Index (NDVI) (*47*) was used as a proxy for changes in resource availability. NDVI data were obtained from the extended global NDVI3g product (third generation Global Inventory Modeling and Mapping Studies (GIMMS)(*229*)) at a bi-weekly resolution for 1990 to 1999 at the study site. This data was accessed using the "gimms" package in R (*230*) and interpolated to a daily resolution. The 0-1 NDVI values were converted into a 0-2 modifier variable, which adjusted the calibrated maximum resource level parameter (see Section 6 for details). A value of 1 maintained the calibrated value as is, a value of 0 reduced the maximum food resource level to zero, and a value of 2 doubled the maximum level. When NDVI values increased, food levels in resource patches rose once per day by the corresponding increase in the maximum level, while any decreases in NDVI were enforced only by capping values to the maximum resource level.

Outputs were collected following the empirical approach as closely as possible. In 1996 to 1998, a number of pregnant females with masses similar to those of the empirical animals (15.7 to 32.4 g, excluding neonate and placental tissues) were selected, using a maximum number of the year-, season-, and manipulation group-specific sample size. At the time of birth, the litter size of selected females was updated to match the empirical values for their assigned manipulation group ('Enlarged' or 'E', 'Reduced' or 'R', and 'Control' or 'C'). The observation dates were selected to align with the seasonal sampling method outlined in the original paper: simulation day 135 for early summer,

day 181 for mid-summer, day 243 for late summer, and day 298 for autumn. For all observation dates, the total abundance of independent individuals was recorded to compare with the reported density dynamics. The selected mothers were tracked throughout the stages of birth, weaning, and subsequent births, during which 12 key patterns were observed for each animal (Table S34). No new females were tracked in autumn, in accordance with the empirical study. One hundred simulation replicates were run to account for stochasticity from ABC parameter combinations and other sources, with outputs analyzed similarly to the empirical results (see Table S34 for details). Since animals in the empirical study couldn't be measured precisely at weaning, independent individuals older than 30 days were observed for weaning transition patterns. To account for this minimum age, the model collected outputs at 37 days to provide some flexibility in the observations.

Table S34. *Empirical patterns used in the replication of a litter manipulation experiment. Outputs were collected for selected females during relevant life history events across 100 simulation replicates, corresponding to the years 1996-1998. All empirical patterns are sourced from Koivula et al., 2003.*

Pattern	Unit	When collected	Grouping for Analysis
28. Relative population density	Proportion of maximum density (N per hectare)	Seasonally	Year & Season
29. Litter size at birth	N offspring	Birth	Season & Manipulation group
30. Litter size at weaning	N offspring	Weaning	Season & Manipulation group
31. Litter size at second birth	N offspring	Second birth	Manipulation group
32. Offspring body mass at birth	grams	Birth	Season
33. Offspring body mass at weaning	grams	Weaning	Season & Manipulation group
34. Weaning success	%	Weaning	Manipulation group
35. Litter mass at birth	grams	Birth	Season & Manipulation group
36. Litter mass at weaning	grams	Weaning	Season & Manipulation group
37. Litter mass at second birth	grams	Second birth	Manipulation group
38. Reproductive effort (litter mass × mean neonate mass$^{0.75}$ / mother's mass$^{0.75}$)	unitless	Birth	Season
39. Survival of mother voles to next sampling season	%	Seasonally - subsequent sampling season	Season & Manipulation group
40. Mothers which gave birth to a subsequent litter	%	Second birth	Manipulation group

The model was found to be able to accurately replicate the majority of the empirical patterns (Figure S29). It captured the seasonal dynamics in population density, showing the highest values in late summer and the lowest in early summer. Notably, it also reflected some relative trends between years, such as the highest density in early summer and the lowest in late summer in 1997 compared to 1996 and 1998 (Figure S29A).

At birth, patterns in litter size (Figure S29B) served as a 'sanity check,' as these values were imposed for selected females. In contrast, litter mass (Figure S29H) and reproductive effort (Figure S29K) at birth emerged from neonate body mass (Figure S29E), driven by energy intake and allocation of the mother during gestation. While

the model outputs closely matched the empirical results for these patterns early in the year (early and mid-summer), the model's prediction of strong declines in neonate body mass in late summer resulted in relatively low litter mass values for that season.

At weaning, litter size was determined by the female's provisioning during lactation, and the outputs varied between manipulation groups and seasons (Figure S29C). The model reproduced observed seasonal patterns, with the largest litter sizes in mid-summer and lowest in late summer. However, offspring survival in the wild is likely influenced by various non-energetic factors, such as predation, and as the empirical study observed animals at a minimum of 30 days old, dispersal processes could already be at play (*231*). These factors likely led to an overall overestimation of litter size at weaning in the model compared to observations. While the model did capture the finding that litter reductions resulted in the smallest litters at weaning, it did not sufficiently capture the pattern that increased litter sizes at birth did not necessarily result in larger litter sizes at weaning, particularly during early and late summer. Instead, the model tended to predict that larger weaning litter sizes correlated positively with litter size at birth across all seasons. This effect was minimal in late summer though, where litter sizes were fairly consistent across manipulation groups. The phenomenon where increased litters at birth do not lead to increased litter size at weaning has been documented in litter manipulation experiments, but the underlying mechanism remains unknown (*56, 57, 67*). This discrepancy could be due to maternal behaviors not represented in the model, such as preferential feeding or infanticide in cases of enlarged litters.

Despite these challenges, the model accurately captured the observed declines in weanling body mass with both season and manipulation group (Figure S29F). However, due to the elevated litter size in the model, total litter mass at weaning remained higher than in the empirical study, though this deviation was again less pronounced in late summer (Figure S29I). The probability of a mother successfully weaning at least one pup was found to be similar to the empirical pattern (Figure S29G), with on average slightly higher values in the model results (mean: Observed: 55.9%; Modelled: 62.6%). Both the empirical and model results found no differences across treatment groups.

For mothers that gave birth to subsequent litters, the litter size at birth closely matched the empirical observations (Figure S29D). The model also successfully replicated the finding that manipulation groups affected subsequent litter mass, with females from enlarged litters having smaller litter masses at birth (mean ± S.E. pups: Observed: R: 11.2 ± 0.71, C: 10.26 ± 0.38, E: 9.79 ± 0.77; Modeled: R: 9.22 ± 0.18, C: 8.74 ± 0.16, E: 8.24 ± 0.17) (Figure S29J). However, the model's average litter mass was lower than the empirical findings (mean: Observed: 10.4 g; Modeled: 8.7 g), due to smaller average neonate sizes in late summer (Figure S29E). The proportion of females producing subsequent litters was also similar between the model and empirical results (Figure S29M), with no consistent pattern observed across manipulation groups (mean: Observed: R: 56%, C: 56.3%, E: 53.4%; Modeled: R: 50%, C: 31%, E: 48%).

Female survival to the next breeding period represents a truly emergent pattern, driven by both energy allocation, foraging success, and mortality processes. The

model successfully captured the decline in survival across seasons and treatment groups (Figure S29L), showing the lowest survival rates in late summer and among females with enlarged litters. While there were some discrepancies, such as the lack of an effect of manipulation group in early summer and relatively low survival of control females in late summer, the model still aligned surprisingly well with the empirical data, especially given the complexity of the pattern.
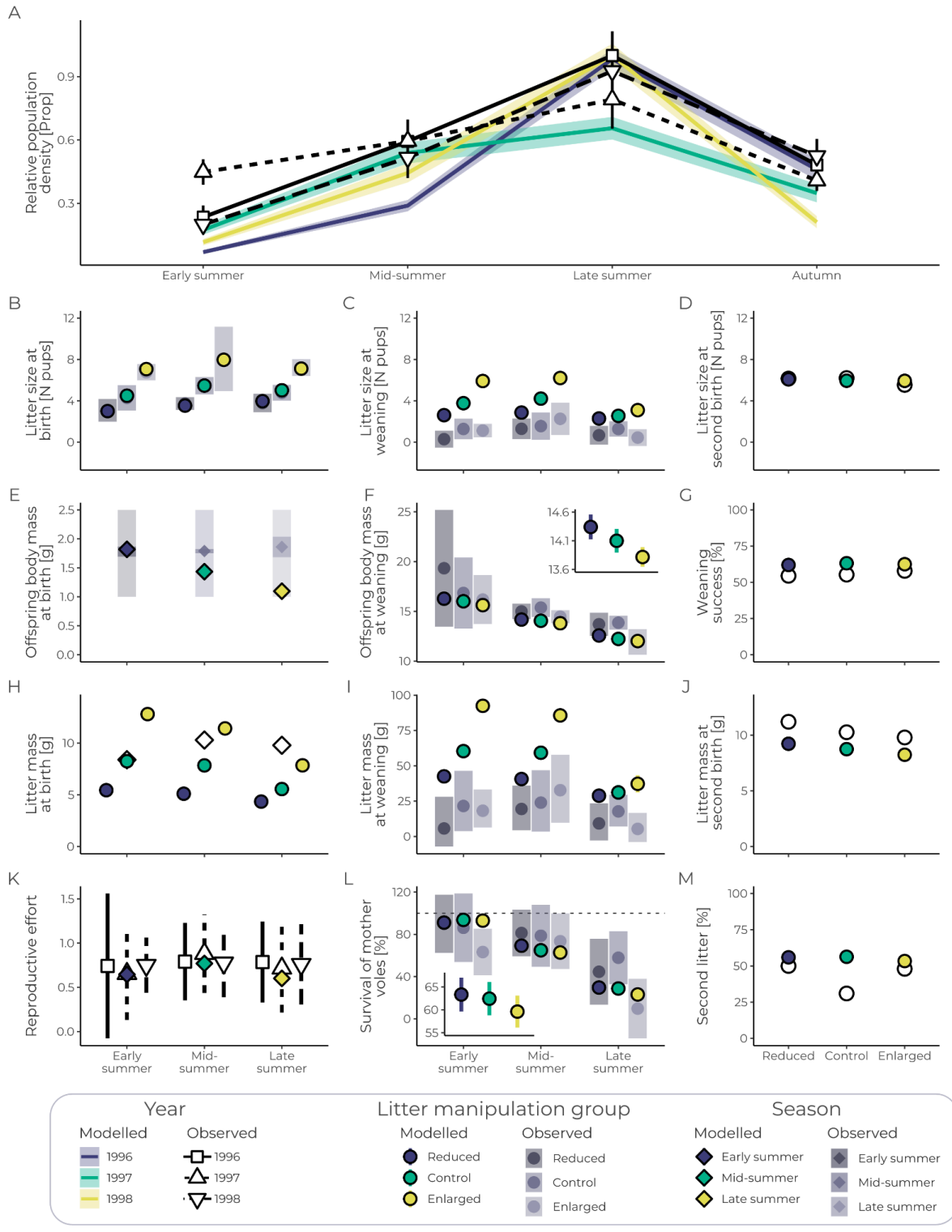
Figure S29. Comparison of model outputs with empirical data from the litter manipulation experiment in Koivula et al. 2003 for the years 1996-1998. (A) Seasonal population density dynamics per year (proportion of maximum value), litter size (count pups) at (B) birth and (C) weaning, and (D) subsequent litters, body mass (in grams) of (E) neonates and (F) weanlings, (G) probability (%) of successfully weaning at least one pup, total litter mass (in grams) at (H) birth, (I) weaning, and (J) subsequent litters, (K) reproductive effort at birth (see Table S34 for calculation), (L) female survival (%) to the next breeding period, and the (M) proportion (%) of females producing subsequent litters. Model outputs are presented from 100 simulation replicates. Model results are shown in color, and empirical findings are in black or grey, with shapes indicating the grouping for analysis: squares for 1996, upward triangles for 1997, downward triangles for 1998, circles for litter manipulation groups, and diamonds for seasons. Statistics for each pattern were matched to those used in the empirical study for comparability: mean ± S.E. is used in panels A, D, E (with the full range in lightest grey), J, and K; mean ± 95% CI is used in panels B, C, F, I, and L; and mean alone is used in panels G, H, and M. Insets in panels F and L display the average mean and 95% CI across seasons.

10. Appendix figures
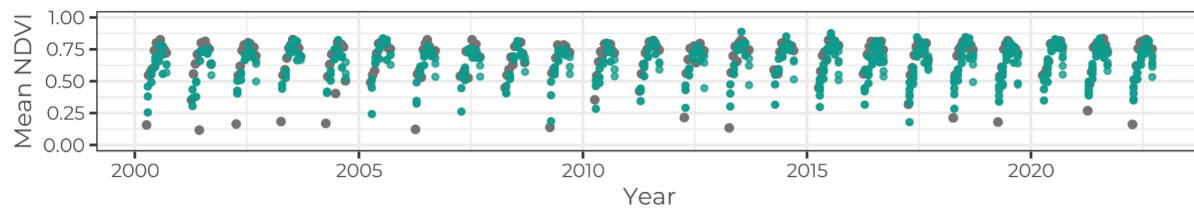
Figure S30. Fit of statistical model (in color) to observed NDVI dynamics (in grey) for Konnevesi, Finland. Observations from winter are not shown as this period was skipped in simulations. NDVI values were obtained from the Terra MODIS mission (Didan, 2021).
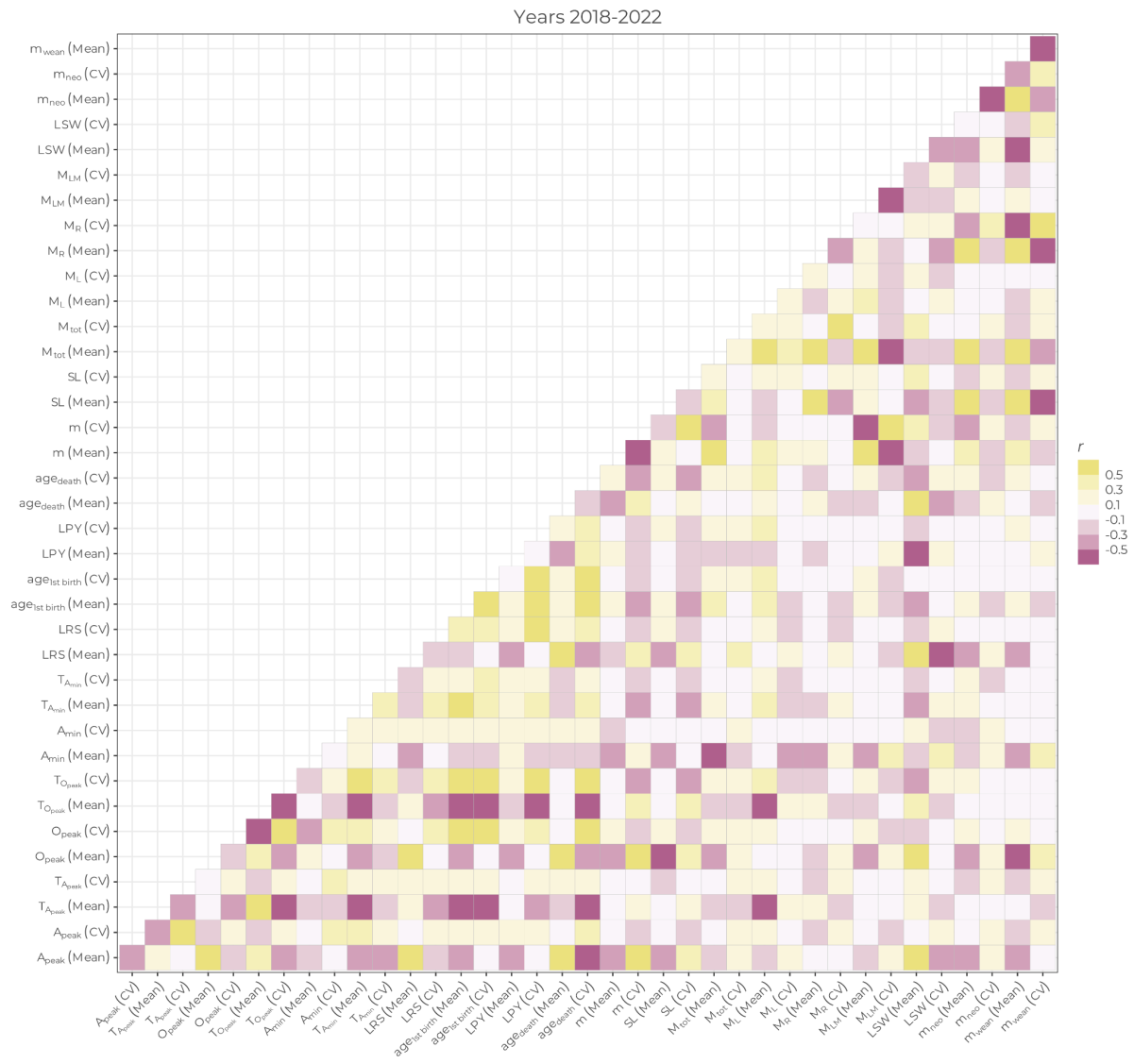
Figure S31. Correlations between individual-level traits and population metrics under observed vegetation dynamics, 2018 to 2022. Pink represents negative correlations and yellow denotes positive correlations, determined via Pearson correlation coefficients, with increasing saturation representing stronger relationships. Abbreviations used include: A_{peak} = peak adult abundance (N), TA_{peak} = timing of peak adult abundance (day of year), O_{peak} = peak offspring abundance (N), TO_{peak} = timing of peak offspring abundance (day of year), A_{min} = adult minimum abundance (N), and TA_{min} = timing of minimum adult abundance (day of year), LRS = lifetime reproductive success (N pups weaned), $age_{1st\ birth}$ = age at first birth (days), LPY = number of litters per year (N), age_{death} = longevity (days), m = body mass (g), SL = body condition (% body fat), M_{tot} = total metabolic rate (J day^{-1}), M_L = locomotion

costs (J day^{-1}), M_R = reproduction costs (J day^{-1}), M_{LM} = cost of lean mass growth (J day^{-1}), LSW = litter size at weaning (N pups), m_{neo} = neonate mass (g), and m_{wean} = weaning mass (g). Both the average '(Mean)' and variation '(CV)' were analyzed for each output. Predictions were generated from 500 simulation runs per site.

Figure S32. Correlations between individual-level traits and population metrics under projected vegetation dynamics, 2094 to 2098. Pink represents negative correlations and yellow denotes positive correlations, determined via Pearson correlation coefficients, with increasing saturation representing stronger relationships. Abbreviations used include: A_{peak} = peak adult abundance (N), TA_{peak} = timing of peak adult abundance (day of year), O_{peak} = peak offspring abundance (N),

TO_{peak} = timing of peak offspring abundance (day of year), A_{min} = adult minimum abundance (N), and TA_{min} = timing of minimum adult abundance (day of year), LRS = lifetime reproductive success (N pups weaned), $age_{1st\ birth}$ = age at first birth (days), LPY = number of litters per year (N), age_{death} = longevity (days), m = body mass (g), SL = body condition (% body fat), M_{tot} = total metabolic rate (J day^{-1}), M_L = locomotion costs (J day^{-1}), M_R = reproduction costs (J day^{-1}), M_{LM} = cost of lean mass growth (J day^{-1}), LSW = litter size at weaning (N pups), m_{neo} = neonate mass (g), and m_{wean} = weaning mass (g). Both the average '(Mean)' and variation '(CV)' were analyzed for each output. Predictions were generated from 500 simulation runs per site.

Figure S33. Predicted spatial and temporal variations in population dynamics, life history, and morphometric traits under observed and projected resource dynamics for shifted NDVI projections, where average annual NDVI was retained from the statistical model projections while within year dynamics were driven by the observed data. These simulations were run under emissions scenario SSP585. For more details, refer to the caption of Figure 5.
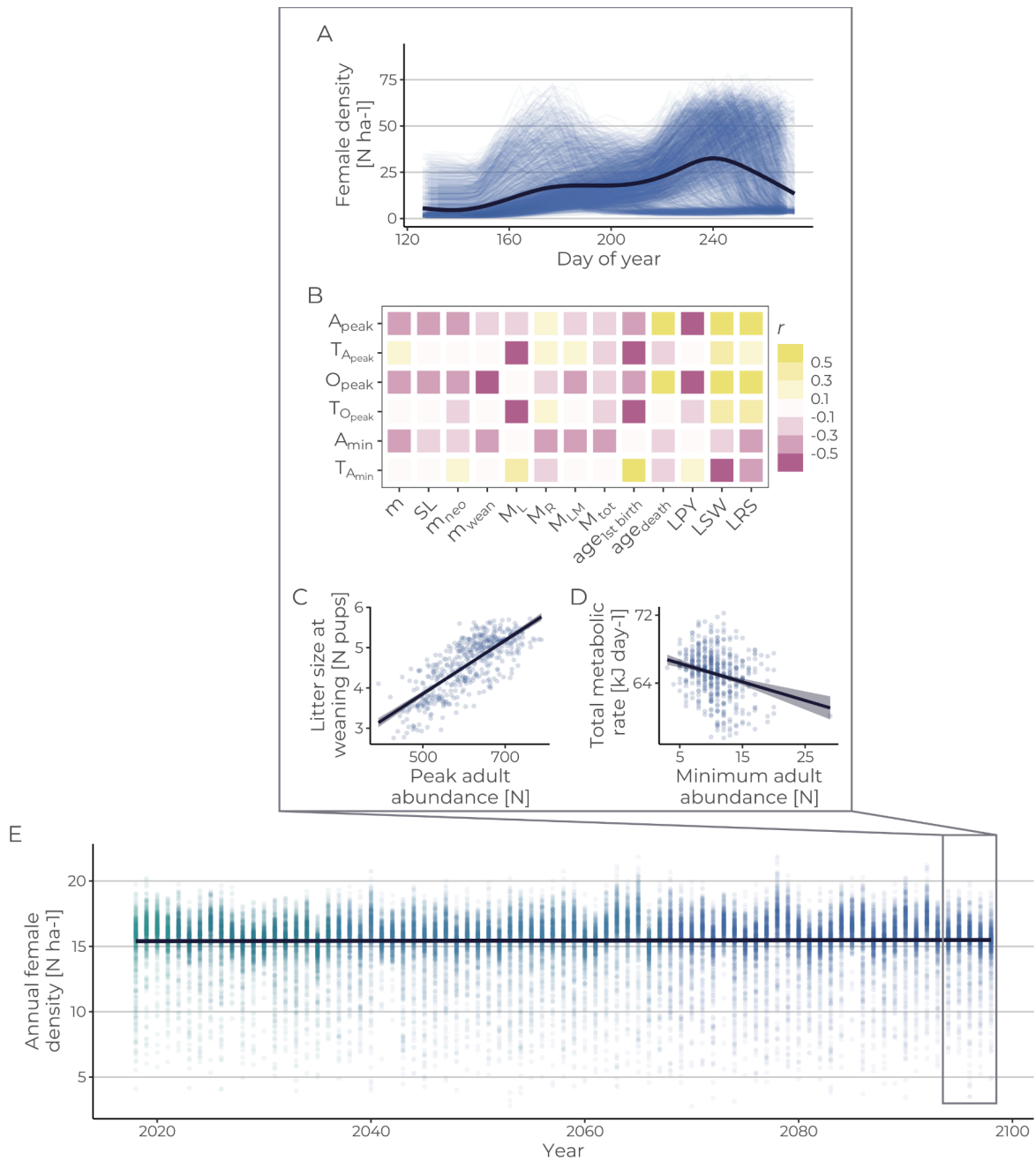
Figure S34. Predicted spatial and temporal variations in population dynamics, life history, and morphometric traits under observed and projected resource dynamics across the ten study sites for emissions scenario SSP245. For more details, refer to the caption of Figure 5.